UNIVERSITAT POLITÈCNICA DE VALÈNCIA

INSTITUTO DE INGENIERÍA ENERGÉTICA

DEPARTAMENTO DE INGENIERÍA MECÁNICA Y MATERIALES

Doctoral program "Ingeniería y Producción Industrial"

Numerical Model for Microchannel Condensers and Gas Coolers with an Improved Air-Side Approach

PhD candidate: Santiago Martínez Ballester

PhD directors: Dr. José Miguel Corberán Salvador

Dr. José Gonzálvez Maciá

Valencia, October 2012

ACKNOWLEDGEMENTS

I would like to start the acknowledgements in general terms, giving special thanks to all the people or institutions who try to do their best for this world, trying to improve or just maintaining our society. And especially to those people who appreciate the knowledge and try to get answers and solutions to our society's questions and problems. These people, organizations and ideas have been my main motivation to carry out this research work.

Of course, I needed something else than ideas or motivations, e.g. friendship, fun, love, advice, time… therefore I want sincerely to acknowledge to all people who have contributed to this thesis, in different ways, with their support, attention and concern:

I am deeply indebted to my supervisor, Prof. José Gonzálvez Maciá, for giving me the opportunity and trust to conduct research works at Institute for Energy Engineering (IIE). Together with him, also special thanks to Prof. José M. Corberán Salvador because of his guidance and advise to do a good job. Both of them were directors of my thesis and I am really grateful for their valuable teaching and advice on numerical modeling.

Most of my research was done at IIE, where we enjoyed a marvelous atmosphere thanks to the friendly relationship we have there. Thus, it is fair to congratulate to the people in charge of this atmosphere: Rafa, Israel, Jesús, Carla, Jorge, Emilio, Pepe, Gerardo, Alicia, and many others… Special thanks to Rafa and David because they did a great job in the first stage of my thesis helping me with the C++ programming.

I had the great opportunity to be hosted by Piotr A. Domaski at National Institute of Standards and Technology in USA for working in the thesis for 6 months. I am deeply grateful to him for hosting me at NIST as well as for giving his valuable time and advice. I will remember always fondly my stay at Gaithersburg thanks to people like: Joanne, Susanne, Nathalie, P. Domanski, D. Yashar, V. Payne, Sunil…

The most important support and special affective gratitude are for those people who had to support the best and the worst of me, before, during and after this thesis, even better than I could have asked for or deserved:

To my parents, my brother and my wife Puri

This thesis work has been supported by the following research grants:

S. Martínez Ballester received a research fellowship from the Program for Training University Teaching Staff (FPU) of the Ministry for Education of Spain.

Part of the contents of the thesis was performed during Santiago's stay for 6 months at National Institute of Standards and Technology (NIST), Gaithersburg (USA). The stay (January 2010-July 2010) was supported by the Santiago´s FPU program and the NIST.

And it has been developed under the frame of the following R&D projects:

"Study and Optimization of Refrigerating and Air Conditioning Systems for Working with Natural Hydrocarbon Refrigerants", funded by the Ministry for Education of Spain (Contract Ref. DPI2008-06707-C02-01).

"Study about Evaporators and Condensers based on Minichannel Technology for application in Refrigerating, Air Conditioning and Heat Pump Steady Systems", funded by the Ministry for Science and Innovation of Spain (Contract Ref. DPI2011-26771-C02-01).

SUMMARY

The following PhD thesis has been carried out in the Institute for Energy Engineering of Universitat Politècnica de València and during a stay at at the National Institute of Standards and Technology (NIST). The main objective of this thesis is to develop a high accuracy model for microchannel heat exchangers (MCHX), which has to be useful for designing purposes in terms of computational cost.

In the author's opinion, there are some drawbacks when existing models are applied to some recent designs of heat exchanger such as serpentine and parallel tubes MCHXs. Thus, the first stage of thesis identifies the phenomena that have the largest effect on the accuracy of a MCHX model. It was also evaluated the degree of accomplishment of some classical assumptions and approaches. To this end, the high accuracy model Fin2D was developed as a tool to carry out the mentioned research.

Fin2D model is a useful tool to analyze phenomena that takes place but requires a large computational cost; not being feasible for design purposes. Therefore, based on the knowledge acquired with Fin2D, a new model was developed: Fin1Dx3 model. This model only accounts for the most important phenomena preserving nearly the same accuracy as Fin2D but with a reduction of one order of magnitude in the required simulation time. It introduces a novel discretization and a unique numerical scheme for modeling the air-side heat transfer. This novel approach allows modeling consistently existing phenomena with great accuracy and with much less simplifying assumptions than current models of literature. Furthermore, it achieves a reasonable computational cost for the objective set. The thesis includes the experimental validation of this model for both a condenser and a gas cooler.

With the aim to present Fin1Dx3 model as a suitable design tool for MCHX, it has been compared in terms of accuracy and computational cost against Fin2D model, simplifications of the Fin1Dx3 model and other representative models from literature.

Finally, as application of the proposed model for design purposes a set of numerical studies were carried out. The studies are about the influence of some design parameters on the MCHX's performance. The importance of these studies is that they cannot be carried out by a model that do not take into account the phenomena modeled by Fin1Dx3.

RESUMEN

La presente tesis se ha llevado a cabo en el Instituto de Ingeniería Energética de la Universitat Politècnica de València y durante una estancia en el National Institute of Standards and Technology (NIST). El objetivo principal de la tesis es desarrollar un modelo de alta precisión para intercambiadores de calor de microcanales (MCHX), que tiene que ser útil, en términos de coste computacional, para tareas de diseño.

En la opinión del autor, existen algunos inconvenientes cuando los modelos existentes se aplican a algunos diseños recientes de intercambiador de calor, tales como MCHXs, bien de tubos en serpentín o en paralelo. Por lo tanto, la primera etapa de la tesis identifica los fenómenos que tienen el mayor impacto en la precisión de un modelo para MCHX. Adicionalmente, se evaluó el grado de cumplimiento de varias simplificaciones y enfoques clásicos. Con este fin, se desarrolló el modelo de alta precisión Fin2D como una herramienta para llevar a cabo la investigación mencionada.

El modelo Fin2D es una herramienta útil para analizar los fenómenos que tienen lugar, sin embargo requiere un gran coste computacional, y por tanto no es útil para trabajos de diseño. Es por ello que en base a los conocimientos adquiridos con el modelo Fin2D, se ha desarrollado un nuevo modelo, el Fin1Dx3. Este modelo tan sólo tiene en cuenta los fenómenos más importantes, reteniendo casi la misma precisión que Fin2D, pero con una reducción en el tiempo de cálculo de un orden de magnitud. Se introduce una novedosa discretización y un esquema numérico único para el modelado de la transferencia de calor del lado del aire. Este nuevo enfoque permite modelar los fenómenos existentes de forma consistente con mayor precisión y con mucho menos simplificaciones que los modelos actuales de la literatura. Por otra parte, se logra un coste razonable de cálculo para el objetivo fijado. La tesis incluye la validación experimental de este modelo tanto para un condensador y un enfriador de gas.

Con el objetivo de presentar el modelo Fin1Dx3 como una adecuada herramienta de diseño para MCHX, éste ha sido comparado en términos de precisión y coste computacional con el modelo Fin2D, otras simplificaciones del modelo Fin1Dx3 y otros modelos representativos de la literatura.

Por último, como aplicación del modelo propuesto a tareas de diseño, se llevaron a cabo una serie de estudios numéricos. Los estudios analizan la influencia de algunos parámetros de diseño en la eficiencia del MCHX. La importancia de estos estudios es que no pueden llevarse a cabo por un modelo que no tenga en cuenta los fenómenos modelados por Fin1Dx3.

RESUM

Aquesta tesi s'ha dut a terme a l'Institut d'Enginyeria Energètica de la Universitat Politècnica de València i durant una estada al National Institute of Standards and Technology (NIST). L'objectiu principal de la tesi és desenvolupar un model d'alta precisió per bescanviadors de calor de microcanals (MCHX), que ha de ser útil, en termes de cost computacional, per a tasques de disseny.

En l'opinió de l'autor, hi ha alguns inconvenients quan els models existents s'apliquen a alguns dissenys recents d'bescanviador de calor, com ara MCHXs, bé de tubs en serpentí o en paral·lel. Per tant, la primera etapa de la tesi identifica els fenòmens que tenen el major impacte en la precisió d'un model per MCHX. Addicionalment, es va avaluar el grau de compliment de diverses simplificacions i enfocaments clàssics. Amb aquesta finalitat, es va desenvolupar el model d'alta precisió Fin2D com una eina per dur a terme la investigació esmentada.

El model Fin2D és una eina útil per analitzar els fenòmens que tenen lloc, però requereix un gran cost computacional, i per tant no és útil per a treballs de disseny. És per això que en base als coneixements adquirits amb el model Fin2D, s'ha desenvolupat un nou model, el Fin1Dx3. Aquest model només té en compte els fenòmens més importants, retenint gairebé la mateixa precisió que Fin2D, però amb una reducció en el temps de càlcul d'un ordre de magnitud. S'introdueix una nova discretització i un únic esquema numèric per a la modelització de la transferència de calor del costat de l'aire. Aquest nou enfocament permet modelar els fenòmens existents de forma consistent amb més precisió i amb molt menys simplificacions que els models actuals de la literatura. D'altra banda, s'aconsegueix un cost raonable de càlcul per a l'objectiu fixat. La tesi inclou la validació experimental d'aquest model tant per a un condensador i un refredador de gas.

Amb l'objectiu de presentar el model Fin1Dx3 com una adequada eina de disseny per MCHX, aquest ha estat comparat en termes de precisió i cost computacional amb el model Fin2D, altres simplificacions del model Fin1Dx3 i altres models representatius de la literatura.

Finalment, com a aplicació del model proposat a tasques de disseny, es van dur a terme una sèrie d'estudis numèrics. Els estudis analitzen la influència d'alguns paràmetres de disseny en l'eficiència del MCHX. La importància d'aquests estudis és que no es poden dur a terme per un model que no tingui en compte els fenòmens modelats per Fin1Dx3.

TABLE OF CONTENTS

LIST OF FIGURES

LIST OF FIGURES

LIST OF TABLES

NOMENCLATURE

A	heat transfer area (m^2)
Ac	cross-sectional area (m^2)
a,b,c,d,e	grid dimensions
Cp	specific heat (J kg^{-1} K^{-1})
D	hydraulic diameter (m)
f	Darcy–Weisbach friction factor (-)
G	mass velocity (kg m^{-2} s^{-1})
g	acceleration of gravity (9.81 m s^{-2})
H	height (m)
h	specific enthalpy (J kg^{-1})
Hp	tube pitch (m)
k	thermal conductivity (W m^{-1} K^{-1})
L	tube length (m)
l	distance between two wall cells (m)
$\dot{m}$	mass flow rate (kg s^{-1})
N	number of cells
Np	number of refrigerant passes
Ns	number of segments
P	pressure (Pa)
pw	wetted perimeter (m)
$\dot{q}$	heat flux (W m^{-2})
$\dot{Q}$	heat capacity (W)
R	thermal resistance (K W^{-1})
s	length in the forward direction of a fluid (m)
T	temperature (K)
t	thickness (m)
U	overall heat transfer coefficient (W m^{-2} K^{-1})
V	volume (m^3)
v	air velocity (m s^{-1})
W	tube depth (m)
X,Y,Z	spatial coordinates (m)
Greek symbols	
α	convective heat transfer coefficient (W m^{-2} K^{-1})
β	tube inclination (deg)
ε	heat exchanger effectiveness (-)
φ	fin height ratio (-)
η	fin efficiency (-)
θ	temperature difference (K)
ρ	density (kg m^{-3})
Subscript	
a	air, air cell index
acc	acceleration
cont	contraction

exp	expansion
f	fin, fin cell index
fB	fin cell at bottom
fr	friction
fT	fin cell at top
g	gravitational
i	fluid cell index
in	inlet
j	matrix column index
k	direction index
N, S, W, E, JB, JT	directions of neighbour wall cell
out	outlet
r	refrigerant, refrigerant cell index
t	tube, tube cell index
w	wall cell index
X,Y,Z	spatial coordinates directions

Abbreviations

BU	both unmixed: air and refrigerant
HX	heat exchanger
LHC	longitudinal heat conduction
MCHX	microchannel heat exchanger
NTU	number of transfer units
RMAU	refrigerant mixed and air unmixed
RTPF	round tube and plate fin heat exchanger

CHAPTER 1

INTRODUCTION

1 INTRODUCTION

Heat exchangers (HXs) are components which are present in lots of industrial processes, ranging from low to high thermal capacities. Depending on the working fluids, application and operating conditions there are several types of heat exchangers. The applications in which the present work focuses are heating, ventilation, air conditioning and refrigeration (HVAC&R) using air as secondary fluid. (Fig. 1.1) shows some of the heat exchangers used in these applications.

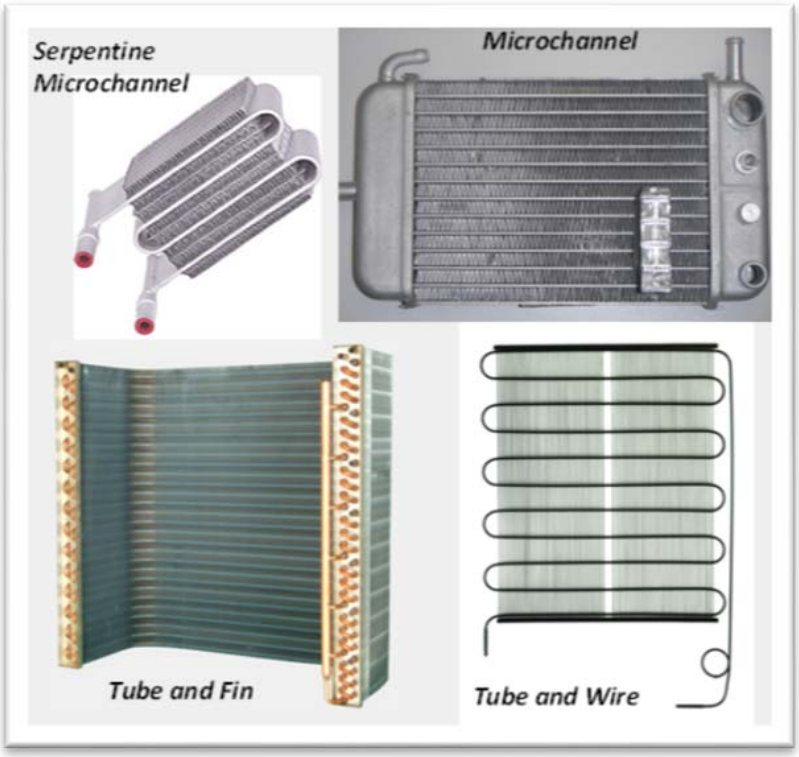

Fig. 1.1 – Types of air-to-refrigerant heat exchangers commonly used in HVAC&R.

As energy costs become very important in today's industrial, residential, and commercial settings, the rational use of energy is now a primary design and management objective. The air-conditioning, refrigeration, and heating equipment consume a large part of electrical energy on a global level. For example, 11.1 % of the total Spain energy consumption is in HVAC&R applications, and 98 % of this consumption corresponds to the commercial sector (IDAE, 2005). The research and progress have been going a long way toward improving the energy efficiency of the systems, by means of innovative system and component design.

As with other products, reliable simulation models can provide substantial cost savings during the design and optimization process of heat exchangers, mainly due to the

reduction of experimental tests. The experimental tests are carried out in expensive laboratories with large human resources requirements, which would have a large impact on final cost. A suitable simulation tools can achieve designs that perform as expected on few tries, which would require less number of experimental tests.

1.1 Microchannel Heat Exchangers

Fin-and-tube HX is the most important kind of air-to-refrigerant HXs. Many parameters can be used to classify fin-and-tube HXs, but hydraulic diameter is the most accepted criteria. There are also many classifications as function of the hydraulic diameter: Kandlikar and Grande (2002) propose the classification shown in Table 1.1. It is important notice that this is not the only classification, and there is not a complete agreement to classify fin-and-tube HXs.

Table 1.1 - Fin-and-tube HXs classification (Kandlikar and Grande, 2002)

Conventional channels	$D_h > 3$ mm
Minichannels	200 μm < D_h < 3 mm
Microchannels	10 μm < D_h < 200 μm
Transitional Channels:	0.1 μm < D_h < 10 μm
- Transitional Microchannels	1 μm < D_h < 10 μm
- Transitional Nanochannels	0.1 μm < D_h < 1 μm
Molecular Nanochannels	D_h < 0.1 μm

The two most common types of fin-and-tube HXs are round-tube and plate-fin heat exchangers (RTPFs) and microchannel heat exchangers (MCHXs). According to Table 1.1, RTPFs correspond to the conventional channel case shown in the table. This kind of HXs are preferred because of their performance, ease of manufacturing and proven reliability.

Regarding MCHXs, the first discussion is the name used to reference them. MCHX commonly used in HVAC&R applications consist of flat multiport tubes, with individual tube hydraulic diameters between 0.5 mm and 1 mm. According to Table 1.1, these HXs would correspond to minichannels HX. However, since there is no full agreement in the classification, microchannel HX is the most common way to reference these kind of HX in the technical literature. Fig. 1.2 shows many MCHX samples and the cross section of some of tubes employed in these heat exchangers.

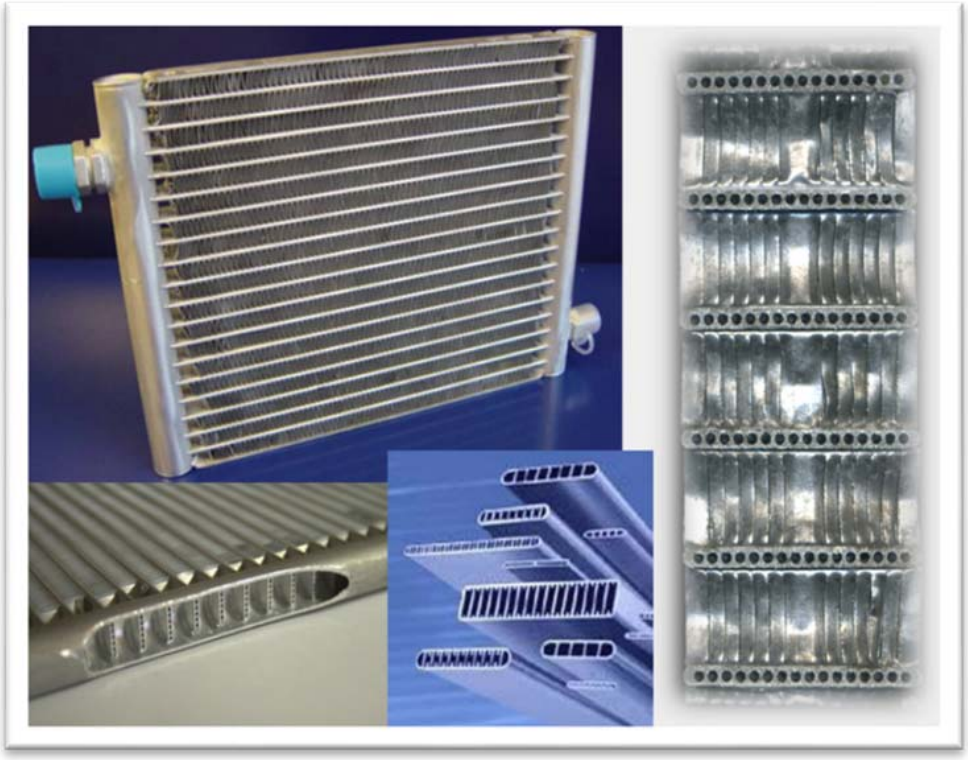

Fig. 1.2 – Different views of microchannel HXs, microchannel tubes and fin surface between tubes.

Currently, an increasing interest on microchannel heat exchangers (MCHXs) is arising in refrigeration and air conditioning applications due to their high compactness (high ratio between *UA* and volume). It is consequence of large heat transfer coefficients as result of using small hydraulic diameters. Given an air side heat transfer area, high compactness means reduced volumes what will result in light heat exchangers and low refrigerant charges.

Getting low refrigerant charges plays an important role on the use of natural refrigerants which are flammable like propane (Palm, 2007; Hrnjak, 2010). Natural refrigerants are considered as more environmentally friendly than others refrigerants commonly used, with a similar or even better performance. The main drawback of working with some natural refrigerants is that they are dangerous in large quantities: ammonia can be toxic and propane is highly flammable, in fact IEC 60335-1 restricts the amount of a hydrocarbon that can be used in a system to 150 g. To this end, a suitable heat exchanger design is a serpentine MCHX (Fernando et al., 2004; Hrnjak and Litch, 2008; Palm, 2007; Hrnjak, 2010). This kind of heat exchangers minimizes the refrigerant charge because it has no headers, thus saving all this volume and the corresponding refrigerant charge.

In the case of transcritical CO2 systems, microchannels have an additional merit related to their high mechanical strength.

However, microchannels also have disadvantages, such as: high cost of manufacture and in case of evaporators: problems to drain the condensate water (Pettersen et al., 1998; Qi et al., 2009; Zhang and Hrnjak, 2010; Moallem et al., 2012a, 2012b) and refrigerant flow mal-distribution (Kulkarni et al., 2004; Brix et al., 2009; Ye et al., 2009; Brix et al., 2010; Nielsen et al., 2012). Additionally, in two-phase flow some of the heat transfer and pressure drop models and/or correlations, traditionally worked out for RTPF heat exchangers, do not work accurately for MCHX because the fluid flow and heat transfer in microchannels is substantially different from those encountered in the conventional tubes and channels. Many authors have worked on this topic: Kandlikar (2002); Thome (2004); Garimella et al. (2005); Cavallini et al. (2005); Revellin and Thome (2007); Bertsch et al., (2008); Cavallini et al. (2009); Revellin et al. (2009); Agarwal et al. (2010). These problems are the goal of much of the research involving microchannels right now.

Microchannels have been widely used in the automotive industry, where RTPF has been almost completely replaced with MCHXs. This application has widely studied by: Joardar and Jacobi, (2005); Zhong et al. (2005); Xia et al. (2006); Lia et al. (2011); Qu et al. (2011); Zilio et al. (2011); Ayad et al. (2012). It is a suitable option for this application because it is light and saves a lot of space, so needed in automobiles. Lately, HVAC&R industry is starting to use MCHX in some systems (Fernando et al. 2008; Shao et al., 2010; Kew and Reay, 2011). In fact, MCHXs are very used in systems that work with CO_2 (Pettersen et al., 1998; Kim and Bullard, 2001; Kim et al. 2002; Kim et al. 2004; Veje and Süss, 2004). Other interesting applications are found in highly specialized fields (Singh, 2009): bioengineering, micro-fabricated fluidic systems, electronics (Zhao and Lu, 2002; Chen and Garimella, 2011; Ramos- Alvarado et al., 2011), and high temperature solar receivers (Li et al., 2011).

1.2 Literature Review and Background

Nowadays, simulation software is a very suitable tool for the design of products in which complex physical processes occur. These tools allow the saving of lots of costs and time in the laboratory working with expensive test benches.

Currently, several models or simulation tools for heat exchanger are available in the literature: for finned tubes (Lee and Domanski, 1997; Corberán et al., 2002; Jiang et al., 2006; Oliet et al., 2007b; Singh et al., 2008; CoilDesigner, 2010; EVAP-COND, 2010;

IMST-ART, 2010; Oliet et al., 2010) and microchannel heat exchangers (Kim and Bullard, 2001; Yin et al., 2001; Asinari, 2004; Jiang et al., 2006; Oliet et al., 2007a; Shao et al., 2009; García-Cascales et al., 2010; MPower, 2010; Fronk and Garimella, 2011). Some of them (Kim and Bullard, 2001; Yin et al., 2001; Corberán et al., 2002; Asinari, 2004; Oliet et al., 2007a; Singh et al., 2008; Shao et al., 2009; CoilDesigner, 2010; IMST-ART, 2010; Oliet et al., 2010) apply energy conservation equations to each control volume, while others (Lee and Domanski, 1997; EVAP-COND, 2010; Jiang et al., 2006; Oliet et al., 2007b; García-Cascales et al., 2010; Fronk and Garimella, 2011) apply directly the solution given by the ε-NTU methodology. The main difference between both methodologies is that the ε-NTU model uses several implicit assumptions resulting in less freedom to describe the actual processes. However, the models based on energy conservation equations usually apply the same assumptions made in ε-NTU approaches. These classical assumptions are the following:

- Steady state.
- Uniform fluid properties.
- Use of fin efficiency: application of the fin theory, which assumes uniform temperature throughout the air in contact with the fin.
- Adiabatic-fin-tip assumption for the fin efficiency evaluation: no heat conduction between tubes trough the fin.
- One-dimensional heat conduction: negligible effect of 2D longitudinal heat conduction (2D LHC).

Steady state is a real assumption, which is satisfied for conditions usually studied.

The fluid properties issue is easily addressed by splitting the heat exchanger into segments. On the other hand, not using the ε-NTU methodology has the disadvantage of losing an accurate fluid temperature function, which requires assuming some temperature profile for the fluids. This problem can be solved by dividing the heat exchanger into smaller segments, which improves the representation of non-uniform air and refrigerant properties. In most published models, this methodology improves only the representation of the refrigerant properties because no discretization is provided in the air flow direction. This leads to approximated air properties for the heat exchanger depth (air flow path) based on the average of the inlet and outlet temperatures.

The fin efficiency is calculated following the fin theory, which is developed assuming uniform temperature for the surrounding air in contact with the fin, and uniform heat transfer coefficients. The assumption of uniform air temperature along the fin height is violated since there is a temperature variation along the fin height and fin depth. The

ε-NTU methodology needs the use of fin efficiency. To the knowledge of the author, all models available in the literature, which use a finite volume method (FVM) (Patankar, 1980), apply the fin efficiency.

One of the most important effects to capture to the author's opinion is the heat conduction between tubes. All the models that apply fin theory assume adiabatic-fin-tip assumption in order to use the corresponding relationship for the fin efficiency (Incropera and DeWitt, 1996). It is a quite simple expression but this efficiency, fundamentally, does not lend itself to accounting for heat transfer via fins between tubes of different temperatures. Some authors (Lee and Domanski, 1997 and Singh et al, 2008) have worked in order to implement this heat conduction in their models for finned tubes. In order to implement it, they apply similar approaches that consist in adding a heat conduction term to the energy conservation equation in the wall. Singh et al. (2008) presented a model, referred to as a "resistance model", to account for heat transfer between tubes through the fins in finned-tube heat exchangers using a segment-by-segment approach. The energy conservation equation in the wall includes the heat transfer from fin to air that is modeled by using fin efficiency. This fin efficiency is based on the fin theory, whose application was discussed above, assuming adiabatic-fin-tip in order to evaluate the fin efficiency. Then, they introduce the heat conduction term as function of temperature gradient between neighbouring tubes despite using the concept of adiabatic-fin-tip efficiency. Singh et al (2008) apply to this term a multiplier which has to be adjusted either numerically or experimentally which depends on the heat exchanger simulated. Basically, this approach corrects a scenario where adiabatic-fin-tip assumption is not correct by applying a correction term to take into account heat conduction between tubes. The authors explained that the use of a set of energy conservation equations is better than the use of ε-NTU methodology with the included heat conduction term because the ε-NTU relationship assumes all heat is transferred from one fluid to another without internal heat transfer within the heat exchanger wall structure itself. The latter methodology was used by Lee and Domanski, 1997. Validation effort of Singh et al (2008) showed improved model predictions when heat conduction effects were included: predicted heat load agreement within ±3% of the experimental data instead of ±5% corresponding to the model without heat conduction between tubes; the temperature distribution prediction showed an agreement within ±3.3 °C of the experimental data instead of ±8.5 °C corresponding to the model without heat conduction between tubes.

To the knowledge of the author there is no model for MCHXs that can evaluate the effect of cutting fins by using a finite volume method (FVM) (Patankar, 1980) for discretizing the equations. This capability means a model able to simulate both scenarios with and without fin cut. Asinari et al. (2004) proposed a three-dimensional

model for microchannel gas coolers using CO_2 as refrigerant which can evaluate such effects but the model employs a finite-volume and finite-element hybrid technique. This model discretizes the equations by means of a finite-volume and finite-element hybrid technique taking into account longitudinal heat conduction (LHC) along all directions for all elements (fins and tubes), thus it does not employ the adiabatic-fin-tip assumption. They investigated the impact of longitudinal heat conduction effects on capacity, and also studied the prediction error due to the adiabatic-fin-tip assumption. The authors concluded that when tube temperatures are different, the use of the adiabatic-fin-tip efficiency gives accurate predictions of the total heat capacity although it does not accurately represent the actual distribution of heat flow between the fin roots. But they did not report the effects in the predicted capacity for the individual tubes of the heat exchanger. It has to be noted that a consequence of a wrong prediction of the individual tube capacity introduces a wrong evaluation of the fluid temperature and pressure at the tube outlet section.

Cutting the fins between tubes for air-to-refrigerant heat exchangers is an improvement studied in literature. Cutting the fins avoids the heat conduction between tubes trough the fins, which degrades the heat exchanger effectiveness. In fact several experimental studies indicated that the heat exchanger performance can be significantly degraded by the tube-to-tube heat transfer via connecting fins. Domanski et al. (2007) measured as much as 23 % reduction in finned-tube evaporator capacity when different exit superheats were imposed on individual refrigerant circuits. For a finned tube gas cooler Singh et al. (2010) reported heat load gain of up to 12% and fin material savings of up to 40%. However, improvements no so large have been achieved for MCHXs, namely: Asinari et al. (2004) who concluded that the impact of this heat conduction can be assumed as negligible in a wide range of applications; Park and Hrnjak (2007) reported measurements of capacity improvements of up to 3.9% by cutting the fins in a CO_2 serpentine microchannel gas cooler. Also Zilio et al. (2007) concluded that heat conduction through fins in a CO_2 gas cooler had a significant impact on the capacity. In fact, cut fin surfaces are increasingly being used in heat exchangers to reduce the heat conduction between tubes and improve the heat exchanger performance.

The one-dimensional heat conduction assumption only accounts for the transverse heat flux trough the wall between two fluids. It does not account for 2D longitudinal heat conduction in the tube and it neglects the longitudinal heat conduction in the fin, along the air flow direction. Asinari et al. (2004) concluded that these effects produce a negligible effect on the performance of the class of CO_2 gas cooler they studied.

A gas cooler working with CO_2 in supercritical pressures is an application where a large impact on the performance could be expected due to 2D LHC in the tube wall and heat conduction between tubes through fins. The reasons are based on the temperature glide of CO_2 during a supercritical gas cooling in contrast with a condenser where the temperature during condensation is approximately constant. Representative values can be extracted from experimental results of Zhao et al. (2001) where CO_2 undergoes temperature variations along a single tube from 25 K up to 85 K while maximum temperature difference between two neighbor tubes range from 30 K to 100 K. Heat conduction between tubes trough fins appears when a temperature difference between tubes exists. This temperature difference will vary depending on the refrigerant circuitry and its temperature difference along the heat exchanger, which will be larger in a gas cooler than in an evaporator or condenser. Thus, gas cooler is an interesting application to be studied in the present thesis, because it is where largest impact of these effects is expected.

Few models take into account all the phenomena explained above. Asinari et al. (2004) presented a model for MCHX gas coolers that included these phenomena but an important difference exists between these similar models and the proposed one in this work related to the computational cost. The method usually applied by these models to discretize governing equations is a finite element method (FEM) (Patankar, 1980) or even a hybrid one as Asinari et al. (2004) employed, which use both the FEM and the finite volume method (FVM) (Patankar, 1980).

1.3 Motivations and Research Objectives

Due to the relatively recent application of MCHXs in HVAC&R industry, a need of developing a simulation tool for this kind of heat exchanger arises in order to aid its design. Thus, the main objective of present thesis is the development of a high accuracy simulation tool for design purposes of MCHX. To this end, this tool should have following features: it should require a reasonable computational cost for design purposes; it has to be robust; it must be able to be used in standard personal computers; and it has to be able to assess the impact on performance of those parameters that the designer has to define.

Other motivation is based on the drawbacks that, in the author's opinion, existing models have when they are applied to some recent designs of heat exchanger such as parallel tubes and serpentine MCHXs. The main drawback of applying existing models to new heat exchangers designs is the implicit application of classical assumptions, which were studied and developed for a specific heat exchanger design and may not

be correct for these new MCHX designs. Some of these assumptions, which were discussed in previous sub-section, have been studied in the literature for many heat exchangers topologies such as RTPF heat exchangers, whilst the effects of these assumptions are not studied so extensively for parallel tubes and serpentine MCHXs. These heat exchangers have a different thermal behavior since the thermal and geometric conditions are different. Thus, the author thinks that it is interesting to evaluate the impact of the classical assumptions, which were exposed previously, for MCHXs working in typical operating conditions.

Given these motivations, the main objectives for the thesis are the following:

- To develop a high accuracy model able to predict the performance of a MCHX with a low computational cost. This model has to be useful for design purposes.
- To identify, understand and quantify all the phenomena that have the largest effect on the heat transfer of a MCHX.

In order to accomplish the previous objectives, additional partial objectives are:

- To develop a model (Fin2D) which can take into account all the phenomena taking place in MCHX, with regard to heat transfer, e.g. 2D longitudinal heat conduction, heat conduction between tubes and the un-mixed air along the fin height. It has to allow evaluating the isolate impact of each phenomenon with high accuracy.
- To check the consistency and accuracy of results for this model.
- To analyze and quantify, by using the Fin2D model, the effect of each phenomenon on the MCHX performance in order to identify the most important effects to include in a model for MCHXs.
- To evaluate the error obtained by using classical approaches for heat exchangers modeling.
- To develop a model (Fin1Dx3) that retains only the most important effects, which were identified previously with the Fin2D model, in order to get a low computational cost with high accuracy.
- To carry out a validation of the model with experimental data for different scenarios.
- To compare in terms of accuracy and computational cost the proposed model with more complicated models, simplified models and representative models of literature.
- To use the developed model for analyzing the influence of some design parameters on the MCHX performance.

1.4 Thesis Organization

The first chapter of the thesis reviews the state of the art related with the problem that the author want to study and presents the objectives of the research.

In order to evaluate the effects exposed in previous subsection a model is going to be developed. First model developed is referred to as Fin2D and is presented in chapter 2. After many consistency tests in order to validate the model, Fin2D was used to evaluate in a more fundamental way all the proposed effects and assumptions, their impact on predicted results. It also allowed studying differences between classical modeling approaches from literature. Results and conclusions by using Fin2D model will be discussed in chapter 2.

Fin2D model was created to obtain accurate results by modeling phenomena in a very detailed way in order to detect inaccuracy sources and to evaluate the degree of accomplishment of some classical assumptions. On the other hand, Fin2D model required a large computational cost. Therefore, according to the objective of developing a suitable model for design purposes, a new model was developed: Fin1Dx3 model. This model only accounts for the most important phenomena preserving nearly the same accuracy. It introduces a novel discretization methodology, which allows be consistent with the assumptions done and it achieves a large reduction of the simulation time required for simulations. Chapter 3 will present Fin1Dx3 model, validation studies with experimental data for both condenser and gas cooler.

Chapter 4 introduces a comparison between different model approaches, namely: some approaches available in literature and some other from Fin1Dx3 modifications. This comparison will show differences concerning computational cost and accuracy.

Once the advantages of using Fin1Dx3 were shown in the comparison of models, chapter 5 presents numerical studies which analyze influence of some design parameters on the performance of MCHXs by using Fin1Dx3 model.

Finally, chapter 6 will summarize the main conclusions and contributions of the research presented in this thesis. Chapter 6 also lists the publications resulting from this thesis.

CHAPTER 2

FIN2D MODEL

2 FIN2D MODEL

This chapter presents a detailed model for microchannel heat exchangers used as gas coolers which does not use the fin efficiency, accounts for 2D LHC in fins and tubes, accounts for the heat conduction between tubes, and applies a detailed discretization for the air, which is independent of the refrigerant discretization. The model, referred to as Fin2D, subdivides the heat exchanger into segments and cells (air, refrigerant, fin, tube wall), to which a system of energy conservation equations is applied without traditional heat exchanger modeling assumptions. Fin2D differs from other models referred to previously in the number of classical assumptions made. The model of Asinari et al. (2004) is the most similar to the present model regarding the number of assumptions, although the discretization method applied by them is a hybrid one, which uses both the finite element method (FEM) and the finite volume method (FVM), whereas the methodology used in the Fin2D model is the FVM.

After a numerical verification, the solution obtained with the Fin2D model is employed to assess the impact of the classical heat exchanger modeling assumptions on the accuracy of the performance predictions for such conditions. The goal of the present chapter is to study the heat transfer processes in a microchannel gas cooler by evaluation of each of individual heat transfer effects described above, rather than propose a model able for heat exchangers design. This chapter will also provide a deeper understanding of the microchannel CO_2 gas coolers.

2.1 Fin2D Heat Exchanger Model

2.1.1 Heat exchanger discretization

Fig. 2.1(a) presents a piece of the studied microchannel heat exchanger. It is discretized along the *X* direction (refrigerant flow) in a number of segments *a*. Each segment (Fig. 2.1(b)) consists of: two streams of refrigerant (top and bottom flows) that are split into *b* channels in the *Z* direction (air flow); two flat tubes (top and bottom) that are discretized into *c* cells in the *Z* direction; and both air flow and fins, which are discretized in two dimensions: *d* cells in the *Y* direction and *e* cells in the *Z* direction. This discretization is summarized in the text as; grid: {*a,b,c,d,e*}. For illustration of the nomenclature, the numerical example shown in Fig. 2.1(a) and (b) corresponds to a grid: {3,5,3,7,4}.

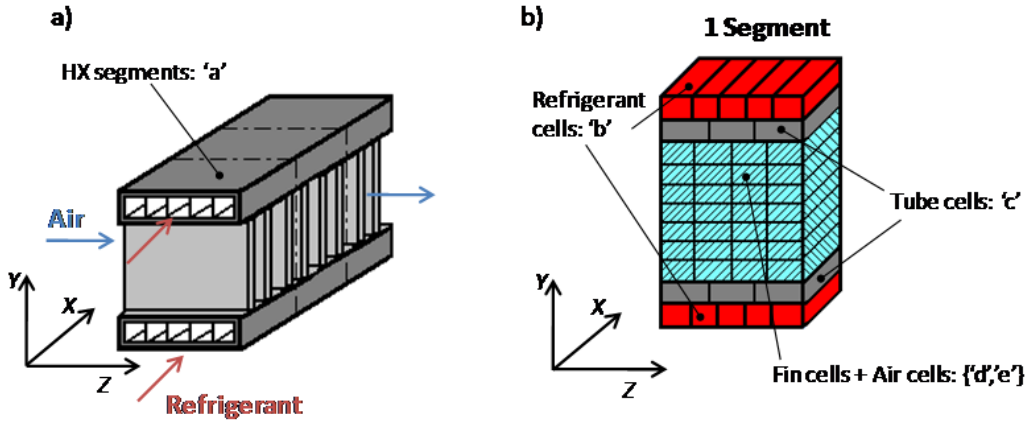

Fig. 2.1 – (a) Piece of the heat exchanger studied in the paper. (b) Schematic of the discretization applied in a segment of the heat exchanger.

The refrigerant flows inside the channels (*b*=5 in Fig. 2.1(a)) along the *X* direction without any mixing between the channels, and it exchanges heat with the tube cells in contact; these tube cells transfer this heat to the air cells in contact by convection, and to its neighbouring tube cells on the plane *X*-*Z* and to the fin roots in contact by conduction. The air exchanges heat by convection with the fin cells, and the air cells at the bottom and top also exchange heat with the tube cells in contact. The fin cells conduct the heat along the plane *Y*-*Z*, and the bottom and top fin cells also conduct heat to the tube wall.

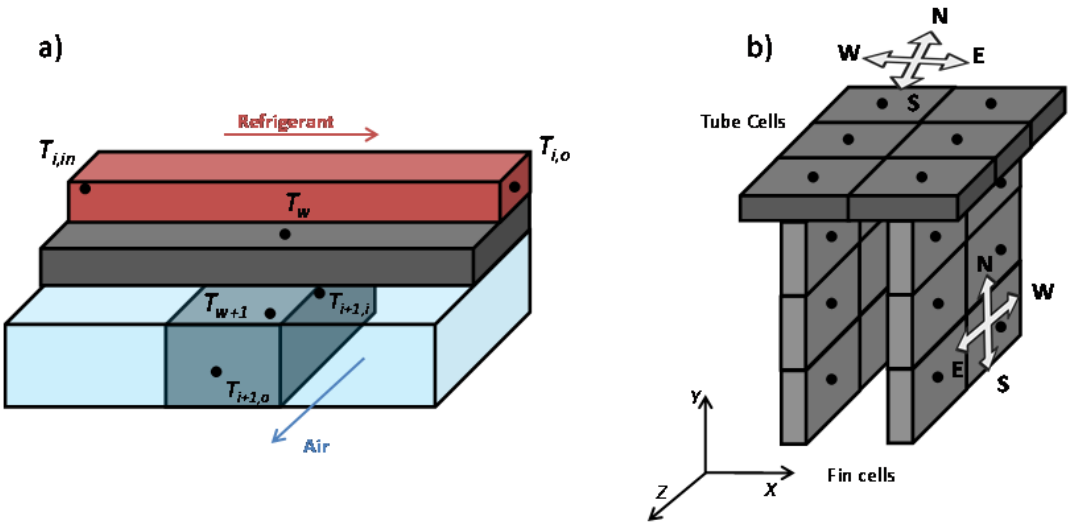

Fig. 2.2 – (a) Cells schematic and definition of the cell nodes. (b) Direction references for fin and tube wall cells.

2.1.2 Governing equations

Every fluid cell (refrigerant or air) has two nodes, which correspond to the inlet and the outlet in the fluid flow direction. The wall cells (tube or fin) have only one node located in the centroid of the cell, as is shown in Fig. 2.2(a). All cell's local variables are referred to the value in these nodes, e.g. $T_{i,in}$ and $T_{i,o}$ are the temperature at the inlet and at the outlet, respectively, of a fluid cell *i*, either refrigerant or air. T_w is the temperature defined for the wall cell *w*, which could be either fin or tube.

In this situation the governing equations at each fluid cell (refrigerant and air) and at each wall cell (tube and fin) can be written as follows:

$$\dot{m}_i \cdot dh_i = \sum_{w=1}^{n_i} \dot{q}_{w,i} \cdot pw_{w,i} \cdot ds_i \tag{2.1}$$

$$\dot{q}_{w,i} = U_{w,i} \cdot (T_w - T_i) \tag{2.2}$$

$$U_{w,i} = \frac{1/A_{w,i}}{\frac{t_w/2}{A_{w,i} \cdot k_{w,k}} + \frac{1}{A_{w,i} \cdot \alpha_{w,i}}}$$

$$\nabla\left(k_{w,k} \cdot t_w \cdot \nabla T_w\right) + \sum_{i=1}^{n_w} \dot{q}_{w,i} = 0 \tag{2.3}$$

where any wall cell *w* is in contact with n_w fluid cells *i*=1, n_w; any fluid cell *i* is in contact with n_i wall cells *w*=1, n_i; $k_{w,k}$ is the thermal conductivity of the wall cell *w* in the *k* direction, thus it is possible to study the influence of 2D LHC at both fin and tube walls. Eq. (2.1) states the energy conservation for a fluid cell, whereas Eq. (2.3) states the energy conservation for a wall cell. Eq. (2.2) represents the heat flow between a wall cell and a fluid cell. Neither pressure losses nor dehumidification has been modeled since it is a gas cooler and the paper only focuses on the understanding of possible differences in heat transfer.

For solving the system of equations a set of boundary conditions is needed. Inlet conditions and velocity distributions are known for both fluids, and velocity distribution is assumed as uniform. Since the heat exchangers are normally well insulated, the heat transferred by the wall edges to the surrounding is considered negligible, and the wall cells are considered to be adiabatic with the surrounding. Only two tubes of the whole gas cooler are going to be modeled in this work, so an additional boundary condition is necessary: both tubes have symmetry condition. This symmetry condition implies that the heat transferred from a tube to each of the

neighboring tubes is the same. This assumption approximates simulations at central tubes of a microchannel slab. It has to be noted that this symmetry condition does not mean that the heat transferred by each tube have to be the same, in fact it will be studied in section 2.5.

2.1.3 Numerical Solution

For the discretization of equations the finite volume method (FVM) (Patankar, 1980) has been applied along with the semi-explicit method for wall temperature linked equations (SEWTLE) proposed by Corberán et al. (2001). The discretization of governing equations does not present any special difficulty, except for the estimation of the integral of the heat transferred to the fluids in contact with a considered piece of wall (Eq. (2.2) and (2.3)). This integration must be consistent with the integration of the coincident terms of fluid energy Eq. (2.1). The numerical scheme corresponding to a linear fluid temperature variation (LFTV), as explained in Corberán et al. (2001), is employed for the discretization of Eq. (2.2). This numerical scheme is basically based on assuming a piecewise distribution of the fluid temperature along the fluid cell, leading to the following expression:

$$A_{\mathrm{w,i}}\ \dot{q}_{\mathrm{w,i}} = U_{\mathrm{w,i}}\, pw_{\mathrm{w,i}} \left(T_{\mathrm{w}} - \frac{T_{\mathrm{i,in}} + T_{\mathrm{i,out}}}{2} \right) \Delta s_{\mathrm{i}} \tag{2.4}$$

The discretization of the Laplacian operator in Eq. (2.3) has been made by the classical finite difference approach according to the adopted FVM. The Eq. (2.3) discretization used in this model is shown in Eq. (2.5).

$$a_{\mathrm{w}} \cdot T_{\mathrm{w}} - \sum_{\mathrm{k=W,E,S,N}} a_{\mathrm{w,k}} \cdot T_{\mathrm{w,k}} = a_{\mathrm{w,J}} \cdot T_{\mathrm{w,J}} - \sum_{\mathrm{i=0}}^{n_{\mathrm{j}}} pw_{\mathrm{w,i}} \cdot U_{\mathrm{w,i}} \cdot (T_{\mathrm{w}} - T_{\mathrm{i}}) \cdot ds_{\mathrm{w,i}} \tag{2.5}$$

$$a_{\mathrm{w,W}} = \frac{k_{\mathrm{w,W}} \cdot A_{\mathrm{w,W}}}{\delta l_{\mathrm{w,W}}} \qquad a_{\mathrm{w,E}} = \frac{k_{\mathrm{w,E}} \cdot A_{\mathrm{w,E}}}{\delta l_{\mathrm{w,E}}} \qquad a_{\mathrm{w,S}} = \frac{k_{\mathrm{w,S}} \cdot A_{\mathrm{w,S}}}{\delta l_{\mathrm{w,S}}}$$

$$a_{\mathrm{w,N}} = \frac{k_{\mathrm{w,N}} \cdot A_{\mathrm{w,N}}}{\delta l_{\mathrm{w,N}}} \qquad a_{\mathrm{w,J}} = \frac{k_{\mathrm{w,J}} \cdot A_{\mathrm{w,J}}}{\delta l_{\mathrm{w,J}}} \qquad a_{\mathrm{w}} = \sum_{\mathrm{k=W,E,S,N,J}} a_{\mathrm{w,k}}$$

All $a_{\mathrm{w,k}}$ terms refer to the conductance between a wall cell *w* and the neighbouring wall cell, adjoined to this one, in the direction *k*. The direction reference is different in the tube and fin cells; the schematic used in the model is shown in Fig. 2.2(b). There is one

exception: $\alpha_{w,J}$, which means the conductance of the joint between a tube wall cell and a fin wall cell.

The global solution method is outlined in Corberán et al. (2001). Basically, this method is based on an iterative solution procedure. First, a guess is made about the wall temperature distribution, and then the governing equations for the fluid flows are solved in an explicit manner, getting the outlet conditions at any fluid cell from the values at the inlet of the heat exchanger and the assumed values of the wall temperature field. Once the solution of the fluid properties is obtained for any fluid cell, then the wall temperature at every wall cell is estimated from the balance of the heat transferred across it (Eq.(2.3)). This procedure is repeated until convergence is reached. The numerical method employed for calculating the temperature at every wall cell is based on the line-by-line strategy (Patankar, 1980) following the *Y* direction for fin cells and the *X* direction for tube cells, so that the global strategy consists of an iterative series of explicit calculation steps. This method can be applied to any flow arrangement and geometrical configuration, and offers excellent computational speed. Additionally, it can easily be extended to other cases, such as two-phase flow or humid air.

2.2 Case Study Definition

In this case study we modelled a microchannel gas cooler for which dimensions were extracted from Zhao et al. (2001). Since the objective of this work was to evaluate the effects of different classical assumptions in the predicted results, operating conditions that produce large temperature variations and high heat fluxes were of interest. Consequently, the chosen operating conditions correspond to the experimental data of the test for gas cooling n° 3b, HX1, from the same work. Table 2.1 shows the most important geometric data while Table 2.2 shows the considered operating conditions. Some data were estimated from the reported experimental values; namely, the CO_2 side heat transfer coefficient was estimated to be 537 W m^{-2} K^{-1}. This coefficient was estimated by using the ε-NTU relationship for cross-flow (Incropera and DeWitt, 1996) working in the mentioned test conditions. For these calculation the air side heat transfer coefficient was required and it was evaluated with convection correlation for fully laminar flow in non-circular tubes (Incropera and DeWitt, 1996) resulting to be 66 W m^{-2} K^{-1} (this value will be used only in the verification studies).

The heat transfer mechanisms that take place along a tube in a gas cooler depend neither on the tube length nor the number of tubes. For this reason, only an

equivalent piece of the heat exchanger has been considered in the detailed analysis of the heat transfer.

Table 2.1 - Geometry of the microchannel heat exchanger

Tube length (cm)	8	Fin pitch (mm)	1.56	Channel diameter (mm)	1
Tube depth (mm)	16	Fin thickness (mm)	0.152	Channels number	10
Tube thickness (mm)	1	Fin height (mm)	8		

Table 2.2 - Operating conditions; Test for gas cooling n° 3b, HX1 (Zhao et al., 2001).

	Inlet pressure (kPa)	Inlet temperature (°C)	Outlet temperature (°C)	G (kg/m^2 s)
CO_2	8937	79.9	42.4*	132.56
Air	100	23.74*	32.4	3.05

*estimated value

The reference case study is shown in Fig. 2.3(a). It consists of two central tubes with their fins attached. The total length of the tubes is five times the tube depth. The refrigerant has only one pass along the heat exchanger with the same mass flow rate in both tubes.

For the evaluation of the thermodynamic and transport properties of fluids, REFPROP (Lemmon et al., 2002) was used. The air, properties were locally evaluated whereas the refrigerant properties were assumed as uniform and evaluated as averaged values between the corresponding values at the inlet and the outlet of the heat exchanger studied in the present work. The thermal conductivity of the fin and tube walls was estimated to be 173 W m^{-1} K^{-1}.

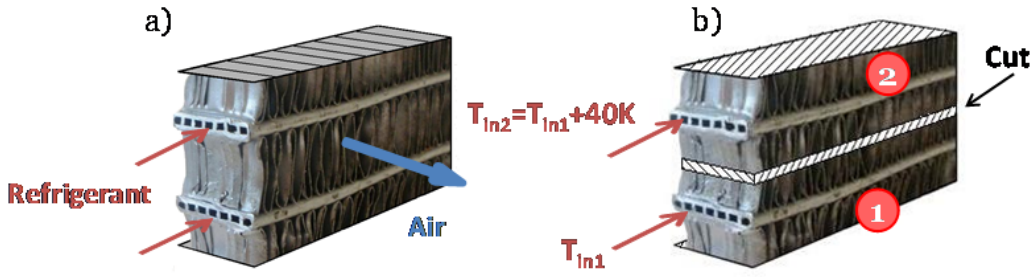

Fig. 2.3 - (a) Schematic of the equivalent heat exchanger studied (b) Schematic of the equivalent heat exchanger used in the study of the adiabatic-fin-tip assumption.

2.3 Numerical Verification of the Fin2d Model

Before employing the newly developed model to produce detailed solutions of heat transfer in the equivalent piece of the microchannel gas cooler, shown in Fig. 2.3(a), it is necessary to validate the model. With this purpose in mind we performed a series of systematic checks against operational cases for which an analytical solution can be obtained.

The detailed discretization of the air flow in the *Y* direction adopted in Fin2D makes it difficult to compare Fin2D predictions with those of analytical solutions. In order to validate the model, many scenarios, listed below, were simulated. These scenarios have an analytical solution, and this solution was adopted as a reference to evaluate the error of the Fin2D model. The following, are different studied scenarios:

- Air side verification (V1): For the refrigerant, the infinite heat capacity rate ($\dot{m} \cdot Cp$) was imposed, which means no temperature change for the refrigerant. Also, we disabled the 2D LHC in the tube walls (LHC_X and LHC_Z) and the LHC_Z in the fin, since these effects are not accounted for by the available analytical solutions.
  The detailed discretization of the air volume, in the Fin2D model, accounts for a non-uniform air temperature along the *Y* direction. Since this effect is not taken into account by any analytical solution, the fin and air were only discretized in the *X* and *Z* directions, using only one cell along the *Y* direction, to make a valid comparison of the Fin2D model with analytical solution. On the other hand, it is not possible to capture the fin temperature variation with only one fin cell along the *Y* direction. Thus, the value of the thermal conductivity for the fin in this direction was set as infinite. In this situation the fin efficiency was equal to 1, and the fin wall temperature was uniform along the *Y* direction. Finally, constant properties and heat transfer coefficients were used, which correspond to those exposed in section 3. For this scenario the analytical solution for the heat exchanger effectiveness is $\varepsilon = 1 - \exp(-NTU)$.
- Refrigerant side verification (V2): The methodology applied was the same as for V1, but the fluid with infinite heat capacity rate was the air. Now, the results were not as sensitive to the air discretization as it was in the V1 case because the air has infinite heat capacity rate and its temperature change is negligible.
- Fin temperature profile verification (V3): The fin conductivity in the *Y* direction had a value corresponding to the case study. Two cases were studied: with the same and different fin root temperatures. The analytical

solutions for both cases were taken from Incropera and DeWitt (1996). These relationships assume a uniform air temperature along the *Y* direction, and uniform air properties and heat transfer coefficient. Thus, to avoid the air temperature change along the *Y* direction, the infinite air flow-stream heat capacity rate ($\dot{m} \cdot Cp$) was imposed. The refrigerant flow-stream capacity rate was also assumed to be infinite to obtain a uniform tube wall temperature along all fin roots.

The fin was discretized only in one cell along the *Z* direction so there was no LHC_Z in the fin.

- Two-dimensional heat conduction in the wall (V4): This case validates the discretization of the Laplacian term of Eq. (2.3). This case studies 2D LHC in the tube assuming no convection and no thermal joint between the fin and the tube. A set of temperatures for each wall's edge was imposed. The analytical solution for this situation can be obtained solving the Laplacian equation for a flat plate given temperatures at the edges.

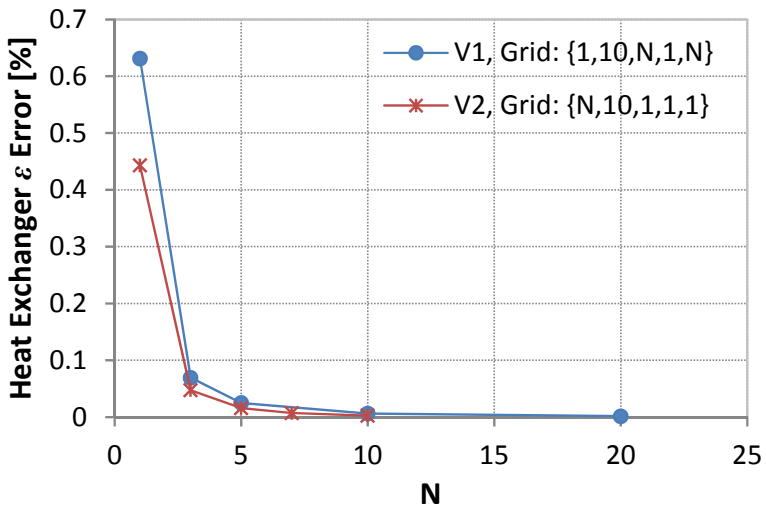

Fig. 2.4 - Validation results for two scenarios: air side when the number of cells in the *Z* direction is varied (V1), and refrigerant side when the number of segments in the *X* direction is changed (V2).

Fig. 2.4 shows the error of the numerical solution with reference to the analytical solution for V1 and V2 cases. The error tends to diminish very quickly with the number of cells used (*N*). In the case of V1, the abscissa shows the number of cells in the *Z* direction. As it can be observed, the error is very small already for *N*=5. In the case of V2, where the air has the infinite flow-stream capacity rate, the abscissa was taken as the number of cells along the *X* direction. Again the analytical solution is almost reached with only five cells.

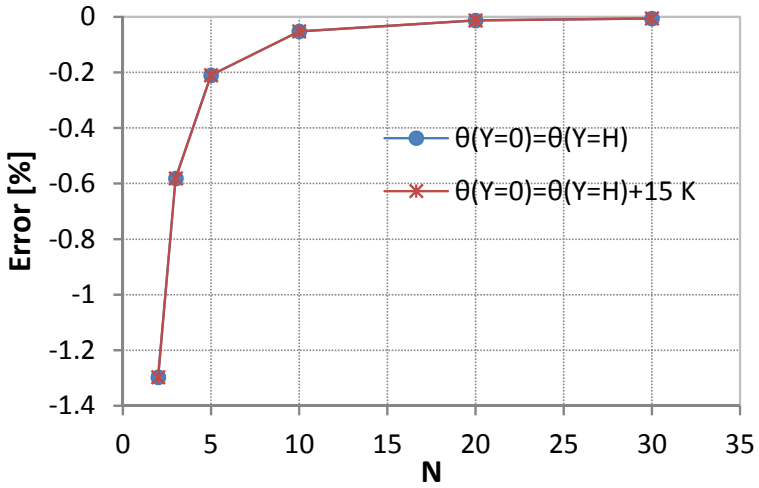

Fig. 2.5 - Fin temperature profile validation (V3): Error of the heat transferred from the fin to the air, for two cases: tubes with the same temperature and with a temperature difference of 15 K, with the grid: {1,1,1, *N*,1}.

Regarding the case V3 verification, Fig. 2.5 shows the error of the numerical solution for the heat transferred from the air film to the fin wall as a function of the number of cells in the *Y* direction for two situations: equal temperatures of the bottom tube and the top tube, and a temperature difference between tubes of 15 K. θ is a difference between the fin temperature and the air temperature. As can be observed, the error is small, -0.2%, with only five cells in the *Y* direction, and quickly approaches zero. The calculated fin temperature profile is shown in Fig. 2.6(a) and (b) for the V3 study in the same two previous cases. The grids differ by the number of fin cells in the *Y* direction. In this manner the accuracy of the numerical model is proved.

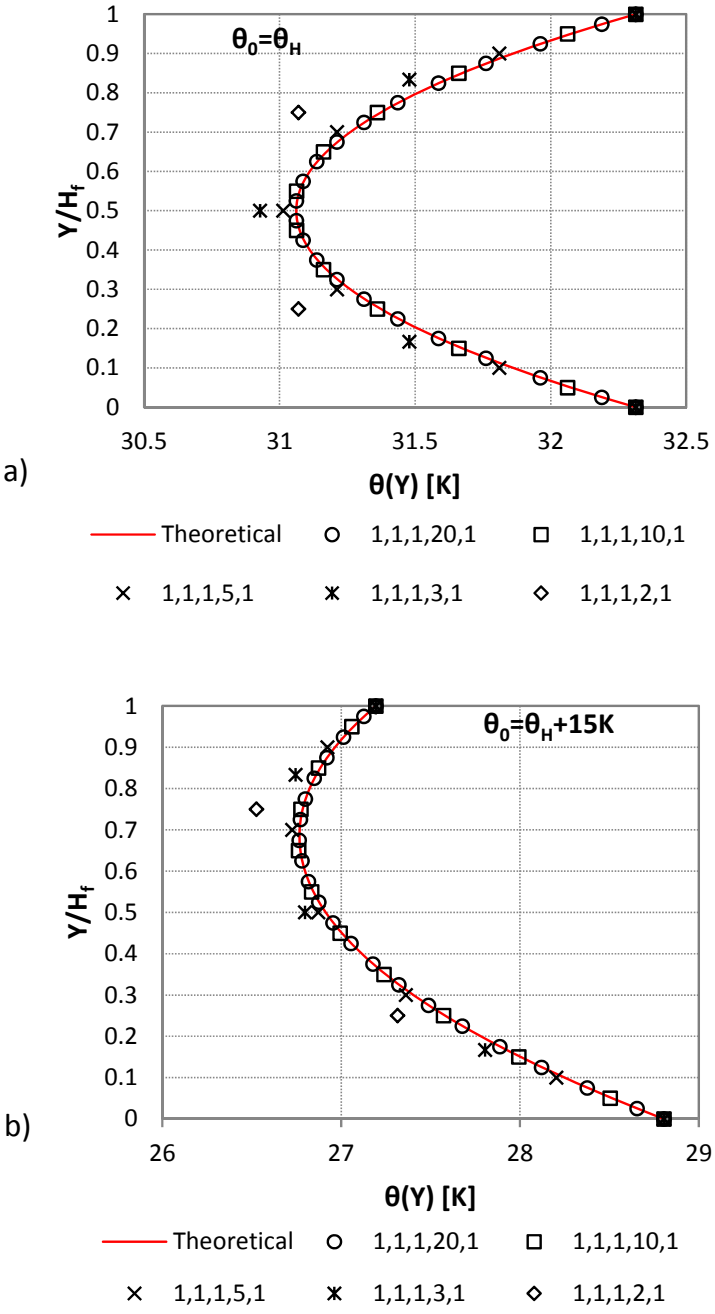

Fig. 2.6 - Fin temperature profile validation (V3): (a) the case with the same inlet tube temperatures and (b) the case with a temperature difference between tubes of 15 K (five grids considered).

Finally, in order to validate the 2D LHC in the Fin2D model, Fig. 2.7(a) presents results for case V4, where the boundary conditions were: $T(X/L=0)$ = 70° C, $T(X/L=1)$ = 50° C, $T(Z/W=0)$ = 25° C, $T(X=0)$ = 35° C. Fig. 2.7 (b) shows the error in the wall temperature field evaluated as a deviation of the Fin2D results from the theoretical solution. It is noticeable that the error ranges from -0.1 K and +0.1 K over almost the entire plate, which is considered as acceptable. The error increases up to 1.3 K only locally near the

corners. The reason is that the actual temperature field imposed along the tube edge is discontinuous just at the corners. The Fin2D model can obtain only continuous solutions, so near the corner the error is increased. This study was also carried out for the fin, resulting in similar results.

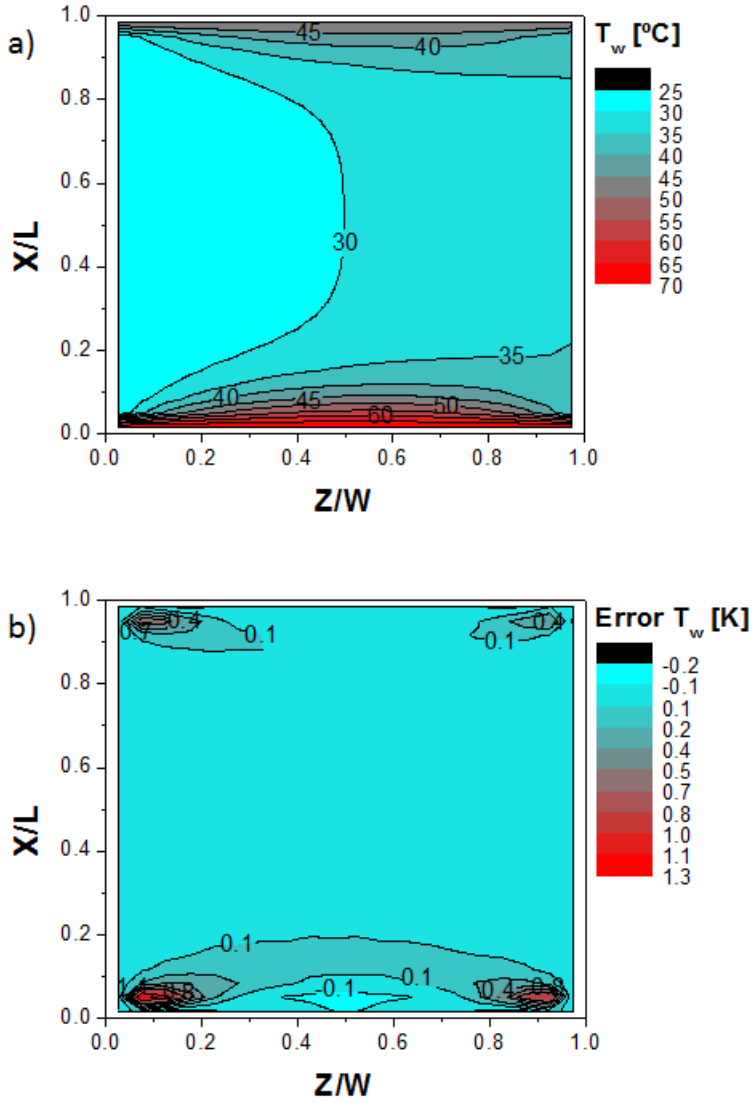

Fig. 2.7 - Two-dimensional conduction (V4): (a) Tube temperature profile predicted with the Fin2D model. (b) Error, evaluated as temperature difference, of the Fin2D model with respect the analytical solution.

2.4 Fin2D Solution for the Case Study

In this section the Fin2D model is used to solve the case study problem. Many thermal variables are analyzed in order to understand the actual heat transfer mechanisms in the case study using a very detailed model able to capture fin and tube two-

dimensional temperature profiles, the refrigerant temperature profile in each channel, and the air temperature profile along the direction between tubes.

This study used test conditions presented in Table 2.2. The air-side heat transfer coefficient was estimated by correlations for a plain fin following the recommendations of Webb (1994). The heat transfer coefficient obtained with this correlation is referred to as α_{air}. Two scenarios were considered: with the air-side heat transfer coefficient equal to α_{air}, and with a value three times larger, consequently the air-side heat transfer coefficient ranged from 60 W m^{-2} K^{-1} to 180 W m^{-2} K^{-1}. This choice was made to cover large variations of possible fin surfaces including enhanced fin surfaces with a high heat transfer coefficient.

Regarding the refrigerant side, constant properties and heat transfer coefficients were used, as listed in Section 2.2. Since the tube length was short, the refrigerant property variations are expected to be negligible; the refrigerant is a gas far from the critical point at which properties change drastically.

In order to set a grid size to obtain the solution in each scenario, with the required accuracy for the comparisons done in this work, the author studied the results accuracy when the grid dimensions were changed. From a very detailed grid, the different grid dimensions were reduced until a further refinement of the grid did not lead to a significant increase in accuracy. The adopted grid dimensions were: {3,10,10,30,10}, following the nomenclature explained in section 2.1.1. The capacities obtained for this case study were 24.21 W and 33.6 W for the scenarios with $\alpha_{air} = \alpha_{air}$ and $\alpha_{air} = 3\ \alpha_{air}$, respectively.

First, results for the refrigerant are shown in Fig. 2.8(a) and (b). Fig. 2.8(a) presents the refrigerant temperature evolution along the *X* direction. Fig. 2.8 (b) presents the temperature profile as a function of the dimensionless tube depth (*Z* direction) at *X*=0.833. In this figure, a case with one equivalent channel (same hydraulic diameter and cross-sectional area) is also plotted in order to study the differences between modeling the actual number of channels and modeling all the fluid as an equivalent fluid cell with the assumption of mixed refrigerant along the tube.

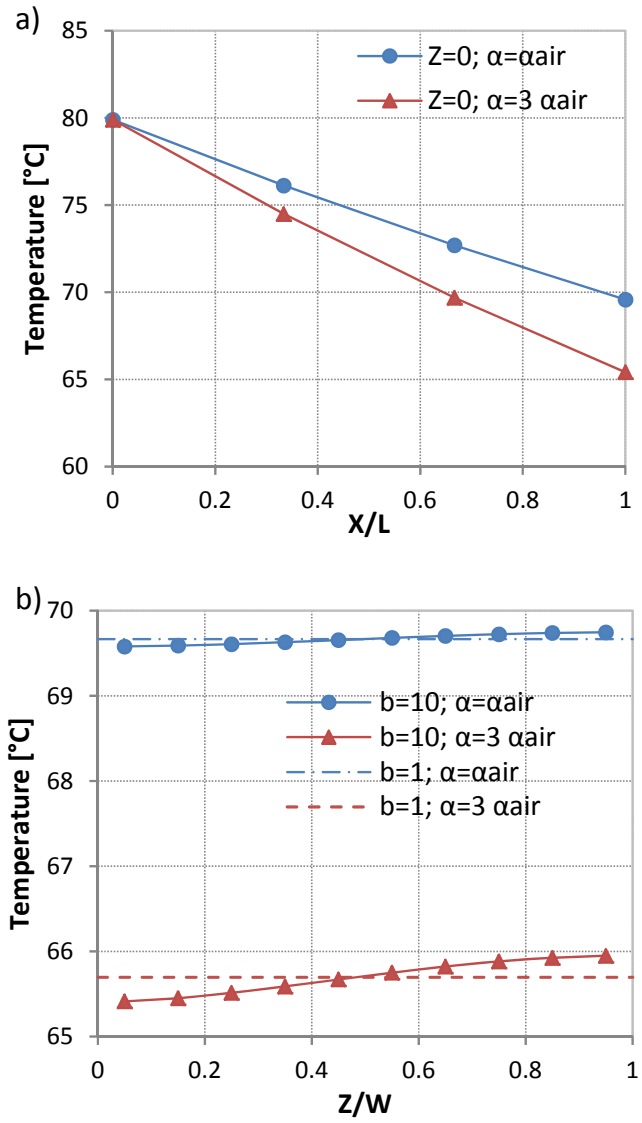

Fig. 2.8 - (a) Refrigerant temperature evolution along the tube length for two values of the air-side heat transfer coefficient. (b) Refrigerant temperature profile along the *Z* direction for two values of the air-side heat transfer coefficient. Each scenario was studied using the actual number of channels (*b*=10) and one equivalent channel (*b*=1).

In Fig. 2.8 (b) the temperature profile for 10 channels describes a typical trend when 2D LHC in the tube is present. It is noticeable how small the temperature variation between different refrigerant channels is in both scenarios (at most 0.5 K). The difference in the total capacity calculated resulted to be less than 0.005 % for both scenarios. This is due to two reasons: the uniform refrigerant temperature for the one channel case almost coincides with the averaged value of the refrigerant temperature in the multichannel case, and the uniformity of the tube temperature along the *Z* direction. The combination of these two facts produces an equal averaged difference of temperatures between the tube and the refrigerant, which produces the same

capacity transferred by the fluid. Thus, for the scenario studied, the modeling of a minichannel tube as one equivalent channel introduces a negligible error.

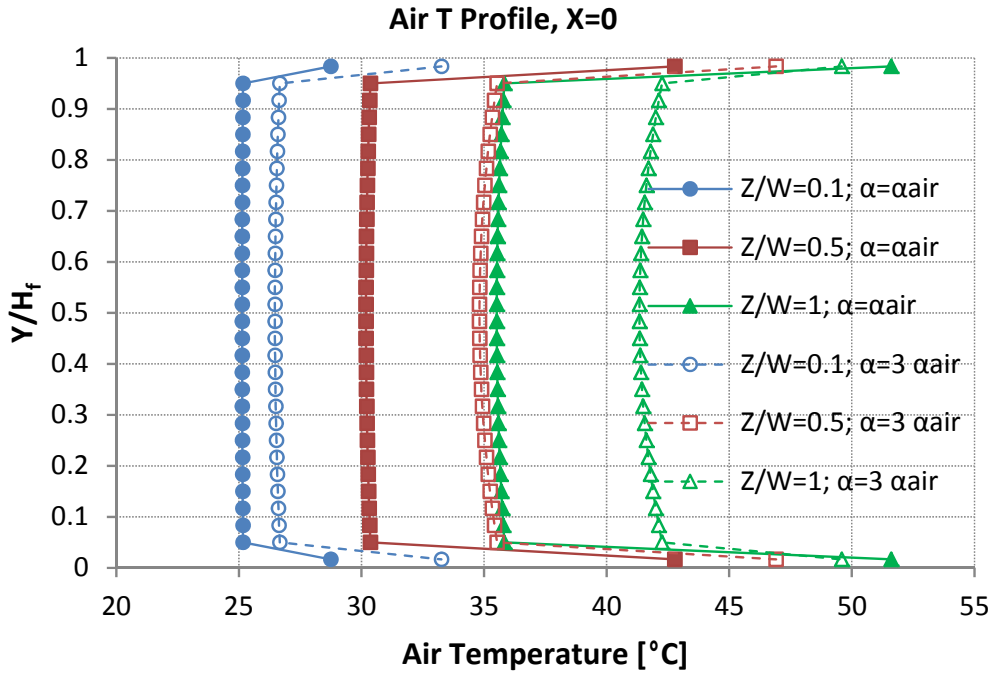

Fig. 2.9 - Air temperature profiles along the *Y* direction at the refrigerant inlet (*X*=0) for three locations along the *Z* direction.

To analyze the thermal evolution of the air, Fig. 2.9 presents air temperature profiles along the *Y* direction at the refrigerant inlet (*X*=0) at three different locations along the *Z* direction. The detailed air discretization makes it possible to study the variation of the air temperature not only along its flow rate direction but also in the direction between tubes. In Fig. 2.9, we can observe that the temperature of most of the air is uniform, except the air close to the tube wall. Only for a high value of the air-side heat transfer coefficient (about 180 W m^{-2} K^{-1}) the air undergoes a small temperature variation along the *Y* direction. This observation agrees quite well with the assumption used in the fin theory development. But, the temperature of air close to the tube wall is higher by up to 15 K with respect to the rest of the air, and this fact is not taken into account in the fin theory development.

Finally, similarly to the aim of Fig. 2.9 to study the air flow evolution, Fig. 2.10 (a) and (b) were plotted to study the fin temperature field at the refrigerant inlet section (*X*=0). When $\alpha=\alpha_{air}$ the temperature field is quite similar to that for a one-dimensional field since the temperature gradient is almost negligible along the *Z* direction. However, when the air-side heat transfer coefficient increases, due to the fact that the air temperature variation along the *Z* direction significantly increases, a strong

temperature gradient in the *Z* direction appears along the fin, leading to a considerable effect of the LHC_Z. This fact points out the big impact of the air-side heat transfer coefficient on these profiles.

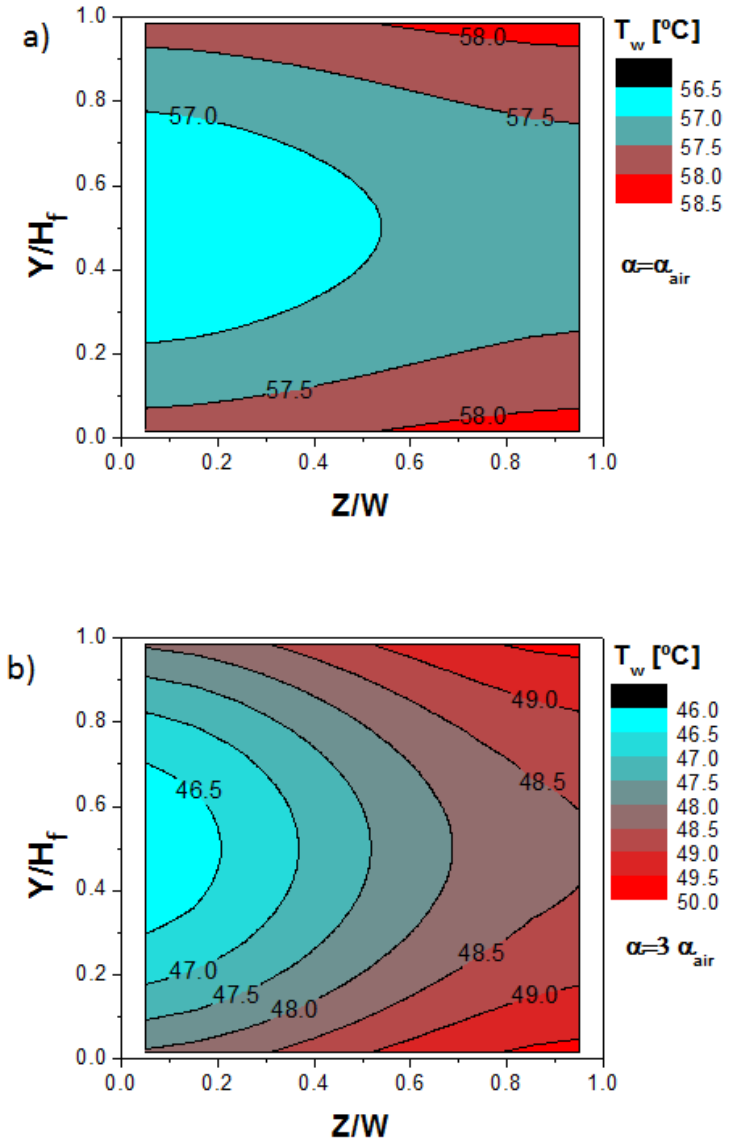

Fig. 2.10 - Fin wall temperature profile at the refrigerant inlet section (*X*=0) for the case study with: (a) $\alpha = \alpha_{air}$ (b) $\alpha = 3\ \alpha_{air}$.

Fig. 2.11 (a) and (b) present the temperature fields for the tube wall. Again, the results depend strongly on the air-side heat transfer coefficient. When the air-side heat transfer is low, basically only the LHC_X in the tube is present, but when this coefficient increases the effects of LHC_Z in the tube also become visible since there is a temperature gradient on the wall tube along the Z direction.

The impact of 2D LHC in the tube and LHC_Z in the fin on the solution are discussed in the following section.

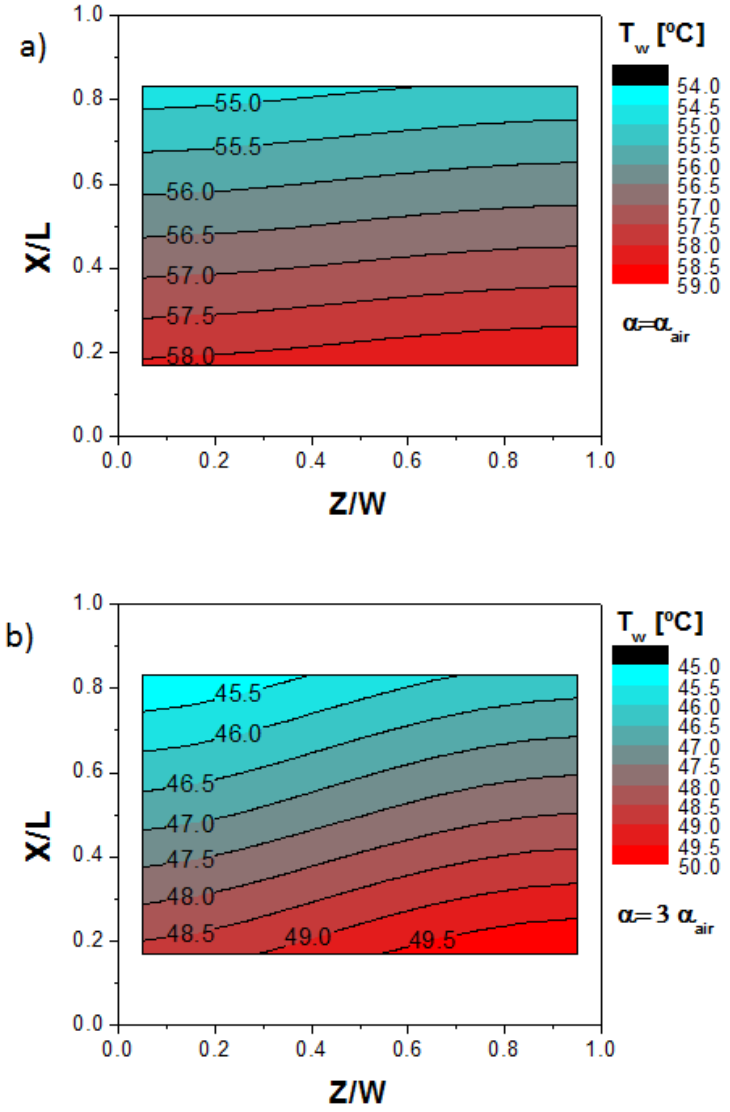

Fig. 2.11 - Tube wall temperature profile for the case study with: (a) $\alpha = \alpha_{air}$ (b) $\alpha = 3\ \alpha_{air}$.

2.5 Analysis of the Segment-by-Segment ε-NTU Modeling and Effect of Classical Assumptions

Once the Fin2D model has been validated it can be used as a reference to check the relative error made by the segment-by-segment ε-NTU modeling of a gas cooler and for studying the impact of the classical assumptions, which are implicit in this methodology. In order to evaluate the relative error, the reference used in this evaluation was the solution for the case study at the same operating conditions and applying the same grid size.

The classical ε-NTU modeling approach divides each heat exchanger tube into segments along the refrigerant flow with its corresponding fins. Some authors use only

one segment per tube, which is commonly referred to as the tube-by-tube approach. When the tube is discretized in more than one segment (*Ns*) the approach is defined as the segment-by-segment approach. Once the heat exchanger is divided into segments, the *ε*-NTU relationships for heat exchangers (Incropera and DeWitt, 1996) are employed for each segment. For multichannel cross-flow heat exchangers the air is always considered to be unmixed because the fins prevent the mixing, but there are two options for the refrigerant: to assume the refrigerant as mixed (RMAU) or as unmixed (BU). In a multichannel tube, the refrigerant is actually unmixed, but some authors assume the refrigerant flow as mixed, applying the RMAU relationship in a segment-by-segment approach, e.g. Jiang (2003). However some other authors, e.g. Fronk and Garimella (2011), apply the BU relationship using also a segment-by-segment approach. Thus, there is no full agreement in the literature regarding using the RMAU and BU options.

The *ε*-NTU models used in this analysis were developed within Engineering Equation Solver (Klein, 1995). Both options available within the *ε*-NTU modeling methodology were included in this study: BU and RMAU. The *ε*-NTU models used the same properties and heat transfer correlations as those used in the Fin2D model.

The classical ε-NTU modeling presents the following drawbacks:

- 2D LHC: As it was explained in the introduction, the *ε*-NTU method does not account for 2D LHC in the tube (LHC_X and LHC_Z) and LHC_Z in the fin.
- Adiabatic-fin-tip efficiency: This assumption is widely used even when a temperature difference between tubes exists.
- Discretization inconsistency of the BU option: discretizing along the *X* direction, i.e. introducing number of segments (*Ns*), involves an implicit mixing of the refrigerant stream since the inlet temperature at one segment is evaluated as the averaged value at the outlet section of the preceding segment. Consequently, for the BU *ε*-NTU case, increasing the number of segments is inconsistent with the hypothesis of unmixed refrigerant stream. Therefore, if the unmixed condition for the refrigerant is the one which better represents the actual process, the best option for the discretization along the *X* direction would be to employ a tube-by-tube approach. This will lead to a full consistent BU solution at each tube with mixing at the outlet. This mixing would be perfectly consistent with the real operation in those microchannel heat exchangers where the tubes end in the collector/distributor head. For serpentine heat exchangers, the BU solution is not consistent because the refrigerant is mixed.

- Air temperature variation along the *Y* and *Z* directions: the *ε*-NTU approach assumes that the air temperature is constant along the *Y* direction since the *ε*-NTU approach uses the fin theory, which is developed under this assumption. This assumption deviates from the reality because the temperature of the air flowing close to the tube and the fin roots becomes much closer to the wall temperature, as it was shown earlier. Additionally, fin theory assumes uniform air temperature along *Z* direction. The impact of temperature variation along the *Z* direction on the fin efficiency evaluation can be reduced by discretizing the fin along this direction. Given this discretization along *Z*, the assumption of uniform air temperature would be only applied to the air along the *Y* direction.

It is important to notice that most of the models for heat exchangers are based on the classical assumptions analyzed above. Therefore, although they do not employ *ε*-NTU approach, they suffer of some of the drawbacks commented above, except the BU discretization inconsistency, that is exclusive for *ε*-NTU models.

2.5.1 Comparison of Fin2D model against *ε*-NTU approaches

The scenarios used to analyze differences between simulation predictions by the Fin2D model and the classical *ε*-NTU approaches are the same as those used for the case study solution. In gas coolers such as serpentine or multitube heat exchangers with large number of refrigerant passes, large temperature differences can appear between the refrigerant in neighboring tubes. In order to study the heat transfer in these gas coolers, a new scenario has been added to the simulation studies. This scenario modifies the cases presented previously by introducing a temperature difference between refrigerant inlets of 40 K, as shown in Fig. 2.3 (b).

Fig. 2.12 (a) and (b) quantify the relative errors obtained when using the classical *ε*-NTU approaches. In these figures *Ns* represents the number of segments used to discretize the tube length. For the RMAU case, the trend of the *ε*-NTU model is asymptotic to the Fin2D solution with a final error of 2.5 % for the α_{air} case, which increases to 3.5 % for the air-side heat transfer coefficient value increased threefold (to about 180 W m^{-2} K^{-1}). The simulations carried out for the scenario with different refrigerant inlet temperatures resulted in identical results, which means that the error does not depend on a temperature difference between the tubes.

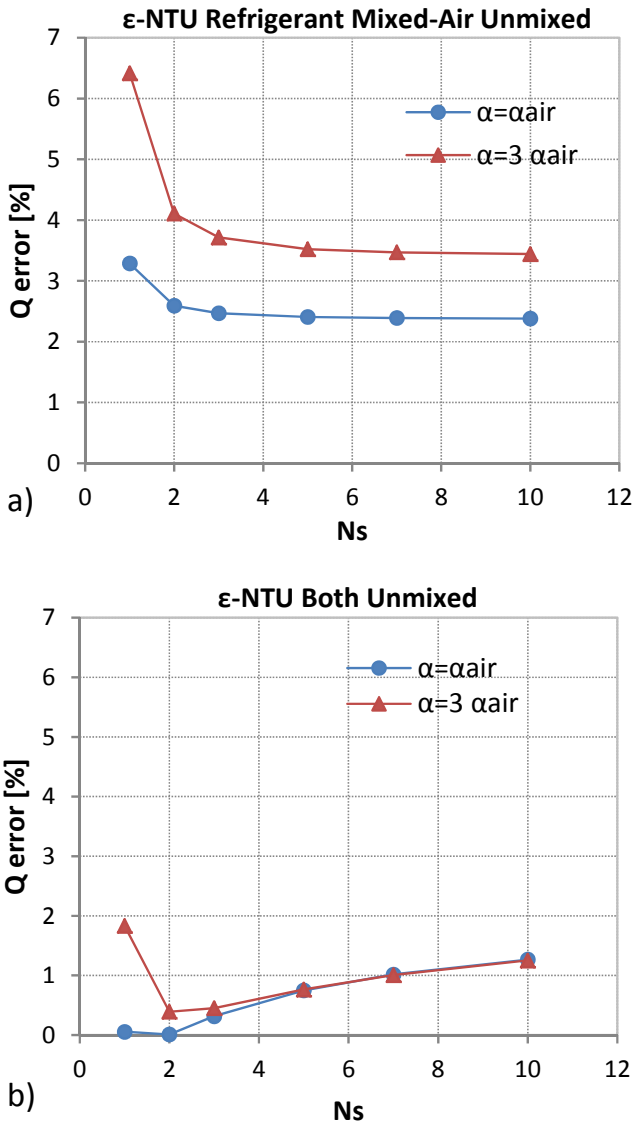

Fig. 2.12 - Comparison of Fin2D model and *ε*-NTU model for different number of refrigerant segments (*Ns*) in the *X* direction used by the *ε*-NTU model: (a) using RMAU relationships, (b) using BU relationships.

For the BU case, the errors are smaller, below 1.5 %, indicating that this approach is much closer to the Fin2D solution. However, as it can be observed in Fig. 2.12 (b), the error increases with the increasing number of cells. This problem is a result of the modelling inconsistency that was pointed out and explained above. Following that explanation, it would be consistent with the assumption of unmixed refrigerant made for the BU case to use only one cell per tube; however, Fig. 2.12 (b) shows the most accurate solution when *Ns*=2. The reason for this result and trend is not clear since many effects occur simultaneously. The main reason could be that one segment (*Ns*=1) produces a linear temperature distribution for the fluids and a poor discretization of the problem, thus when the number of segments is increased, the accuracy is improved despite the modeling inconsistency. But with values *Ns* larger than two

segments, the modeling inconsistency takes an overriding influence on the accuracy, and the error begins to increase.

After observing these results it could be thought that the effect of the temperature difference of the refrigerant between neighboring channels is important. However, Fig. 2.8 (b) and the comments made regarding Fig. 2.8(b) in the previous sections do not support this idea.

2.5.2 Analysis of classical assumptions with Fin2D model

This section analyzes the impact of individual classical assumptions used in a heat exchanger model on the simulation results. The impact was evaluated with respect to the complete Fin2D model prediction by imposing selected assumptions within the Fin2D model, and performing additional simulations. The considered assumptions are: no 2D LHC in the tube, no LHC_Z in the fin, adiabatic-fin-tip, and uniform air temperature along the fin height (*Y* direction). The case study CO_2 gas cooler was used in these simulations.

2.5.2.1 LHC effects

To evaluate the impact of the LHC effects and to identify the most dominant areas with heat flow and its direction, four cases of simulations were performed with the following modeling constraints: (1) no LHC_Z in the fin, (2) no LHC_X in the tubes, (3) no LHC_Z in the tubes, and (4) all LHC effects disabled for all wall elements, except conduction along the *Y* direction in the fin. Table 2.3 shows the error in the capacity predictions associated with eliminating from consideration selected LHC phenomena with respect to the complete solution (case study solution which includes LHC in all elements and directions enabled) and same refrigerant inlet temperature.

Table 2.3 - Effect of 2D LHC on capacity

	Q error case 1 [%]	Q error case 2 [%]	Q error case 3 [%]	Q error case 4 [%]
$\alpha = \alpha_{air}$	0.03	0.12	0.09	0.66
$\alpha = 3\,\alpha_{air}$	0.24	0.10	0.55	2.54

The effect of LHC depends strongly on the air-side heat transfer coefficient. When the air-side heat transfer coefficient is equal to the reference value, α_{air}, the influence of LHC is negligible. But when the air-side heat transfer coefficient has a three times as high value (about 180 W m^{-2} K^{-1}), the effect is noticeable, 2.54 %. This impact increase,

when the air-side heat transfer is increased, can be explained by observing Fig. 2.10(b) and 12(b). In these figures the temperature gradient along the *Z* direction in the fin and along the *X* and *Z* directions in the tube rises when the air-side heat transfer coefficient increases, whereas the temperature gradient along the *Z* direction in the tube and fin is almost negligible for the lowest air-side heat transfer coefficient value.

This increase in the prediction error due to neglecting the LHC effects when the air-side heat transfer coefficient is increased is consistent with the increase in the prediction error shown in Fig. 2.12(a) for the ε-NTU models. When the LHC has the largest influence, the dominant component is the LHCZ in the tube. It is important to notice that the LHC effects are strongly non-linear.

The case with a temperature difference between tubes was also studied in the same way as described above. The results and conclusions are the same. This fact indicates that the LHC effects in an element do not depend on the conditions of its neighboring elements. These conclusions are not valid for the heat conduction in the fin between tubes, which is studied below.

2.5.2.2 Adiabatic fin tip

To study the effect of assuming the adiabatic tip at the half length of the fin, as it is usually accepted, the case with the 40 K temperature difference between refrigerant inlets was chosen, since the adiabatic-fin-tip assumption is exact for the case with the same refrigerant inlet temperature. To quantify this error and isolate only the effect of the adiabatic-fin-tip assumption, this scenario was modeled by introducing a cut along the fin surface and leaving all remaining LHC effects enabled. The cut was modeled as a cut along the air direction in the middle section of the fin surface between tubes (Fig. 2.3(b)). Under these conditions the adiabatic-fin-tip assumption is strictly correct, even though there is a temperature difference between neighbouring tubes. Thus, the difference between results for a scenario solved with and without modelling a cut along the fin corresponds to assuming an adiabatic-fin-tip when a temperature difference between tubes exists.

Table 2.4 contains a summary of the obtained results. Tubes 1 and 2 referred to in this table are depicted in Fig. 2.3(b). The difference between the capacity with the fin cut and without it is negligible, which means that the improvement in the capacity is almost zero. Nevertheless, Table 2.4 shows large errors, more than 300%, in the heat capacity per tube calculated assuming adiabatic-fin-tip efficiency with respect to using the actual fin efficiency. This fact means that refrigerant temperature at the outlet of one tube would be wrongly predicted in case of using adiabatic-fin-tip efficiency;

nevertheless the impact on total capacity would result negligible for the analyzed scenario. These deviations produce a different heat flux distribution in the gas cooler. In fact, these results agree with the findings of Asinari et al. (2004). They also concluded that the heat flux distribution per tube results different depending on the fin efficiency used, but the total heat transferred by the fin between two tubes (sum of the heat flux for both fin roots) is exactly the same assuming either the adiabatic-fin-tip or the actual one. This conclusion is independent of the temperature difference between neighboring tubes. They studied a three passes gas cooler, and concluded that the impact of adiabatic-fin-tip assumption involves a modest effect on the total capacity prediction, about 1%. However, Park and Hrnjak (2007) reported improvements in capacity up to 3.9 % by cutting fins for a microchannel serpentine gas cooler. A possible explanation of this contradiction is that the effect, of the heat flux distribution in the gas cooler on the total heat capacity, depends of the number of passes. It results in a noticeable total capacity difference when the number of passes is large, as is the case of the serpentine gas cooler studied by Park and Hrnjak (2007). Currently, Fin2D does not have the capability to simulate complex circuitry arrangement to validate the above hypothesis, but the work to enhance Fin2D in this direction is underway.

Table 2.4 - Effect of assuming adiabatic-fin-tip efficiency on capacity

	Q without fin cut [W]	Q with fin cut [W]	Q without fin cut tube 1 [W]	Q error tube 1 [%]	Q without fin cut tube 2 [W]	Q error tube 2 [%]
$\alpha = \alpha_{air}$	15.35	15.37	-1.87	-274.87	17.22	-29.73
$\alpha = 3\,\alpha_{air}$	21.32	21.35	1.1	313.64	20.23	-16.96

The wall temperature profiles for each solution (when $\alpha = \alpha_{air}$) are plotted in Fig. 2.13. The profiles are shown along the *Y* direction at the refrigerant inlet section (*X*=0) in the middle of the tube depth. The error in the capacity of the fin roots, explained above, can be interpreted from Fig. 2.13. It can be observed how different the actual temperature profile is from the temperature profile when the adiabatic-fin-tip is assumed. The slope of these curves in the *Y* direction gives the local heat flux along the fin and from the fin to the tubes. Consequently, if the slope of the curves is analyzed, it is easy to notice the deviation of the adiabatic-fin-tip assumption from the reality; the Fin2D solution presents a significant slope in the middle section of the fin whereas the adiabatic-fin-tip assumption imposes a null slope in the middle section. Fig. 2.13 shows that the solution temperature slope does not change its sign in any section along the fin height, which means that the fin receives heat from tube 2 and transfers heat to the tube 1 (and to the air). The slope for the cut fin changes its sign depending the fin root analyzed, hence the adiabatic-fin-tip assumption results in a wrong heat flux sign

calculation (not only the absolute value) for the fin root of tube 1. The consequence of these differences is a large error in the heat capacity predicted for each tube and, therefore, in the refrigerant outlet properties.

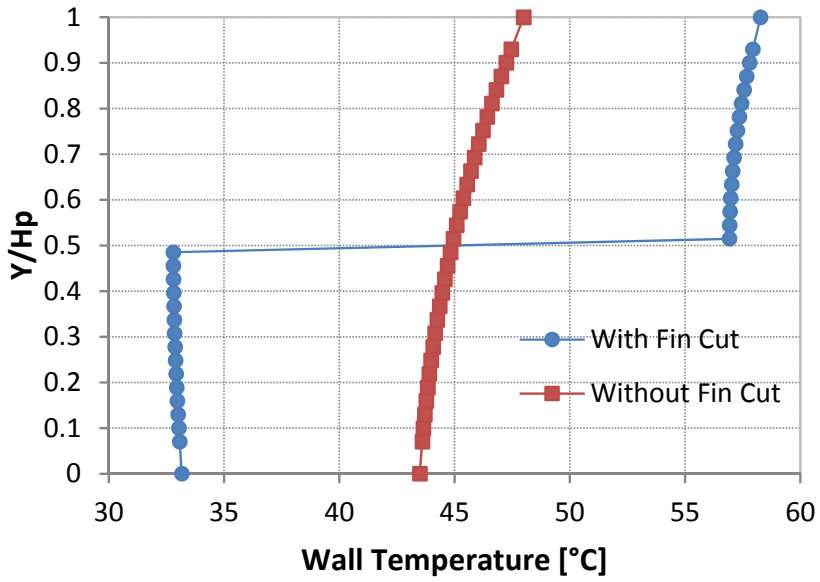

Fig. 2.13 - Wall temperature profile (fin and tubes) along the *Y* direction at the refrigerant inlet section (*X*=0) in the middle of the tube depth (*Z*/*W*=0.5) for both scenarios solved with Fin2D model: fin cut and without cut, $\alpha = \alpha_{air}$.

2.5.2.3 Uniform air temperature along fin height

To study the assumption of constant air temperature along the *Y* direction, Fig. 2.14 presents the corresponding air temperature profile in the same locations as those studied in Fig. 2.9, but now the studied scenario includes a 40 K temperature difference between refrigerant inlets.

The results shown in Fig. 2.14 are similar to those shown for Fig. 2.9 except two differences: the temperature difference between the air close to the tube and the rest of the air is now within 10 K, and the air temperature profile is less flat, particularly at the air outlet with the highest air-side heat transfer rate, due to the temperature difference between refrigerant inlets. This aspect is not accounted for by the fin theory, since it assumes a uniform air temperature. Although not studied here, an additional impact on the prediction results can be expected in an evaporator simulation due to the large temperature difference between the bulk air and the air close to the tube wall. In an evaporator model in the presence of dehumidification, the heat and mass transfer processes are strongly a function of local properties, which depend on the local temperatures.

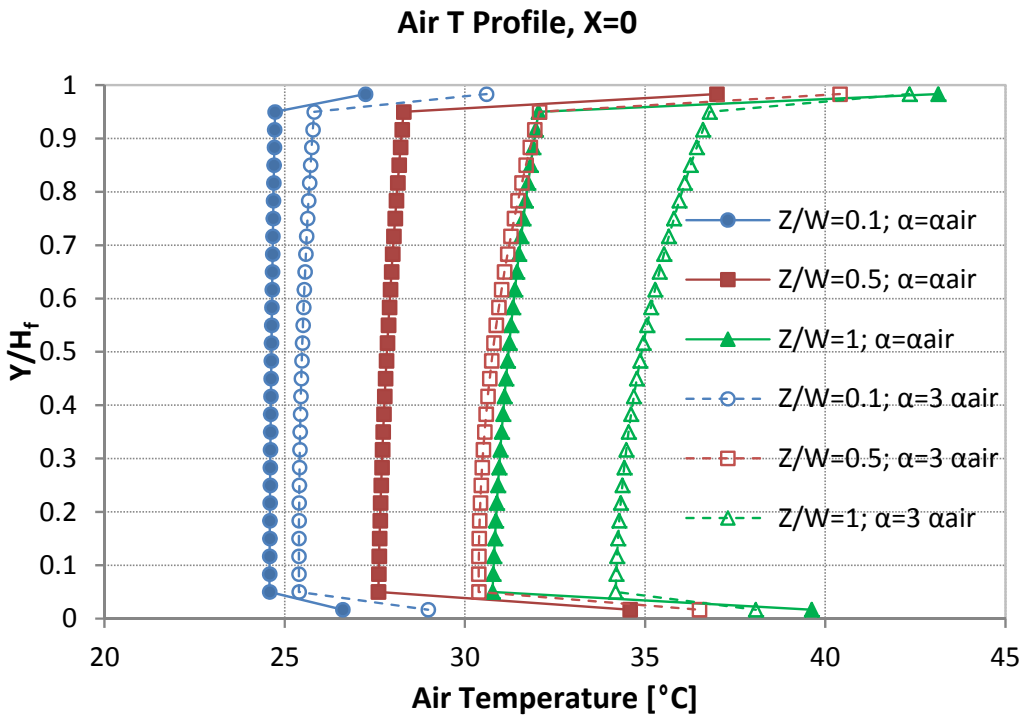

Fig. 2.14 - Air temperature profiles along the *Y* direction at the refrigerant inlet (*X*=0) for three different locations along the *Z* direction when a difference temperature of 40 K exists between refrigerant inlets.

2.6 Conclusions

A model for microchannel heat exchangers, Fin2D, accounting for heat conduction in all directions and in all heat exchanger elements was presented. The model allows for independent discretization for the refrigerant, tube and fins. The air has the same discretization as the fins. After verification against known analytical solutions, the model was employed to quantify prediction errors associated with the classical ε-NTU modelling approach. Also, the classical assumptions were studied to evaluate their impact on the accuracy of simulation results. The following are the main conclusions of the study:

- The error obtained using the ε-NTU method depends on the ε-NTU relationship employed to calculate the effectiveness of each segment. For the studied case it is smaller than 3.5% for RMAU, smaller than 1% for BU and becomes larger as the air-side heat transfer coefficient increases. In general, the best option for the studied case is to use the tube-by-tube approach and to consider both fluids as unmixed although the effect of the mixed refrigerant assumption turned out negligible in the scenarios studied. However, this option can lead to larger errors when long length tubes are

simulated because refrigerant properties and heat transfer coefficients can have significant variations, particularly when the refrigerant undergoes a phase change. It is not consistent to apply a segment-by-segment approach when the RMAU relationship is adopted.

- For the operating conditions studied, the impact of LHC effects along each direction in fins and tube walls, if considered separately, is not significant. The combined effect is more noticeable and may result in a capacity prediction error of as much as 2.5%, with the LHC_Z in the tube being the dominant effect. The impact of LHC depends on the air heat transfer coefficient.
- Using the adiabatic-fin-tip efficiency, which is commonly applied, leads to large errors in heat distribution per tube, and therefore in the prediction of temperature at the tube outlet, when a temperature difference between tubes exists. However impact of this assumption in the total gas cooler capacity is much less. This assumption affects the global capacity prediction of gas coolers with large number of refrigerant passes. Thus, the fin cuts are justified in these heat exchanger topologies.
- The temperature of air close to the tube wall is very different than the bulk air temperature. This fact could have an important impact on local effects controlling the heat and mass transfer, e.g. dehumidification. It would have been interesting to evaluate the isolated effect of the non-uniform temperature profile of the air along the fin height.
- The developed model is able to capture most of the secondary heat transfer effects not taken into account by the classical ε-NTU approach or any model which applies the described classical assumptions; however, simulation of the 2D LHC problem in the wall requires a considerable computation time. The authors will continue working on a simplified model that will retain the most important effects. This will lead to much lower computation times while providing high accuracy of prediction of the complex heat transfer phenomena taking place in air-to-refrigerant microchannel heat exchangers.

CHAPTER 3

FIN1Dx3 MODEL

3 FIN1Dx3 MODEL

Previous chapter proposed a model for a microchannel gas cooler referred to as Fin2D model. The aim of developing Fin2D model was to evaluate the prediction errors of classical modelling assumptions and techniques described above, in an equivalent piece of a microchannel gas cooler, and identify error sources.

Fin2D model was sufficient to identify the deficiency sources of the classical methodologies in such kind of heat exchangers, but was no good to evaluate the global performance prediction errors when an actual MCHX is simulated regarding dimensions, number of tubes and number of refrigerant passes. The main reason which did not allow studying an actual microchannel gas cooler was the computational cost of the Fin2D model. This model has a large computational cost, mainly due to the fin surface discretization: the model needs to employ a large number of fin cells because any fin efficiency is used to solve the heat transfer equation along the fin, which involves heat convection and heat conduction. Furthermore the Fin2D model applies the same discretization for both air and fin, so the air also introduced an important computational effort.

The goal of the present work is to develop a model based on the Fin2D model, without modelling the negligible effects and changing the model structure and/or discretization in order to reduce the computational cost, providing a simulation tool for MCHXs with reasonable computational cost for design purposes. To this end, the authors developed the Fin1Dx3 model, with a novel formulation to take into account heat conduction between tubes without applying adiabatic-fin-tip assumption, thus any correction term was needed. The result is a much faster model with almost the same accuracy as Fin2D model.

Given this computational time reduction, the proposed model is able to simulate either a microchannel gas cooler or a condenser with any refrigerant circuitry. Thus, experimental data from measurements of an actual condenser and a gas cooler was used to validate the model. This model will also allow evaluate the isolated effect of the non-uniform air temperature profile along the fin height; fact that could not be studied with Fin2D model.

3.1 Fin1Dx3 Heat Exchanger Model

The model proposed in this chapter, which will be referred to as Fin1Dx3, is based on the Fin2D model, performing some changes in order to reduce the computational cost but preserving accuracy. The changes are based on the following considerations:

- Chapter 2 revealed that the longitudinal conduction in the fin along the air flow direction resulted in a negligible effect on the predicted performance results. In addition, several current fin surfaces have cuts along this direction (louvered, slit, lanced…) cancelling LHC in that direction. Thus, in the present model this effect is cancelled, what means in practice no thermal connections between neighbouring fin cells along the air flow direction, even though a discretization of both the fin and air exists along this direction.
- Chapter 2 revealed that the air temperature profile is quite flat along the direction between tubes, excepting the air close to the tube wall. In those studies the height of the fin occupied by the air close to the tube with a temperature different from the rest of air was about 1/30 of the fin height. The discretization of air along that direction increases the computational cost. On the other hand it would be quite interesting to capture the effect of accounting for the temperature difference between the air close to the tube wall and the rest of the air. A possible solution for this conflict of interests is to discretize the air with three air cells along the *Y* direction, as shown in Fig. 3.1. For this discretization, the height of the air cells close to the tube wall is unknown: this dimension (φH_f) should be that one which provides the best results, so this dimension is a parameter to adjust either experimentally or numerically, even by observation. The only restriction is that both fin cells (cells close to the tubes), for the same *Z*, will measure the same. What actually these three air cells represent is the consideration of non-mixed air along the *Y* direction between them. This idea makes sense for air flowing through louvered fins and for laminar flows, i.e.: the air could be assumed as mixed along all the louver height but as non-mixed with the rest of air close to the tube walls, since the fin height is greater than louver height, as it is shown in Fig. 3.1; laminar flow represents a non-uniform temperature distribution along the *Y* direction.
- The Fin2D model solved the heat transferred from the air to the fin without applying the fin theory. Consequently Fin2D model needs a large number of fin cells along the *Y* direction to solve accurately the 2D heat conduction in the fin. This calculation is the procedure which required more computational cost within the Fin2D model.

The fin temperature, for a uniform fin, is governed by Eq. (3.1). Only when the air temperature is constant throughout the fin, Eq. (3.1) can be expressed as Eq. (3.2), (Incropera and DeWitt, 1996). If heat transfer properties are constant, or they are evaluated with mean values, the general solution for the Eq. (3.2) is Eq. (3.3).

$$\frac{d^2T_f}{dY^2} - m^2\left(T_f - T_a\right) = 0 \tag{3.1}$$

$$\frac{d^2\theta_{f,a}}{dY^2} - m^2\,\theta_{f,a} = 0 \tag{3.2}$$

$$m^2 = \frac{\alpha\ pw}{k\ A}$$

$$\theta_{f,a}(Y) = C_1 e^{mY} + C_2 e^{-mY} \tag{3.3}$$

First, fin theory assumes uniform air temperature along *Z* direction. The impact of temperature variation along the *Z* direction on the fin efficiency evaluation is reduced by discretizing the fin along this direction, as the model proposed in this chapter does. Given this discretization along Z, the assumption of uniform air temperature would be only applied to the air along the *Y* direction. Thus, when equations (3.1), (3.2) and (3.3) are used, the main assumption of the fin theory which is not satisfied in an actual fin surface is that the air temperature is not uniform along the *Y* direction. In the model proposed in this chapter, the discretization for the fin and the air is the same and the discretization in the air has been chosen in order to represent air cells with uniform temperature, so it could be possible to apply the fin theory solution (Eq. (3.3)) for each air-fin cell connection without failing the assumption of uniform air temperature. The result of this methodology is a great reduction, in comparison with Fin2D, of the grid size and consequently of the computational cost.

It is should be noted that Eq. (3.3) does not imply the classical adiabatic-fin-tip assumption (in the cross section at half fin height), since boundary conditions have not been applied yet. The evaluation of the constants C_1 and C_2 will be exposed in the subsection 3.1.2.

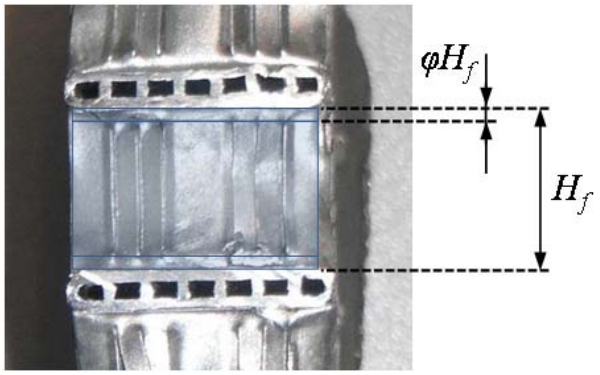

Fig. 3.1 - Detail of a louvered fin surface in a microchannel heat exchanger, where the non-louvered height and the total fin height are depicted.

3.1.1 Heat Exchanger Discretization

Fig. 3.2 presents a sample of a MCHX that can be simulated with the proposed model. The model can simulate any refrigerant circuitry arrangement: any number of refrigerant inlets and outlets; and any connection between different tube outlets/inlets at any location.

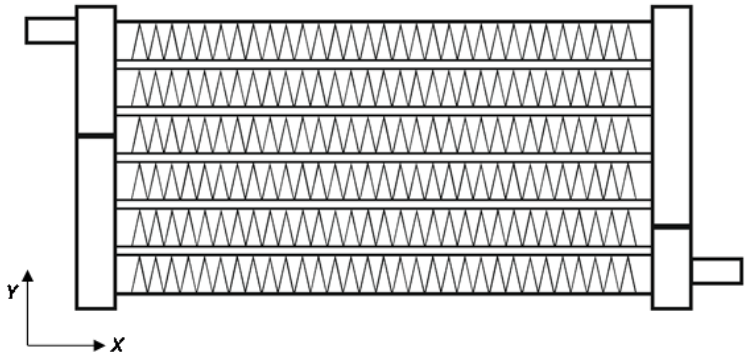

Fig. 3.2 - Example of a microchannel heat exchanger that can be simulated by Fin1Dx3.

Fig. 3.3 shows the discretization in segments of the heat exchanger shown in Fig. 3.2, where the thinner lines correspond to thermal connections between wall cells, whereas the thicker lines correspond to the refrigerant flow path. First, the heat exchanger is discretized along the *X* direction (refrigerant flow) resulting N_s segments per tube. The discretization for each segment is the same and it is shown in Fig. 3.4. Each segment consists of: a refrigerant stream that is split into $N_{r,Z}$ channels in the *Z* direction; a flat tube which is discretized into $N_{t,Z}$ cells in the *Z* direction; and both air flow and fins, which are discretized in two dimensions: $N_{a,Y}$=3 cells in the *Y* direction and *N*a,Z cells in the *Z* direction. Since the discretization for the air and fin wall is the same, $N_{f,Y}=N_{a,Y}$ and $N_{f,Z}=N_{a,Z}$.

The discretization for a heat exchanger is summarized in the following as a grid: {N_s, $N_{r,Z}$, $N_{t,Z}$, $N_{a,Z}$}. For illustration of the nomenclature, the numerical example shown in Fig. 3.3 and Fig. 3.4 corresponds to a grid: {3,4,3,2}.

The refrigerant flows inside the channels along the *X* direction without any mixing between the channels, and it exchanges heat with the tube cells in contact; these tube cells transfer heat to the air cells in contact by convection, to its neighboring tube cells on the plane *X-Z* by conduction, and to the fin roots in contact by conduction. The air exchanges heat by convection with the fin cells, and the air cells at the bottom and top also exchange heat with the tube cells in contact. The fin cells conduct the heat along the *Y* direction, and the bottom and top fin cells also conduct heat to the neighbor tube wall.

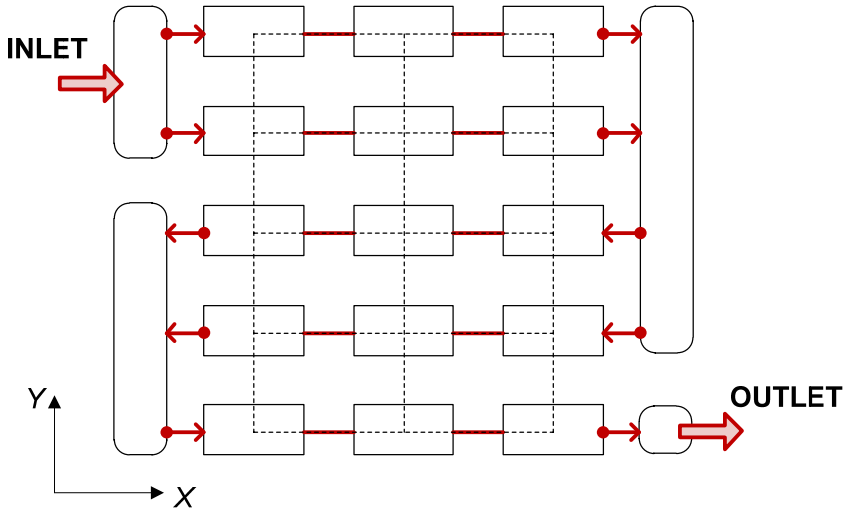

Fig. 3.3 - Discretization in segments of the heat exchanger showed in Fig. 3.2, which includes the thermal connections between different segments and flow arrangement.

Regarding the fluid cells, either air or refrigerant, there are two typologies: elemental cell and mixture cell. The elemental cell corresponds to the one described above, exchanging heat with the surrounding wall cells. The mixture cell is adiabatic and its function is collecting the fluid from a number of tubes and distributing into the next tubes according the heat exchanger circuitry. The inlet and outlet ports of each tube are connected to the corresponding mixture cells. The distribution of these fluid cells and the definition of the tubes connected to these cells determine the flow path of each fluid. In the proposed model, any configuration can be fixed, thus heat exchangers such as serpentine or parallel tubes MCHXs can be simulated with any refrigerant circuitry.

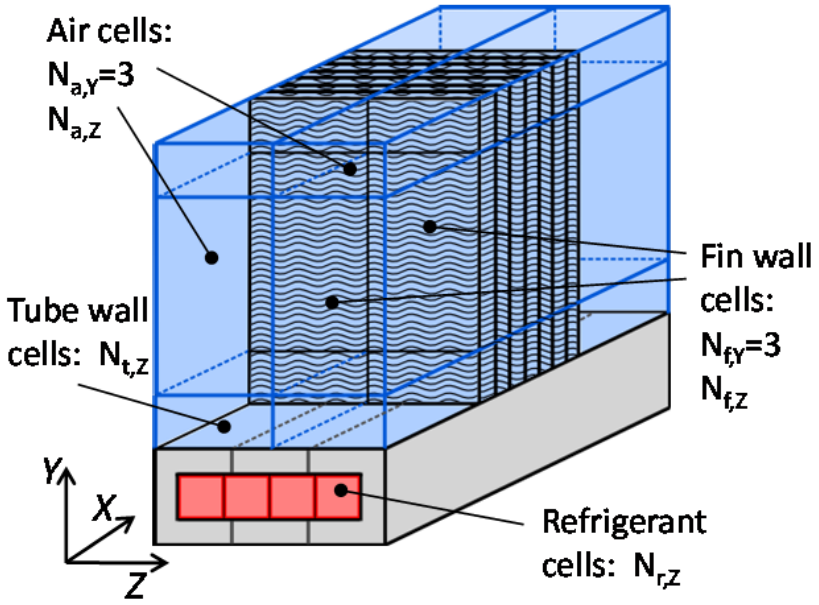

Fig. 3.4 - Schematic of a segment discretization into cells.

The model is designed to allow this methodology also with the air, but in this work, these mixture cells were only used for the refrigerant fluid. In Fig. 3.3, these refrigerant cells are represented with the round shape boxes.

3.1.2 Governing Equations

Every fluid cell (either refrigerant or air) has two nodes, which correspond to the inlet and outlet sections in the fluid flow direction. The tube wall cells have only one node located in the centroid of the cell, as shown in Fig. 3.5(a). All cell local variables are referred to the value in these nodes, e.g. $T_{r,in}$ and $T_{r,out}$ are the temperature at the inlet and outlet, respectively, of a refrigerant cell *r*; for the air flow would be the same but with subscript *a*; T_t is the temperature of the tube cell *t*. The fin does not have any node because a continuous function governs in the fin.

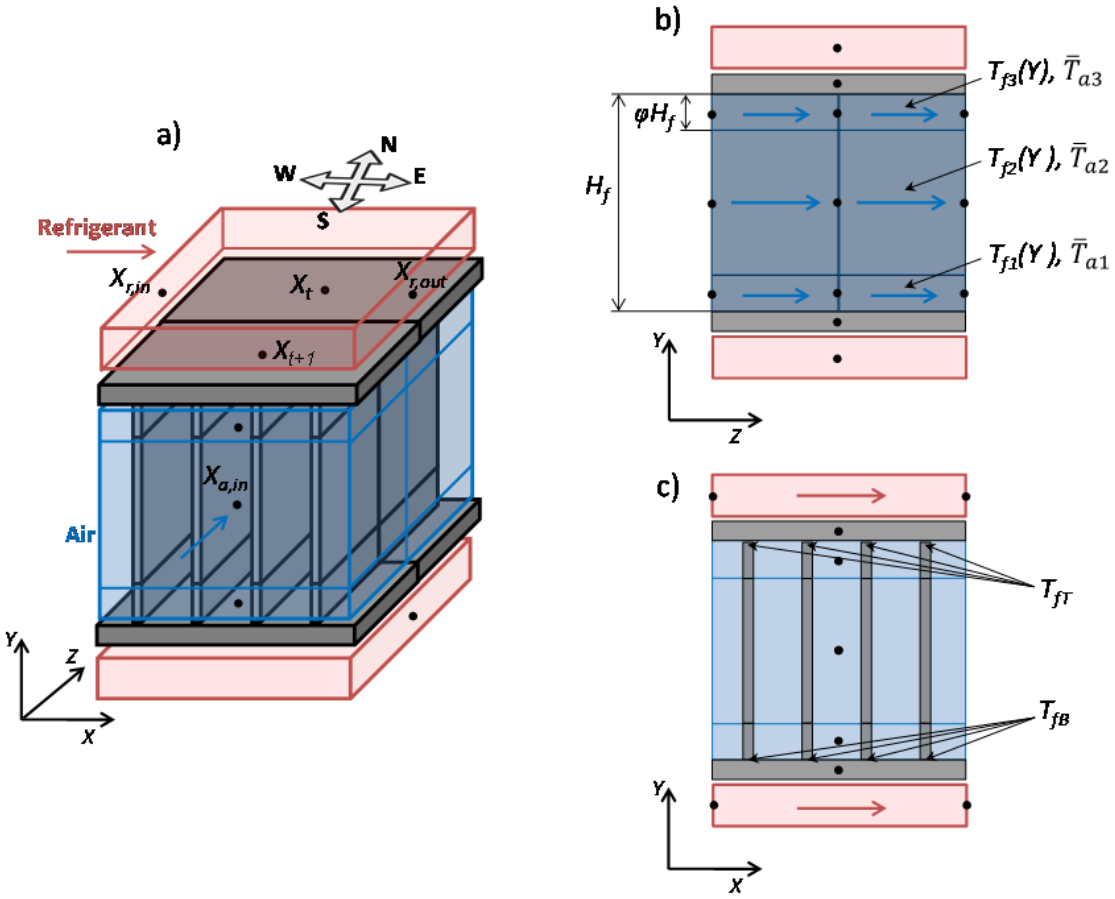

Fig. 3.5 - Different views of a discretized portion of heat exchanger: (a) global view illustrating fluid nodes and tube directions; (b) *Z*-*Y* plane, which shows main geometric data of the fin and regions where is defined the corresponding T_f (*Y*) and $\overline{T}_a$; (c) *X*-*Y* plane, which shows the location of the T_{fT} and T_{fB} temperatures.

According to the assumptions and methodology explained above, the governing equations for the tube wall will be different from those applied to the fin wall. So, the description of the governing equations is going to be structured in four blocks: refrigerant flow, air flow, tube wall and fin wall with their corresponding thermal connections between neighbor fluids or wall cells.

3.1.2.1 Tube wall and its thermal connections

The energy conservation equation for a tube cell can be written as:

$$\nabla\left(k_{t,k}\nabla T_t\right)dV+\sum_{r=1}^{n_r}\dot{q}_{t,r}\,pw_{t,r}\,ds_{t,r}+\sum_{a=1}^{n_a}\dot{q}_{t,a}\,pw_{t,a}\,ds_{t,a}=0 \qquad (3.4)$$

where any tube wall cell *t* is in contact with n_r refrigerant cells *r*=1, n_r and with n_a air cells *a*=1, n_a; $k_{t,k}$ is the thermal conductivity of the tube cell *t* in the *k* direction. The Laplacian term is the term that allows studying the influence of 2D LHC along the tube walls, and it also takes into account the heat transferred by conduction between a tube cell and the adjoined fin cells. The heat fluxes $\dot{q}_{t,r}$ and $\dot{q}_{t,a}$ for a thermal connection between a tube wall cell *t* and a fluid cell *i*, either air or refrigerant, are evaluated as follows,

$$\dot{q}_{t,i} = U_{t,i}\left(T_t - T_i\right) \tag{3.5}$$

where the overall heat transfer coefficient $U_{t,i}$ for this connection corresponds to:

$$U_{t,i} = \frac{1/A_{t,i}}{\dfrac{t_t/2}{A_{t,i}k_{t,k}} + \dfrac{1}{A_{t,i}\alpha_{t,i}}}$$

By using Eq. (3.5), Eq. (3.4) can be rewritten as follows,

$$\nabla\left(k_{t,k}\nabla T_t\right)dV + \sum_{i=1}^{n_i} pw_{t,i}U_{t,i}\ \left(T_t - T_i\right)\ ds_{t,i} = 0 \tag{3.6}$$

where $n_i = n_r + n_a$.

3.1.2.2 Refrigerant flow

Eq. (3.7) states the energy conservation for a refrigerant cell *r* in contact with n_t tube wall cells *t*=1, n_t.

$$\dot{m}_r dh_r = \sum_{t=1}^{n_t} \dot{q}_{t,r}\, pw_{t,r}\, dX \tag{3.7}$$

The fluid pressure drop along length of the refrigerant cell *r*, is obtained by integration of the momentum equation,

$$\Delta P_r = \Delta P_{r,fr} + \Delta P_{r,acc} + \Delta P_{r,g} \tag{3.8}$$

where the friction term is evaluated in the form:

$$\Delta P_{r,fr} = f_r \frac{\Delta X_r}{D_r A c_r^2 \left(\rho_{r,in} + \rho_{r,out}\right)} \dot{m}_r^2 \tag{3.9}$$

The friction factor f_r can be evaluated by several correlations available in the literature (Kays and London, 1984). The acceleration term, can be expressed by:

$$\Delta P_{r,acc} = \left(\frac{\dot{m}_r}{A c_r}\right)^2 \left(\frac{1}{\rho_{r,out}} - \frac{1}{\rho_{r,in}}\right) \tag{3.10}$$

Finally, the gravitational term, can be evaluated as follows:

$$\Delta P_{r,g} = \frac{1}{2} g \left(\rho_{r,in} + \rho_{r,out}\right) \Delta X_r \sin\beta \tag{3.11}$$

The mixture cells, which in this work are only used for the refrigerant flow, have another formulation since they are adiabatic and only collect and/or distribute the refrigerant flow. The governing equations implemented in these cells determine the fluid flow distribution: uniform or non-uniform. In the present work, uniform flow distribution was assumed. An object-oriented programming allows an easier change of a model which assumes uniform flow distribution to one which does not, because the equations to describe this phenomena are only located in the mixture cell due to the modular capability of this programming technique. According to the assumption of uniform flow distribution, any outlet of the mixture cell *r* has the same conditions which are calculated with:

$$\dot{m}_{r,out} = \frac{\sum_{1}^{n_{r,in}} \dot{m}_{r,in}}{n_{r,out}} \tag{3.12}$$

$$h_{\mathrm{r,out}} = h_{\mathrm{r,in}} \tag{3.13}$$

where a mixture cell *r* is connected to $n_{\mathrm{r,in}}$ inlet tubes and $n_{\mathrm{r,out}}$ outlet tubes.

A mixture cell in this kind of heat exchanger would be a portion of header tube, so there is a pressure drop due to the insertion of the tubes into the header, which can be treated as a sudden expansion or contraction. Additionally, frictional and gravitational pressure drop along the headers could be evaluated applying Eq. (3.9) and Eq. (3.11) to the corresponding mixture cell.

3.1.2.3 Fin wall and its thermal connections

The present model discretizes the fin height, together with the air in contact, into three cells (Fig. 3.5(b)); two short cells of equal height, which are in contact with the corresponding tubes, and a central cell. The reason to apply this discretization is that in this way, the assumption of uniform temperature along Y direction of the air cell in contact with each fin cell is more correct. In this manner, Eq. (3.3) can be applied more fundamentally to each fin-air connection than in a situation with just one air cell. Thus, in the proposed model the fin theory is applied to each fin-air connection, what means applying Eq. (3.3) for each fin cell, resulting for a column of fin cells the system of Eq. (3.14). That is the reason for the model's name: 1D because it applies a one-dimensional equation for each fin-air connection and "x3" because it is applied for three connections per fin.

$$\theta_{f,a}(Y)=\begin{cases}\theta_{f,a1}(Y)=C_1\,e^{m_{f,a1}Y}+C_2\,e^{-m_{f,a1}Y}, 0\le Y\le \varphi\,H_f\\ \theta_{f,a2}(Y)=C_3\,e^{m_{f,a2}\left(Y-\varphi\,H_f\right)}+C_4\,e^{-m_{f,a2}\left(Y-\varphi\,H_f\right)}, \varphi\,H_f\le Y\le (1-\varphi)\,H_f\\ \theta_{f,a3}(Y)=C_5\,e^{m_{f,a3}\left[Y-(1-\varphi)H_f\right]}+C_6\,e^{-m_{f,a3}\left[Y-(1-\varphi)H_f\right]}, (1-\varphi)\,H_f\le Y\le H_f\end{cases} \tag{3.14}$$

In Eq. (3.14) H_f is the fin height and φ is the non-dimensional height of fin and air cells at the bottom and top of the fin. Eq. (3.14) assumes uniform air temperature inside each region, on the *Y-Z* directions, thus to obtain the fin wall temperature (Eq. (3.15)), an integrated mean value is used for the air temperature, which corresponds to $\overline{T}_a$. Actually this value corresponds to an integrated value along the *Z* direction since the air temperature for each corresponding region is uniform along the *Y* direction.

$$T_f(Y)=\begin{cases}T_{f1}(Y)=\theta_{f,a1}(Y)+\overline{T}_{a1}, 0\le Y\le \varphi\,H_f\\ T_{f2}(Y)=\theta_{f,a2}(Y)+\overline{T}_{a2}, \varphi\,H_f\le Y\le (1-\varphi)\,H_f\\ T_{f3}(Y)=\theta_{f,a3}(Y)+\overline{T}_{a3}, (1-\varphi)\,H_f\le Y\le H_f\end{cases} \tag{3.15}$$

The unknown constants: C_1, C_2, C_3, C_4, C_5, C_6 must be evaluated from the boundary conditions of the heat transfer problem along the fin height, i.e. the temperature field must be continuous and derivable. Therefore, for a continuous fin, the conditions to evaluate the constants are:

$$\begin{cases} T_{f1}(Y=0)=T_{fB} \\ T_{f1}(Y=\varphi H_f)=T_{f2}(Y=\varphi H_f) \\ T_{f3}(Y=H_f)=T_{fT} \\ T_{f2}(Y=(1-\varphi)H_f)=T_{f3}(Y=(1-\varphi)H_f) \\ \left.\dfrac{dT_{f1}}{dY}\right|_{Y=\varphi H_f}=\left.\dfrac{dT_{f2}}{dY}\right|_{Y=\varphi H_f} \\ \left.\dfrac{dT_{f2}}{dY}\right|_{Y=(1-\varphi)H_f}=\left.\dfrac{dT_{f3}}{dY}\right|_{Y=(1-\varphi)H_f} \end{cases} \tag{3.16}$$

where T_{fB} and T_{fT}, illustrated in Fig. 3.5(c), correspond to the temperature at the bottom and top of the fin in the base of contact with the bottom and top tube cells, respectively. In this way it is possible to define T_f as follows,

$$T_f(Y)=\begin{Bmatrix} T_{f1}(Y) \\ T_{f2}(Y) \\ T_{f3}(Y) \end{Bmatrix}=[A(Y)]\begin{Bmatrix} \overline{T}_{a1} \\ \overline{T}_{a2} \\ \overline{T}_{a3} \\ T_{fB} \\ T_{fT} \end{Bmatrix} \tag{3.17}$$

[$A(Y)$] is a 3x5 matrix that depends on Y, geometry, air-side heat transfer coefficient and fin conductivity. Note that T_f has the interesting feature that is a pseudo-linear function with respect to $\overline{T}_a$, T_{fB} and T_{fT}.

Governing equations are presented for a continuous fin, as it has been exposed above, but this methodology allows modeling either a continuous fin or a fin with a cut along the air flow direction and located at half the fin height. Motivations for this fin cut were mentioned in Introduction and they will be widely discussed in subsection 3.3. The way to include this cut only affects to the definition of the boundary conditions in order to get the unknown constants of Eq. (3.14): C_1, C_2, C_3, C_4, C_5, C_6, and consequently [$A(Y)$]. Appendix A includes the definition of these boundary conditions for a particular case. Rest of model would be just the same.

Once we have an expression for the fin wall temperature function, the governing equations for the thermal connections between fin and tube (Eq. (3.18) and (3.19)) can be obtained by imposing that the heat conduction at the bottom (Eq. (3.18)) and top (Eq. (3.19)) of the fin are equal to the heat conduction, in the *Y* direction, through the n_t wall tube cells in contact. The conduction areas between a tube cell *t* and the top and bottom of the fin are A_{J_T} and A_{J_B}, respectively; the corresponding conduction areas for the bottom and top of the fin are A_{fB} and A_{fT}, respectively.

$$\sum_{t}^{n_t} A_{t,J_B} \frac{\partial}{\partial Y}\left(k_{t,J_B} T_t\right)\Big|_{Y=0} = A_{fB} \frac{d}{dY}\left(k_{f1} T_{f1}\right)\Big|_{Y=0} \tag{3.18}$$

$$\sum_{t}^{n_t} A_{t,J_T} \frac{\partial}{\partial Y}\left(k_{t,J_T} T_t\right)\Big|_{Y=H_f} = A_{fT} \frac{d}{dY}\left(k_{f3} T_{f3}\right)\Big|_{Y=H_f} \tag{3.19}$$

3.1.2.4 Air flow

Eq. (3.20) states the energy conservation in an air cell *a* in contact with a fin cell *f* and n_t tube cells *t*=1, n_t.

$$\dot{m}_a dh_a = d\dot{Q}_{f,a} + \sum_{t=1}^{n_t} \dot{q}_{t,a} pw_{t,a} dZ \tag{3.20}$$

The heat flux $\dot{q}_{t,a}$ exchanged with each tube cell *t* is calculated by applying Eq. (3.5), while the heat transferred to the neighbour fin cell *f*, can be evaluated by:

$$d\dot{Q}_{f,a} = \alpha_{f,a} pw_{f,a} \theta_{f,a} dY \tag{3.21}$$

The air pressure drop along the fluid cell *i* length is obtained by applying the momentum equation,

$$\Delta P_a = \Delta P_{a,fr} + \Delta P_{a,acc} + \Delta P_{a,cont} + \Delta P_{a,\exp} \tag{3.22}$$

where $\Delta P_{a,fr}$ and $\Delta P_{a,acc}$ are evaluated with the Eq. (3.9) and (3.10), respectively. The pressure drop terms due to the sudden contraction and expansion in the heat exchanger are obtained following Kays and London (1984).

For solving the system of equations a set of boundary conditions is needed. Inlet conditions and velocity distributions are known for both fluids. Additionally, the heat

transferred by the wall edges to the surroundings is usually considered negligible, so the edges of the extreme wall cells are adiabatic with the surrounding. The two extreme tubes, in the *Y* direction, of the heat exchanger are usually modelled using a fin package, which is placed in the surrounding side, with a height of half a fin height of the rest of fins. However, in real heat exchangers, these extreme tubes are finned with whole fins, in both sides of the tube, and the heat exchanger is closed, at the bottom and top, with two metal plates. In the proposed model, these two metal plates have been modelled as empty tubes, i.e. tubes with the same geometry as the rest but without refrigerant flowing inside, which are adiabatic with the surrounding.

3.1.3 Numerical Scheme

In order to discretize the governing equations presented in the previous subsection, a finite volume method (FVM) was applied. In the governing equations the wall temperature has been considered as the iterative variable of the problem, and the semi-explicit method for wall temperature linked equations (SEWTLE) proposed by Corberán et al. (2001) has been employed to solve the problem. The use of the wall temperature as independent variable gives more freedom to formulate the heat transfer phenomena, allowing the formulation of equations for energy conservation with fewer assumptions than classical *ε*–NTU approaches. Additionally, using the wall temperature as independent variable of the thermal problem, converts an implicit problem into a semi-explicit problem, by solving at each iteration a series of explicit steps.

In order to integrate the Laplacian operator in Eq. (3.6), it has been discretized by a classical finite difference (finite volume) approach.

$$a_t T_t - \sum_{k=W,E,S,N} a_{t,k} T_{t,k} = a_{t,J_B} T_{t,fB} + a_{t,J_T} T_{t,fT} - \sum_{i=1}^{n_i} pw_{t,i} U_{t,i} \left(T_t - T_i\right) ds_{t,i} \qquad (3.23)$$

$$a_{\mathrm{t,W}} = \frac{k_{\mathrm{t,W}} \cdot A_{\mathrm{t,W}}}{\delta l_{\mathrm{t,W}}} \quad a_{\mathrm{t,E}} = \frac{k_{\mathrm{t,E}} \cdot A_{\mathrm{t,E}}}{\delta l_{\mathrm{t,E}}} \quad a_{\mathrm{t,S}} = \frac{k_{\mathrm{t,S}} \cdot A_{\mathrm{t,S}}}{\delta l_{\mathrm{t,S}}} \quad a_{\mathrm{t,N}} = \frac{k_{\mathrm{t,N}} \cdot A_{\mathrm{t,N}}}{\delta l_{\mathrm{t,N}}} \; a_{\mathrm{t,J_B}} = \frac{k_{\mathrm{t,J_B}} A_{\mathrm{t,J_B}}}{\delta l_{\mathrm{t,J_B}}}$$

$$a_{\mathrm{t,J_T}} = \frac{k_{\mathrm{t,J_T}} A_{\mathrm{t,J_T}}}{\delta l_{\mathrm{t,J_T}}} \qquad a_{\mathrm{t}} = \sum_{k=W,E,S,N,J_B,J_T} a_{\mathrm{t,k}}$$

Notice that the term in Eq. (3.23) of the heat transferred to the fluids in contact is applied to both refrigerant and air cells in contact with a tube cell *t*. The direction reference used in the model for *k* is shown in Fig. 3.5(a). All $a_{\mathrm{t,k}}$ terms refer to the

conductance between a tube cell *t* and the neighbour tube cell in the *k* direction. a_{t,J_B} and a_{t,J_T} are the conductance of the connection between a tube cell *t* and the correspondent fin base, at either the bottom or the top of each fin respectively. For this formulation it has been assumed that the tube wall temperature T_t is uniform in the *Z-X* direction.

To continue discretizing the set of governing equations, first it is necessary to assume a temperature profile for the tube walls, or for the fluids, in order to obtain the estimation of the integral of the heat transferred to the fluids in contact with a considered piece of wall (Eq. (3.5) and (3.6)) in the fluid flow direction. This integration must be consistent with the integration of the coincident terms of fluid energy Eq. (3.7) and Eq. (3.20). The linear fluid temperature variation scheme (LFTV) has been assumed for both fluids, as Corberán et al. (2001) suggested for this application, leading to the following expression:

$$A_{t,i}\,\dot{q}_{t,i} = U_{t,i}\,pw_{t,i}\left(T_t - \frac{T_{i,in}+T_{i,out}}{2}\right)\Delta s_{t,i} \tag{3.24}$$

Eq. (3.24) is valid for both refrigerant and air cells in contact with a tube cell *t*. Substituting Eq. (3.24) in Eq. (3.18), the tube wall temperature can be evaluated as follows,

$$T_t = \frac{\sum_{k=W,E,S,N} a_{t,k}T_{t,k} + a_{t,J_B}T_{t,fB} + a_{t,J_H}T_{t,fH} + \sum_{i=1}^{n_i} pw_{t,i}U_{t,i}0.5\,(T_{i,out}+T_{i,in})\Delta s_{t,i}}{a_t + \sum_{i=1}^{n_i} pw_{t,i}U_{t,i}\Delta s_{t,i}} \tag{3.25}$$

By combination of Eq. (3.7) and Eq. (3.24), the outgoing temperature of a refrigerant cell *r*, can be expressed by,

$$T_{r,out} = \frac{T_{r,in}\left(1-0.5\sum_{t=1}^{n_t} NTU_{t,r}\right) + \sum_{t=1}^{n_t} NTU_{t,r}T_t}{\left(1+0.5\sum_{t=1}^{n_t} NTU_{t,r}\right)} \tag{3.26}$$

$$NTU_{t,i} = \frac{pw_{t,i}U_{t,i}\Delta s_{t,i}}{\dot{m}_i Cp_i}$$

Eq. (3.26) is used for a one-phase flow whereas for two-phase flow the outlet temperature depends on the outlet pressure.

To obtain the outgoing temperature of the air, Eq. (3.20) has to be solved, so the integration of Eq. (3.21) must be done previously. The total heat transfer along the fin cell can be expressed as:

$$\int d\dot{Q}_{f,a} = \int \alpha_{f,a} pw_{f,a} \theta_{f,a} dY = \alpha_{f,a}\ A_{f,a}\ \bar{\theta}_{f,a} \tag{3.27}$$

where $\bar{\theta}_{f,a}$ is the integrated mean value of $\theta_{f,a}(Y)$. A novel aspect of this model is that in order to include heat transfer from fin to air, integration of temperature difference $\theta_{f,a}$ is implemented in the model, while rest of models use directly a fin efficiency by applying the analytical relationship for adiabatic-fin-tip assumption, $\tanh(mL)/mL$.

The advantage of using the integration of $\theta_{f,a}$ is that allows taking into account the heat conduction between tubes more easily and fundamentally than other fin efficiency based approaches. Furthermore a fin efficiency cannot be always be defined, e.g. when temperature at fin roots are not identical. This fact leads to some models, which use the adiabatic-fin-tip efficiency, to apply more or less artificial approaches in order to include heat conduction between tubes. It is important notice that this idea is independent on the discretization applied in air and fin, i.e. with just one air cell, instead of three as this paper proposes, applying this idea is possible. Thus, there is neither accuracy nor computational cost reason to apply an approach based on the use of an adiabatic-fin-tip efficiency instead of the previous methodology, which is fundamentally more appropriated. Following section 3.2 will present an accuracy comparison on results between both methodologies, when one air and fin cell is used instead three.

By using Eq. (3.27), Eq. (3.20) can be written for each region of the fin on the following way,

$$\begin{Bmatrix} \dot{m}_{a1}\Delta h_{a1} \\ \dot{m}_{a2}\Delta h_{a2} \\ \dot{m}_{a3}\Delta h_{a3} \end{Bmatrix} = \begin{Bmatrix} \alpha_{f,a1} A_{f,a1} \bar{\theta}_{f,a1} \\ \alpha_{f,a2} A_{f,a2} \bar{\theta}_{f,a2} \\ \alpha_{f,a3} A_{f,a3} \bar{\theta}_{f,a3} \end{Bmatrix} + \begin{Bmatrix} \sum_{t=1}^{n_t} \dot{q}_{t,a1} pw_{t,a1} \Delta Z_{t,a1} \\ 0 \\ \sum_{t=1}^{n_t} \dot{q}_{t,a3} pw_{t,a3} \Delta Z_{t,a3} \end{Bmatrix} \tag{3.28}$$

The linear fluid temperature variation (LFTV) approach was also assumed for the air, along the *Z* direction, thus the set of Eq. (3.28) is rewritten as,

$$\begin{Bmatrix} 2\left(\overline{T}_{a1}-T_{a1,in}\right) \\ 2\left(\overline{T}_{a2}-T_{a2,in}\right) \\ 2\left(\overline{T}_{a3}-T_{a3,in}\right) \end{Bmatrix} = \begin{Bmatrix} NTU_{f,a1}\,\overline{\theta}_{f,a1} \\ NTU_{f,a2}\,\overline{\theta}_{f,a2} \\ NTU_{f,a3}\,\overline{\theta}_{f,a3} \end{Bmatrix} + \begin{Bmatrix} \sum_{t=1}^{n_t} NTU_{t,a1}\left(T_t-\overline{T}_{a1}\right) \\ 0 \\ \sum_{t=1}^{n_t} NTU_{t,a3}\left(T_t-\overline{T}_{a3}\right) \end{Bmatrix} \tag{3.29}$$

$$NTU_{f,a} = \frac{\alpha_{f,a} A_{f,a}}{\dot{m}_a Cp_a}$$

where, $NTU_{t,a}$ is defined for the thermal connections between a tube cell *t* and an air cell *a*, whereas $NTU_{f,a}$ is defined for the thermal connection between the air cell *a* and the attached fin cell *f*.

In Eq. (3.29) the term $\overline{\theta}_{f,a}$ corresponds to $\overline{T}_f - \overline{T}_a$, whilst $\overline{T}_f$ can be obtained by integration of Eq. (3.17) resulting the following equations,

$$\overline{T}_f = \begin{Bmatrix} \overline{T}_{f1} \\ \overline{T}_{f2} \\ \overline{T}_{f3} \end{Bmatrix} = \begin{bmatrix} \dfrac{\int_0^{\varphi H_f} [A(Y)]_{1,j}}{\varphi H_f} \\ \dfrac{\int_{\varphi H_f}^{(1-\varphi) H_f} [A(Y)]_{2,j}}{(1-2\varphi) H_f} \\ \dfrac{\int_{(1-\varphi) H_f}^{H_f} [A(Y)]_{3,j}}{\varphi H_f} \end{bmatrix} \cdot \begin{Bmatrix} \overline{T}_{a1} \\ \overline{T}_{a2} \\ \overline{T}_{a3} \\ T_{fB} \\ T_{fT} \end{Bmatrix} \tag{3.30}$$

Now, if $\overline{T}_a$ is subtracted from $\overline{T}_f$ and rearranging the result, $\overline{\theta}_{f,a}$ can be expressed as,

$$\begin{Bmatrix} \overline{\theta}_{f,a1} \\ \overline{\theta}_{f,a2} \\ \overline{\theta}_{f,a3} \end{Bmatrix} = \begin{Bmatrix} \overline{T}_{f1} - \overline{T}_{a1} \\ \overline{T}_{f2} - \overline{T}_{a2} \\ \overline{T}_{f3} - \overline{T}_{a3} \end{Bmatrix} = [B] \cdot \begin{Bmatrix} \overline{T}_{a1} \\ \overline{T}_{a2} \\ \overline{T}_{a3} \\ T_{fB} \\ T_{fT} \end{Bmatrix} \tag{3.31}$$

[*B*] is a 3x5 matrix that depends on the same parameters as [*A*(*Y*)] excepting *Y*. $\overline{\theta}_{f,a}$ depends on the outlet temperatures of all the air cells located at the same *Z* (of the same segment), however note that $\overline{\theta}_{f,a}$ has the interesting characteristic, same as $T_f(Y)$, that is a pseudo-linear function with respect to $\overline{T}_a$, T_{fB} and T_{fT}. This fact will report interesting computation capabilities, which will be described in next section. In order to get the matrix [*B*] many algebraic operations have to be done, thus Appendix A contains the definition of these terms, for both continuous fin and cut fin.

If Eq. (3.31) is substituted in Eq. (3.29), and rearranging, the system of equations to solve is the set of Eq. (3.32). The average air temperature and consequently the outlet air temperature for each segment are obtained simultaneously by solving the system of Eq. (3.32). The solution for a system of 3 linear equations is known and easy to compute.

$$\begin{bmatrix} \dfrac{2+\sum_{t=1}^{n_t} NTU_{t,a1}}{NTU_{f,a1}} - B_{1,1} & -B_{1,2} & -B_{1,3} \\ -B_{2,1} & \dfrac{2}{NTU_{f,a2}} - B_{2,2} & -B_{2,3} \\ -B_{3,1} & -B_{3,2} & \dfrac{2+\sum_{t=1}^{n_t} NTU_{t,a3}}{NTU_{f,a3}} - B_{3,3} \end{bmatrix} \cdot \begin{bmatrix} \overline{T}_{a1} \\ \overline{T}_{a2} \\ \overline{T}_{a3} \end{bmatrix} =$$

$$\begin{bmatrix} \dfrac{2T_{a1,in} + \sum_{t=1}^{n_t} T_t\, NTU_{t,a1}}{NTU_{f,a1}} + T_{fB}B_{1,4} + T_{fT}B_{1,5} \\ \dfrac{2T_{a2,in}}{NTU_{f,a2}} + T_{fB}B_{2,4} + T_{fT}B_{2,5} \\ \dfrac{2T_{a3,in} + \sum_{t=1}^{n_t} T_t\, NTU_{t,a3}}{NTU_{f,a3}} + T_{fB}B_{3,4} + T_{fT}B_{3,5} \end{bmatrix} \tag{3.32}$$

Now, we have to discretize Eq. (3.18) and (3.19) in order to relate temperature at the bottom and top of a fin with the temperature at the corresponding connected tube cells. The discretization of these equations, considering the proposed heat exchanger discretization and using some terms of Eq. (3.23), is

$$\left\{\begin{array}{l}\displaystyle\sum_{t=1}^{n_t} a_{t,J_B}\left(T_t - T_{fB}\right) = -A_{fB}k_{fB}\left.\frac{dT_{f1}}{dY}\right|_{Y=0} \\ \displaystyle\sum_{t=1}^{n_t} a_{t,J_T}\left(T_t - T_{fT}\right) = A_{fT}k_{fT}\left.\frac{dT_{f3}}{dY}\right|_{Y=H_f}\end{array}\right\} \tag{3.33}$$

where the derivative of the temperature at the bottom and top of the fin can be evaluated from Eq. (3.17), resulting

$$\left\{\begin{array}{l}\left.\dfrac{dT_{f1}}{dY}\right|_{Y=0} \\ \left.\dfrac{dT_{f3}}{dY}\right|_{Y=H_f}\end{array}\right\} = [C]\left\{\begin{array}{l}\overline{T}_{a1} \\ \overline{T}_{a2} \\ \overline{T}_{a3} \\ T_{fB} \\ T_{fT}\end{array}\right\} \tag{3.34}$$

where [*C*] is obtained by deriving the corresponding rows of [*A*(*Y*)] (Eq. 3.17) and evaluating them at $Y=0$ or $Y=H_f$, respectively. Because of same reasons as for matrix [*B*], the coefficients of matrix [*C*] are exposed in the Appendix A, for both continuous fin and cut fin.

By substitution of Eq. (3.34) in Eq. (3.33) results the following system of equations,

$$\begin{bmatrix}\left(C_{1,4} - \displaystyle\sum_{t=1}^{n_t}\chi_{t,B}\right) & C_{1,5} \\ -C_{2,4} & -\left(\displaystyle\sum_{t=1}^{n_t}\chi_{t,T} + C_{2,5}\right)\end{bmatrix}\cdot\begin{bmatrix}T_{fB} \\ T_{fT}\end{bmatrix} = \begin{bmatrix}-C_{1,1}\overline{T}_{a1} - C_{1,2}\overline{T}_{a2} - C_{1,3}\overline{T}_{a3} - \displaystyle\sum_{t=1}^{n_t}\chi_{t,B}T_t \\ C_{2,1}\overline{T}_{a1} + C_{2,2}\overline{T}_{a2} + C_{2,3}\overline{T}_{a3} - \displaystyle\sum_{t=1}^{n_t}\chi_{t,T}T_t\end{bmatrix} \tag{3.35}$$

Where the following expressions have been used, for the thermal conductance at the bottom and top of the fin:

$$\chi_{t,B} = \frac{a_{t,J_B}}{A_{fB} k_{fB}}, \ \chi_{t,T} = \frac{a_{t,J_T}}{A_{fT} k_{fT}}$$

This system is again a linear system of equations, and it is employed to relate T_{fB} and T_{fT} with $\overline{T_a}$ and T_t .

At this point all the equations which describe the thermal problem have been discretized. The pressure drop equations, presented in the previous subsection 3.1.2, were already in discretized form.

To summarize, the proposed model applies to each segment the equations: (3.25), (3.26), (3.32), (3.35), with T_{fB}, T_{fT}, T_t, $T_{r,out}$ and $T_{a,out}$ being the unknown variables of the problem for each of the cells of the heat exchanger. Once these variables are known, any performance parameter of the heat exchanger can be calculated, including the fin temperature at any position *Y* by means of Eq. (3.17).

3.1.4 Solution Methodology

The global solution method is based on the SEWTLE method, outlined by Corberán et al. (2001), with some differences due to the particularities of the present model.

The proposed system of equations consists of a system of non-linear equations since coefficients and properties depend on the temperature and pressure field. The functions of the properties and coefficients are strongly non-linear and too complex to introduce directly in the system of equations. Thus, the solution needs an iterative process. A first option could be to start solving the problem assuming constant coefficients and properties. Corberán et al. (2001) concluded that it is not worth finding the exact solution for such a system, since even with the exact solution the properties/coefficients have to be recalculated and the system must be solved again and again. They proposed that a better strategy would be "*combine the iterative calculation of the solution with the continuous updating of the coefficients, in such a way that both calculations progress together toward the solution of the nonlinear problem*". The proposed numerical scheme fits quite well with this strategy, since it consists of a set of explicit equations.

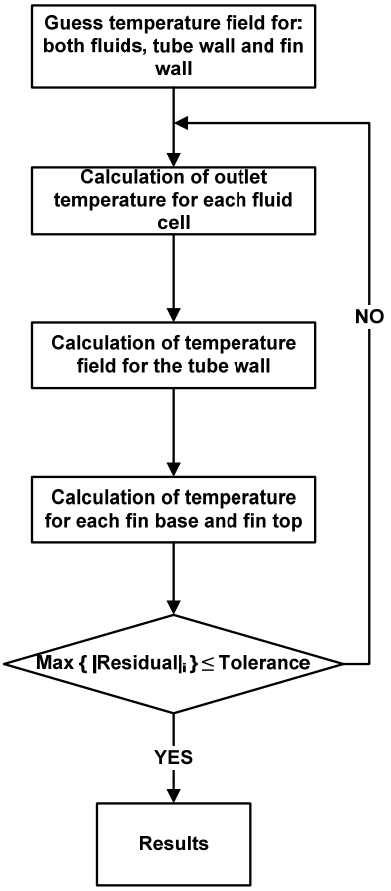

Fig. 3.6 – Solution methodology for solving the problem.

The solution methodology applied in the present work is summarized in Fig. 3.6. In the first step, the fluid outlet temperatures at each cell are initialized for both fluids, with the corresponding inlet temperature. Any wall cell is initialized using the average temperature of the fluid cells in contact with it. Since the temperatures at the bottom and top of the fin are required, these temperatures are initialized with the same value as those adopted at the attached tube cells.

The first step in the iterative procedure is the fluid outlet temperature calculation for both streams: refrigerant and air. First, Eq. (3.26) is used to obtain the refrigerant field temperature. Secondly, for the air flow, the solution of Eq. (3.32) gives the outlet temperature of each air cell along the fin height of a fin. Although Eq. (3.32) represents a system of three equations, note that the solution for such a system is known, and can be easily expressed as an explicit equation for each air cell, so that it is not necessary solving numerically the inverse matrix of Eq. (3.32). Thus, the outlet temperatures of the three air cells of each fin column (in a segment) are obtained explicitly.

Once the fluid temperature has been evaluated at each cell, Eq. (3.25) must be solved for the tube wall temperature. Note that at this step the temperature field of fluids, fin

bottom and fin top temperatures are known. In presence of LHC, Eq. (3.25) shows that the wall temperature of a wall cell *t* depends on the wall temperature of the neighbouring wall cells. When there is no LHC the exact solution, at this step, consists of explicit calculations.

In case of LHC being present, it is necessary to solve a system of linear equations, involving all the tube cell temperatures. If we take into account that it is not worth to obtain the exact solution in each step, as it was explained above, the best methodologies to deal with this calculation are:

- Using for each tube cell equation values of the temperature of neighbouring tube cells corresponding to the previous iteration. This way converts Eq. (3.25) into an explicit equation, but this method will increase considerably the time to reach the convergence.
- Line-by-Line iteration method (Patankar, 1980). Due to the characteristics of the system, it converts the system of equations into a tridiagonal system of equations, which is easily solved. When the LHC is only one direction, this methodology gives the exact solution.
- Block-by-Block (Patankar, 1980). It is based on the line-by-line method, but it adds a correction to the solution after finishing each iteration. It has the advantage of a faster convergence than the line-by-line method but it needs twice the number of operations.

Regardless of the selected methodology, this step calculates the wall tube temperature field along a set of explicit calculations. Particularly, these calculations will be the exact solution in case that no LHC is present or when LHC is present only in the tube along one direction and the line-by-line method is used.

The last step consists of solving the temperature field for the fin wall cells at the bottom and top of the fins. For each fin, both temperatures are obtained from Eq. (3.35). This system has only two equations and the solution can be easily expressed as two explicit equations. Note that due to no existence of longitudinal heat conduction in the fin, along the *Z* direction, the fin wall temperature field does not need an iterative resolution as it occurred in the Fin2D model, so that the process to obtain the fin wall temperature field results explicit. An interesting point of the fin discretization is that though fin wall is discretized into three cells, computationally it behaves as just one fin cell. In fact, the total number of unknown variables for each fin, regardless the number of fin cells, are two: temperatures at fin and bottom of fin.

At the end of the iterative process, the residual is compared with the accepted tolerance. Several variables can be used to evaluate the residual such as wall

temperature, heat exchanged by a fluid flow… In this model, the authors used as residual for each cell the scaled heat balance (absolute value) in that cell, applying the maximum one for all the cells as the decision parameter.

3.2 Model Validation

In order to validate the proposed model, a set of existing experimental results are going to be compared with the thermal capacity predicted by the model, when inlet conditions and mass flow rates are provided for both fluids. The model is able to simulate both gas cooler and condenser, thus both scenarios are validated.

Table 3.1 - Correlations used in the model for coefficients evaluation.

	Heat transfer coefficient	Pressure drop	Expansion/Contraction pressure losses
Refrigerant			
One-phase	Gnielinski (1976)	Churchill (1977)	Kays and London (1984)
Two-phase	Cavallini et al. (2002)	Friedel (1980)	Kays and London (1984)
Air			
	Kim and Bullard (2002)	Kim and Bullard (2002)	Kays and London (1984)

The grid size was chosen as the one that gave a good balance between accuracy and computational cost. According to the definition exposed in subsection 3.1.1, the grid employed for all the predicted results was: {5,1,3,3}. The authors studied in section 2 the effect of simulating the actual number of channels or just one channel with identical hydraulic diameter, and they concluded that the differences were negligible. Therefore, regardless the actual number of channels per tube, only a hydraulic equivalent channel was modeled.

The fin height ratio φ, has still not been evaluated. This parameter could be adjusted experimentally, numerically or even by observation. According to the corresponding explanations in section 3.1, it is possible to get a first approach from: typical dimensions of louvered fins used in this type of heat exchangers; the value reported in section 2 was about 3%. Thus, a value of φ equal to 4% was assumed for the validation and for the different scenarios studied in next section. At end of this section, a simulation study was carried out in order to analyze the influence of this parameter on the solution.

The different correlations employed to evaluate the heat transfer and pressure drop coefficients are listed in Table 3.1.

Table 3.2. Geometric characteristics of the condensers used for the model validation (García-Cascales et al., 2010)

Condenser #1			
Face area (cm^2)	1604	Refrigerant side area (m^2)	1.16
Airside area (m^2)	3.9	Tubes number	33
Tube length (mm)	483	Refrigerant passes	4
Fin type	Louvered	Tube depth (mm)	19
Number of ports	19	Fin depth (mm)	21.5
Wall thickness (mm)	0.32	Fin density (fins/in)	14
Hydraulic diameter (mm)	1.276	Fin height (mm)	8.1
Fin thickness (mm)	0.11		
Condenser #2			
Face area (cm^2)	5939	Refrigerant side area (m^2)	3.76
Airside area (m^2)	16.51	Tubes number	66
Tube length (mm)	889	Refrigerant passes	2
Fin type	Louvered	Tube depth (mm)	19
Number of ports	19	Fin depth (mm)	21.5
Wall thickness (mm)	0.32	Fin density (fins/in)	14
Hydraulic diameter (mm)	1.276	Fin height (mm)	8.1
Fin thickness (mm)	0.11		

3.2.1 Microchannel condenser validation

The experimental data used was measured by García-Cascales et al. (2010). They measured two condenser arrangements (one-row and two-row) for two refrigerants (R410A and R134a), but for the present work only the experimental data corresponding to the one-row condenser is going to be used for the model's validation. For this arrangement, two condensers working with R410A were tested and have been simulated; their main geometry is described in Table 3.2. Differences between both condensers are mainly the number of tubes, finned length and therefore the capacity.

Usually, predicted capacity is reported as the mean value between refrigerant and air side capacities. However, measured capacity for refrigerant side had differences about 10% with respect to measured capacity in the air side. Since air is harder to measure, the authors consider that the actual capacity should be closer to the refrigerant side. Thus, in order to present the model's validation, predicted capacity is compared against measured refrigerant side capacity and measured mean capacity (arithmetic average of both capacities).

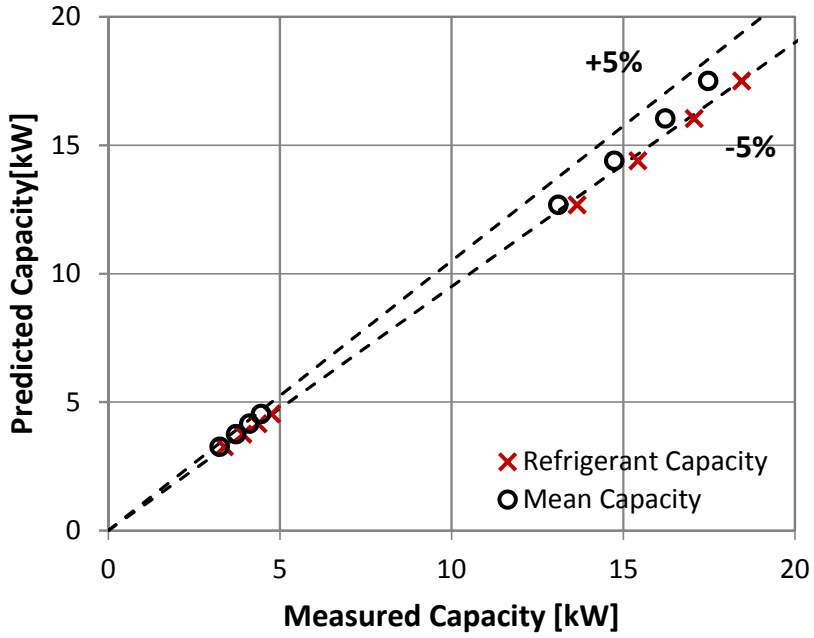

Fig. 3.7 - Model validation for two condensers by means of comparison between experimental and predicted capacity.

Fig. 3.7 presents the predicted capacity against the whole set of experimental values, for both condensers. The figure shows two plots, which correspond to the measured heat capacities mentioned above. The model agrees well with the mean measured capacity while it underestimates the refrigerant capacity, when an error band of ±5% is considered.

In order to obtain these results an adjustment factor of 1.15 was applied to the air side heat transfer coefficient obtained with the corresponding correlation of Table 3.1. The main reason to use this factor concerns to an adjustment of the φ factor to the real fin surface measured whose meaning was introduced in subsection 3.1, but basically it represents the effects of non-mixed air along Y direction and it depends on the fin surface and operating conditions. Next subsection will assess the influence of this parameter on the predicted results. In addition to the influence of φ factor on the validation study, the correlation used for the air side heat transfer coefficient (Kim and Bullard, 2002) reported rms errors of 14.5% for the Colburn factor. The authors found as a suitable way to use an adjustment factor for the air side heat transfer of 15% to take into account all the deviations explained above.

The predicted pressure losses of refrigerant were quite underestimated with regard the experimental data, with mean errors of 50% and 75% for condenser #1 and condenser #2 respectively. Microchannel tube geometry is hard to measure accurately since small manufacturing defects produce large geometry variations, thus pressure losses variations. A different mean error for both condensers also supports this idea.

3.2.2 Microchannel gas cooler validation

The experimental data used corresponds to a CO_2 gas cooler tested by Yin et al. (2001), who measured the performance of the gas cooler over a wide range of operating conditions. The uncertainty for the capacity measurement in those experiments was ±5%. The gas cooler modeled is a parallel tube MCHX of three refrigerant passes, whose main geometric data is summarized in Table 3.3.

Table 3.3. Geometric characteristics of gas cooler (Yin et al., 2001)

Face area (cm^2)	1950	Refrigerant side area (m^2)	0.49
Airside area (m^2)	5.2	Tubes number	34
Tube length (mm)	545	Refrigerant passes	3
Fin type	Louvered	Core depth (mm)	16.5
Number of ports	11	Fin density (fins/in)	22
Wall thickness (mm)	0.43	Port diameter (mm)	0.79
Fin thickness (mm)	0.1	Fin height (mm)	8.89

Fig. 3.8(a) presents the predicted gas cooler capacity against the whole set of experimental values. As it can be observed, all the predicted values are within the error bound of ±5 %. The accuracy is quite high since a linear function fitted to the predicted capacity had a slope of 0.9972, what represents an error of -0.28%, for the whole set of experimental data. Overall, the model slightly underpredicts the gas cooler capacity. For this scenario, it was not applied any adjustment factor to the heat transfer coefficients.

The outlet refrigerant temperature was also compared against experimental data in Fig. 3.8(b). The figure includes the bounds of ± 2 K around the measured temperatures. As it can be observed, all the points deviate from the experimental data less than ±2 K.

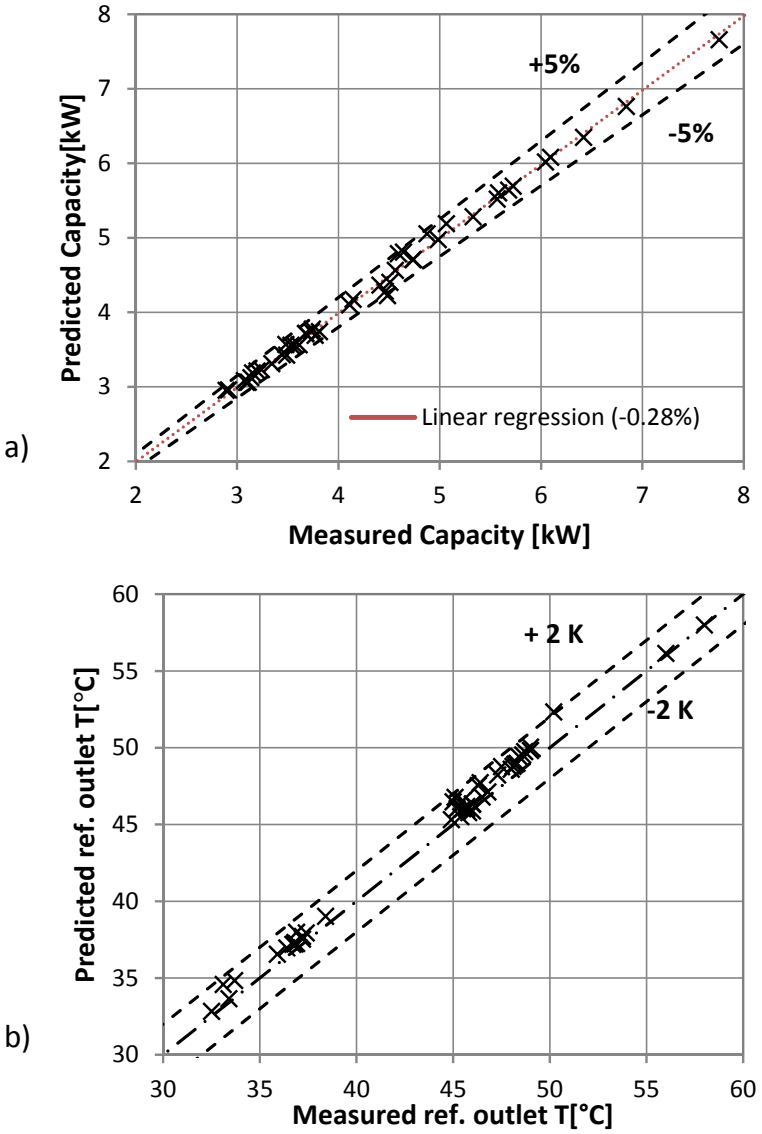

Fig. 3.8 - Model validation for a gas cooler by means of comparison between experimental data against (a) predicted capacity; (b) predicted refrigerant outlet temperature.

The predicted pressure losses of refrigerant were far from the experimental data, with a mean error of -80%. These errors are similar to those errors reported by Asinari et al. (2004) and Yin et al. (2001) when they evaluated this error with their own models for the same cases. Yin et al. (2001) solve this disagreement introducing some dimensional changes in ports, produced by manufacturing defects. Asinari et al. (2004) demonstrate that introducing arbitrary multiplying factors pressure losses agree well with a negligible effect on the capacity results. They argue that the reason for the disagreement between predicted and experimental pressure drop is based on underestimation of the pressure losses when traditional correlations are used for this particular geometry and conditions.

An important factor to take into account in a model validation is the effectiveness of the gas cooler employed for obtaining the experimental data. If we define the temperature approach as the temperature difference between the refrigerant outlet and the air inlet, this factor will be quite representative of the gas cooler effectiveness. A robust validation of a model will imply large approach values. For the experimental data used, the approach ranged from 1 K to 7 K, with an average value of 4.1 K. This value indicates a high gas cooler effectiveness, in fact, for the data used it had an average value of 83%.

3.2.3 Impact of parameter φ on predicted capacity

The meaning of the fin height ratio φ in the model has been discussed in section 3.1 whilst its estimation has been discussed in subsection 3.2. A value of 4% was finally proposed for the validation cases, even though this value depends on the fin surface and operating conditions. To this end, authors carried out a numerical study about the impact of φ on the model results in order to analyze the model sensitivity to this parameter, what implicitly means the impact of un-mixed air flow along *Y* direction.

The scenario chosen for this study corresponds to the gas cooler introduced in the gas cooler validation working in the operating conditions of test #2 (Yin et al., 2001), which has the largest capacity of all the tests.

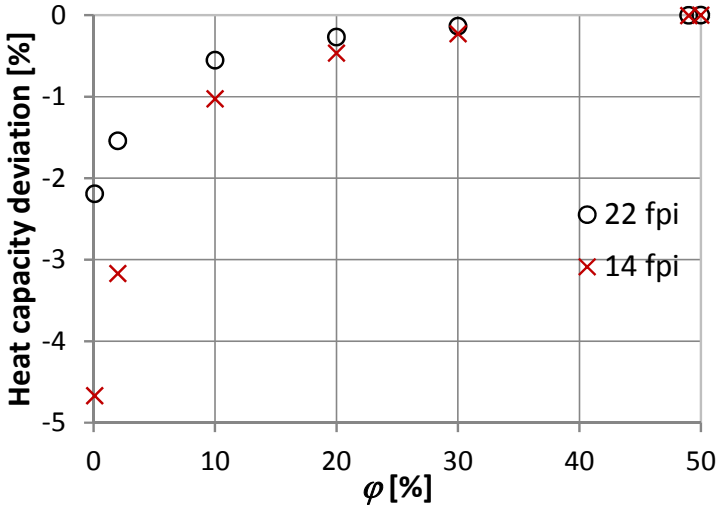

Fig. 3.9 - Influence of fin height ratio φ on heat duty of gas cooler for different fins densities.

Fig. 3.9 shows the deviation between the heat exchanged by the gas cooler when the parameter φ is modified with respect to the heat exchanged when φ tends to be 50%. This study is carried out for two fins densities: 22 fpi and 14 fpi. The variation of φ ranges between two limit situations: 0% and 50%. A value close to 50% means that air

flow has a temperature profile corresponding to a mixed air flow along the fin height. In fact, for this φ value, if temperatures of attached tubes to the fin are identical, air flow has uniform temperature along the whole fin height. The opposite behaviour is when the φ tends to be 0% which means that the non-mixed air along *Y* direction has the maximum effect. In this situation, a thin air layer is in contact with each wall tube. These air layers have a quite different temperature from the rest of air because air flow rate in these cells is very small and its temperature will be very close to the tube wall temperature. Therefore, these air layers will have an insulating effect on the tube wall in contact. Both situations are not real and what actually happens is between both of them.

The effects described above for extreme values of φ value agree quite well with the trend shown in Fig. 3.9; the lower the φ value, the less capacity is exchanged by the gas cooler. It is interesting notice that the trend is asymptotic for large φ values whereas the effect of φ changes sharply for low φ values. Louvered fins would have low φ values while it would be much greater for plain fins. Fig. 3.9 also shows that impact of φ on the solution depends on the fin density, resulting values from 2% to 5% for fin densities of 22 fpi and 14 fpi respectively.

This parameter is actually unknown, but fortunately the deviation in predicted capacity would be less than 5%, for the fins densities evaluated.

3.3 Simplification of Fin1Dx3 model: Fin1D

The objective of the thesis work is to develop a detailed MCHX model considering not only accuracy reasons but also to computational cost. To this end, reduction of number of cells plays an important role. Thus, authors decided to simplify the Fin1Dx3 model in order to assess in further studies the potential of this simplificated model.

The simplification consists in discretizing air and fin only in one cell along *Y* direction. Fig. 3.10 shows an example of this discretization.

Governing equations and numerical scheme for Fin1D model are not presented in the section because they are obtained in same way and with same assumptions as made in section 3.1. Instead of the piecewise function proposed for Fin1Dx3, now only one continuous function for the fin wall temperature is used. This function is obtained by imposing same boundary conditions in the fin: temperatures at fin roots are given. In the air flow, now there is only a temperature variable for one air-fin column.

Integration of the air-to-fin heat transfer is obtained in the same way as for Fin1Dx3 but now is much simpler.

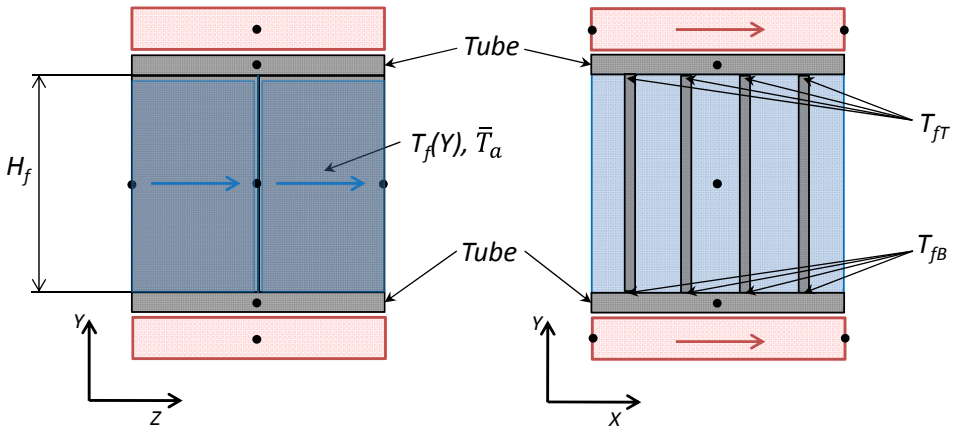

Fig. 3.10 - Different views of portion of heat exchanger discretized by Fin1D model which uses only one cell along *Y* direction for fin and air.

Phenomena that Fin1D model takes into account are the same as for Fin1Dx3, with just one exception: Fin1D cannot takes into account the effect on the heat transfer of the un-mixed air *Y* direction.

The validation for this Fin1D model is not carried out since an accuracy study against Fin1Dx3 model is worked out in the following chapter.

3.4 Conclusions

This chapter presents the Fin1Dx3 model which reduces significantly the computational cost of the Fin2D model retaining its accuracy. In this way, it allows using that model to analyze microchannel condensers and gas coolers with any refrigerant circuitry, including serpentine heat exchangers.

The main conclusion is that it is possible to take into account the heat conduction between tubes in a more fundamental way than other fin efficiency based approaches, which have to apply heat conduction terms to an approach that uses the adiabatic-fin-tip assumption, which is not satisfied in such cases. The alternative methodology, proposed in this work, consists in evaluating the heat transfer by integration of the corresponding fin temperature profile instead of using a fin efficiency which cannot always be defined, e.g. when temperature at fin roots are different. It has been shown that this integration does not represent an obstacle since it can be easily discretized consistently with the rest of governing equations; therefore there is neither accuracy nor computational cost reason to apply adiabatic-fin-tip assumption when it is not

satisfied. The approach proposed in this paper is developed for a three air-fin cells discretization but this conclusion is equally applicable to a single air-fin discretization.

The rest of conclusions regarding the Fin1Dx3 model and its validation that can be drawn from this section are the following:

- The Fin1Dx3 model accounts for all the same effects than Fin2D model except the LHC in the fin along *Z* direction which, in any case, has been found not to be important. Fin1Dx3 is based on a novel discretization methodology for the air and fin wall that only needs three air cells along the *Y* direction. This methodology allows reducing drastically the number of cells to compute, with regard to the Fin2D model, and consequently the simulation time but keeping a high resolution along *Y* direction.
- The large number of fin cells needed by Fin2D model to solve accurately the air-side heat transfer, is compensated in Fin1Dx3 with a novel methodology to describe the air-side heat transfer, using a piecewise function for the fin temperature. This piecewise function, together with the employed air discretization, allows applying in a more fundamental way the analytical solution given by the fin theory.
- The main capabilities of Fin1Dx3 are: 2D-LHC in the tube wall; non-mixed air effects due to temperature difference between bulk air and the air close to the tubes; and it accounts fundamentally for heat conduction between tubes since it does not apply adiabatic-fin-tip assumption.
- The equations have been discretized, with the interesting characteristic of resulting in a system of pseudo-linear equations with respect to the variables of the problem. A numerical scheme has been proposed to solve the problem as a series of explicit steps. The numerical scheme proposed allows computing the three fin cells with the computational effort of just one fin cell.
- Fin1Dx3 model was validated with experimental data, for both condenser and gas cooler. The predicted capacity is within ±5% error, being much more accurate for the gas cooler scenario. Although pressure drop was underpredicted, it did not affect the heat transfer results.
- The study about the influence of the factor φ, which accounts for the effects of un-mixed air flow along Y direction, showed deviations less than 5% for extreme values of φ and for the simulated conditions.

Finally, a simplification of FinDx3 has been presented: Fin1D. It reduces the number of cells employed in the discretization at the expense of accuracy. In next chapter it is compared against Fin1Dx3 model regarding to accuracy and computational cost.

CHAPTER 4

NUMERICAL COMPARISON OF MODELS

4 NUMERICAL COMPARISON OF MODELS

This section will discuss and compare accuracy skills and computation time for two groups of models for MCHX.

First group of models to compare are those developed by present authors for MCHX modeling: Fin2D, Fin1Dx3 and Fin1D. The goal of Fin1Dx3 model is to be a suitable tool for simulation and design of MCHXs. It has been explained that the Fin1Dx3's discretization is based on the Fin2D model, which had large computational requirements, but the new discretization of Fin1Dx3 allows, for same accuracy, reducing considerably the number of both air and fin cells, so that a large computational cost reduction is expected. Therefore, the first results presented in this section are oriented to assess the degree of accomplishment got to this end. Another way to reduce the computational cost is to reduce the number of cells employed in the discretization, which a priori means accuracy degradation. To this end authors developed a model referred to as Fin1D which applies same assumptions as Fin1Dx3 model but it discretizes the whole fin and air column of each segment into just one cell along the fin height direction.

In Introduction, it was explained that most of models available in literature do not account for heat conduction between tubes. A model that uses the adiabatic-fin-tip without any correction term, to take into account the heat conduction between tube, is always predicting results as if the heat exchanger had all fins cut, hence these models are always overpredicting the heat transfer. Only few authors (Lee and Domanski, 1997; and Singh et al., 2008) model, for finned tube heat exchangers, this phenomenon by using a correction term which takes into account, in a more or less artificial way, the heat conduction between tubes, despite using the adiabatic-fin-tip assumption in the governing equations. Thus, the second group of models compared in this section consists of the models proposed in this paper (Fin1Dx3 and Fin1D) and a model which represents what other authors (Lee and Domanski, 1997; and Singh et al., 2008) do in their models in order to take into account the heat conduction between tubes in a MCHX. Although these approaches were originally proposed for finned tubes heat exchangers, in this chapter they have been adapted to MCHXs.

The accuracy comparison between the different models has been worked out by comparing the models with regard to the most detailed model, which depends on the scenario studied. Experimental results have not been used as reference to perform the accuracy comparison since the deviation between results is affected by several factors hard to identify such as experimental uncertainty, moreover this deviation could be

non-linear adding a complex factor in order to draw conclusions about the models comparison.

4.1 Comparison among different developed models: Fin2D, Fin1Dx3 and Fin1D

Below are listed and briefly summarized each of the models compared in this subsection:

- Fin2D: It corresponds to the model presented in chapter 2. It is a very detailed model which discretizes fin and air into a two-dimensional grid. Its main capabilities are: it takes into account 2D longitudinal heat conduction (LHC) in both fin and tube wall, it does not applies fin theory and it accounts for heat conduction between tubes. Its main drawback is the simulation time employed to solve a case, due to the detailed grid adopted in the fin and air elements.
- Fin1Dx3: It corresponds to the model presented in chapter 3. For each segment it discretizes air and fin into three cells along the direction between tubes, while for the tube wall it applies the same discretization as Fin2D model. The phenomena modeled are the same as Fin2D model excepting the LHC in the fin along air flow direction with a large reduction in the number of cells employed.
- Fin1D: It is basically the same model as Fin1Dx3, and same phenomena modeled, but now neither air nor fins are discretized along the fin height. The analytical solution given by fin theory, for the case of given temperatures at fin roots, is used to get the fin temperature profile. Thus, it also takes into account heat conduction between tubes.

The geometry of the tubes and fins, of the case study for this section, are the same as used by Yin et al. (2001) (Table 3.3). The operating conditions for the simulations are those used for the tests nº: 9, 17, 25, 33 and 41 (Yin et al., 2001). All the models applied the same grid, with the exception of the fin and air cells along *Y* direction. Due to the model differences, Fin2D model needs a large number of these cells; in chapter 2 it was proposed using 30 cells in the *Y* direction. The grids applied for these scenarios are: {5,1,3,30,3} for Fin2D model and {5,1,3,3} for Fin1Dx3 and Fin1D models. Regarding the correlations used by the model, they are listed in the Table 3.1.

The results for the accuracy comparison are presented in Fig. 4.1. The figure shows the deviation on predicted capacity for models Fin1D and Fin1Dx3 with respect the

predicted results of Fin2D model. Therefore, the zero for ordinates axis corresponds to the predicted results with Fin2D model. Fin2D model has been chosen as reference because it is the most accurate of them since it applies the finest discretization to the heat exchanger.

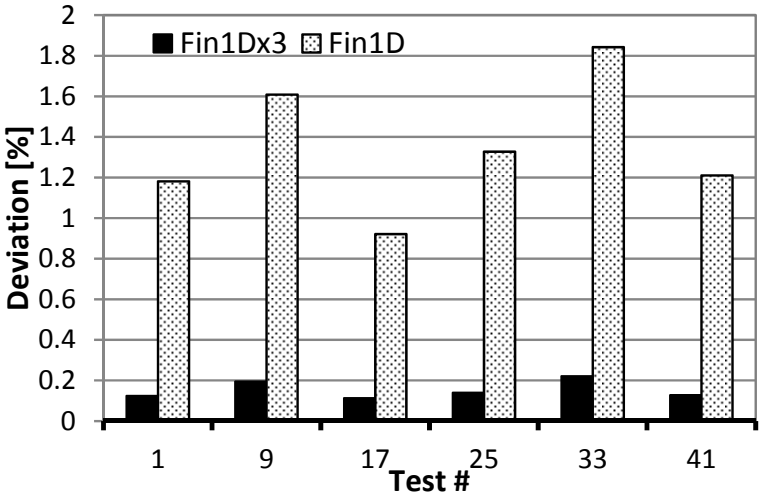

Fig. 4.1 – Heat transfer deviation, for different test conditions, of Fin1Dx3 and Fin1D models with regard to Fin2D model.

Fig. 4.1 shows that the deviation between Fin2D and Fin1Dx3 model is at most 0.2%, which means that predicted results could be considered as the same ones. However, this deviation turns to be as much 2% in the case of Fin1D model. The negligible difference between Fin2D and Fin1Dx3 models means that longitudinal heat conduction in fin surface along air direction, which is not modeled in Fin1Dx3 model, can be neglected for this scenario. These results also confirms that the approach of using three fin/air cells with a piecewise function for the fin temperature profile gives a good solution with much lower computational cost.

Fin1D and Fin1Dx3 take into account same phenomena and differences between them are only due to the fin/air discretization. According to this, the deviation between predicted results of both models is consequence only of a more accurate application by Fin1Dx3 model of fin theory for the air-to-fin heat transfer evaluation. In other words, this difference could be interpreted as the effect of non-mixed air along *Y* direction. Nevertheless, this deviation can be interpreted as small, though the effect would depend on the operating conditions, heat exchanger and application. The present work, analyses the case of a gas cooler that corresponds to a case with an expected impact of these phenomena larger than for the case of a condenser. For an evaporator, dehumidification appears and plays an important role and what happens depends strongly on local properties, thus authors foresee to include dehumidification in future works.

With regard to the computational cost, Fig. 4.2 presents the simulation time employed by each model to solve several cases which were described above. In the figure, a large computing time reduction, from Fin2D model to Fin1Dx3 model, is noticeable. This reduction represents one order of magnitude. The main reason is the large difference of air and fin cells used by both models. In the case of Fin1Dx3 model, a piecewise function which consists of three one-dimensional functions is enough to capture accurately the actual fin temperature profile and consequently the heat transfer from fin to air. However, as explained in the introduction, Fin2D needs to apply a large discretization to the fin height, in practice 30 fin and air cells are required to get accurate results.

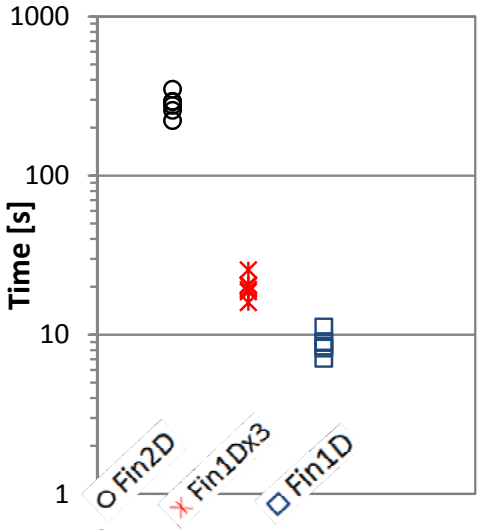

Fig. 4.2 – Comparison of the simulation time employed by each model.

The simulation time reduction from Fin1D to Fin1Dx3 model is not as drastic as for Fin2D case, Fin1D needs half the time spent by Fin1Dx3. A priori, a larger simulation time reduction could be expected since Fin1D uses just one air and fin cell along the fin height direction instead of three air and fin cells as Fin1Dx3 model does. However an interesting fact of the piecewise function applied in the Fin1Dx3 model is the following; the piecewise function uses as unknown variables the temperatures of the three air cells and the fin roots. The Fin1D model also includes as unknown variables the fin roots temperatures, since it takes into account heat conduction between tubes, but only one air temperature value. Thus only two variables are added to the Fin1D model with regard to Fin1Dx3 model, which corresponds to the air temperature values. These temperature values are obtained in the same way as Fin1D model does, i.e. with an explicit calculation given the wall temperature field, so that in Fin1Dx3 model there are only two more explicit calculations. In other words, the only cells that add computational cost to the Fin1Dx3 models are the air cells whilst the three fin cells behave numerically as just one.

If both factors accuracy and computational cost are taken into account, Fin2D model is not a cost effective solution since Fin1Dx3 provides the same results with a simulation time reduction of one order of magnitude. In contrast, Fin1Dx3 offers better results than Fin1D with only double simulation time, thus Fin1Dx3 model is considered by the authors as the best option for modeling this kind of heat exchangers. Despite the fact that for a condenser or a gas cooler the Fin1D could be an interesting option, for an evaporator the accuracy difference between both approaches is expected to be larger than for the presented results due to local effects on dehumidification.

4.2 Comparison with other authors' approaches

This subsection compares, in a similar way as the previous subsection did, the models proposed in the paper (Fin1D and Fin1Dx3) against other approaches used in literature for heat exchanger modelling. To this end, it has been necessary to develop two new models:

- Fin1D_Cut: It reproduces the results of the most common models available in literature (Yin et al., 2001; Corberán et al., 2002; Jiang et al., 2006; García-Cascales et al., 2010; Fronk and Garimella, 2011). It applies a segment-by-segment discretization, uses the adiabatic-fin-tip assumption and it does not take into account heat conduction between tubes. The model is just the same as Fin1D but it includes a cut along the fin to reproduce always adiabatic-fin-tip assumption. The needed changes in the model to include this fin cut are the same as those explained in previous chapter, when the Fin1Dx3 model was modified to simulate a MCHX with fin cuts.
- Corrected-Fin: It is based on the approaches proposed by Singh et al. (2008), and Lee and Domanski (1997). They have been chosen as references since they account for heat conduction between tubes in a different way to the proposed in the present paper, though these approaches model that phenomenon in a more artificial way. This model tries to be representative of what referred authors' models do. It is based on Fin1D model and it applies the same discretization but now it uses the analytical solution given by fin theory when adiabatic-fin-tip is assumed. In order to account for the heat conduction in the same way as referred authors do, correction terms are included in the corresponding energy conservation equations, which will be described in detail below.

The approaches of Singh et al. (2008), and Lee and Domanski (1997) were originally developed for fin-and-tube heat exchangers but they have been adapted in this paper

for a MCHX. Fig. 4.3 shows the geometric parameters of both arrangements regarding the heat conduction phenomenon.

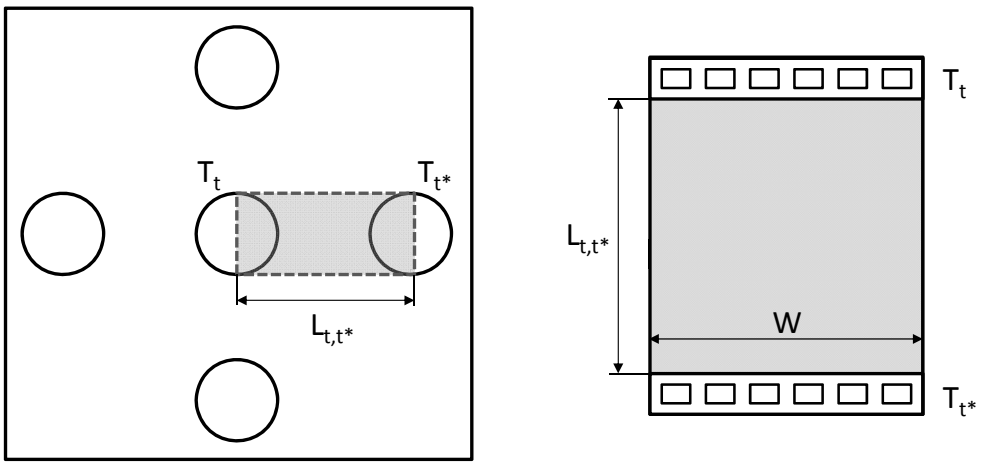

Fig. 4.3 – Analogy between a finned tube and a MCHX for the heat conduction resistance evaluation between two neighbors tubes along the fin.

These approaches (Singh et al., 2008; Lee and Domanski, 1997) apply the fin theory to each volume control and use a fin efficiency to include the fin-to-air heat transfer that is evaluated with Eq. (4.1), where $\theta_{fB,a}$ is the temperature difference between the bulk air temperature and the corresponding fin root temperature, and η_f is the fin efficiency. The relationship used for evaluation of the fin efficiency corresponds to the case of adiabatic-fin-tip assumption, Eq. (4.2).

$$\dot{Q}_{f,a} = \eta_f \; \alpha_{f,a} \; A_{f,a} \; \theta_{fB,a} \tag{4.1}$$

$$\eta_f = \frac{\tanh(m_{f,a} \; H_f / 2)}{m_{f,a} \; H_f / 2} \tag{4.2}$$

$$m_{f,a}^2 = \frac{\alpha_{f,a} \; pw_{f,a}}{k_f \; A_f}$$

Eq. (4.3) establishes the energy conservation in a segment. The segment consists of the wall tube cell *t*, the corresponding fin wall cell *f* attached to the tube, and the fluids in contact with it: refrigerant cell *r* and air cell *a*.

$$\dot{Q}_{f,a} + \dot{Q}_{t,a} + \dot{Q}_{t,r} + \dot{Q}_{t,t^*} = 0 \tag{4.3}$$

Since tubes have different temperatures, the correction term $\dot{Q}_{t,t^*}$ is introduced in Eq. (4.3) in order to take into account the heat conduction between tubes, which corresponds to the total heat transfer by conduction between neighboring tubes. Fig. 4.3 shows 4 tubes *t** connected to a central tube *t* by the fin surface. For this example the total heat conduction between central and neighboring tubes can be modeled as Eq. (4.4).

$$\dot{Q}_{t,t^*} = \sum_{t^*} \lambda \left(\frac{T_t - T_{t^*}}{R_{t,t^*}} \right) \tag{4.4}$$

Different approaches could be applied to get the value of thermal resistance R_{t,t^*} together the use of λ ,which is a multiplier that can be used to adjust the heat conduction term. Singh et al. (2008) explain that this multiplier has to be adjusted either numerically or experimentally which on the heat exchanger simulated. The need to use this correction factor which a priory is unknown and its dependency on the modeled case are the main drawbacks of this methodology.

Corrected-Fin model evaluates R_{t,t^*} with Eq. (4.5) and applies λ =1.

$$R_{t,t^*} = \frac{L_{t,t^*}}{t_f \; W \, k_f} \tag{4.5}$$

The simulations were carried out for the gas cooler (Yin et al., 2001) that was validated in previous chapter. The operating conditions for the simulations are those used for the tests nº: 9, 17, 25, 33 and 41 by Yin et al. (2001). The correlations for heat transfer and pressure losses coefficients were also the same as described in previous subsection.

All the cases analyzed have tubes with different temperatures and heat conduction is present, therefore Fin1D will be more accurate than Fin1D_Cut since adiabatic-fin-tip assumption is not valid. Fin1D model should be also more accurate than Corrected-Fin because the latter applies a correction term to take into account heat conduction between tubes, while Fin1D takes into account implicitly the heat conduction without simplifying assumptions.

First study compares the models that apply same discretization level, i.e. fin is discretized just in one cell. Fig. 4.4 shows the deviation on predicted capacity for models Fin1D_Cut and Corrected-Fin with regard to the predicted results of Fin1D model, which is expected to be the most accurate of them. First, it is noticeable that deviations between these models for these conditions are quite small, what means

that adiabatic-fin-tip assumption, despite not being valid, does not have a large impact on the solution which is less than 0.8 %. The deviation between Fin1D_Cut and Fin1D is always positive what implies that by cutting the fins, heat transfer is always increased. As can be observed in Fig. 4.4, Corrected-Fin can take into account heat conduction between tubes with negligible deviations, what means that the approaches of Singh et al. (2008) and Lee and Domanski (1997) are a good alternative for modeling finned tubes heat exchangers in presence of heat conduction between neighboring tubes.

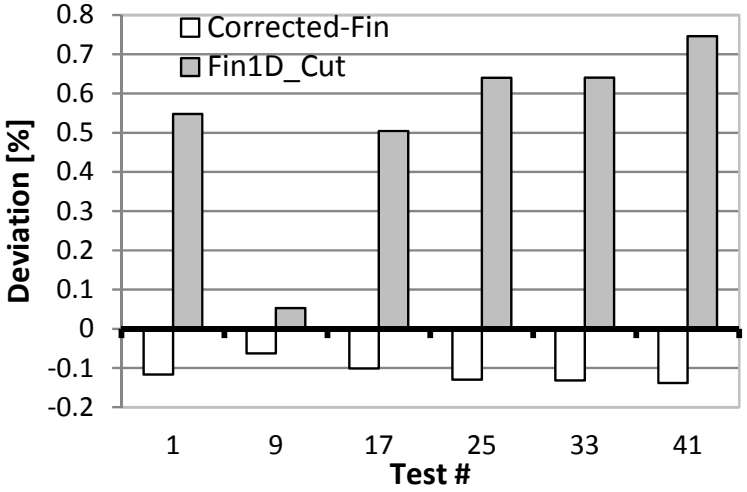

Fig. 4.4 – Deviation of predicted heat transfer of models Fin1D_Cut and Corrected-Fin with regard to Fin1D for different test conditions.

The following study compares the models which apply same discretization level (Fin1D, Fin1D_Cut and Corrected-Fin) with Fin1Dx3 model that applies a more detailed discretization, resulting in the most accurate of them. Fig. 4.5 presents the deviation in capacity for models Fin1D, Fin1D_Cut and Corrected-Fin with regard to the predicted results of Fin1Dx3 model. Therefore, the zero for ordinates axis corresponds to the predicted results with Fin1Dx3 model.

As can be observed in Fig. 4.5 the accuracy of all the models is good, resulting errors as much of 2% with respect to Fin1Dx3 model. The largest deviation is produced by the Fin1D_Cut model which uses the adiabatic-fin-tip. Fin1D and Corrected-Fin models have a similar deviation ranging from 1% to 2%. This deviation indicates that the major impact in the prediction error is considering the air as mixed in the direction between tubes; in fact, this is the only difference between Fin1D and Fin1Dx3 models; Fin1Dx3 discretizes the fin height into 3 cells being able to account for non-mixed air along fin height.

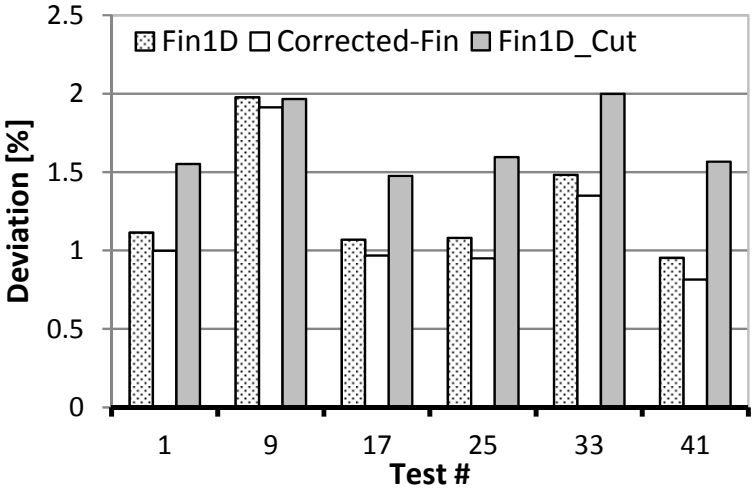

Fig. 4.5 – Deviation of predicted heat transfer of models Fin1D, Fin1D_Cut and Corrected-Fin with regard to Fin1Dx3 for different test conditions.

Regarding computational cost, it is not necessary to perform an evaluation of the simulation time required by Fin1D_Cut and Corrected-Fin models because they apply same discretization as Fin1D and therefore they have the same computational cost, which was presented above (Fig. 4.2).

4.3 Conclusions

Numerical studies about accuracy and computational cost were presented in order to compare the different developed models: Fin2D, Fin1Dx3 and Fin1D, and other representative models from literature. The main conclusions of these comparisons were the following:

- The solving time of Fin1Dx3 has been reduced one order of magnitude with regard to the time employed by Fin2D, whereas the differences on the results are less than 0.3%, which are considered as negligible for practical applications. The solving time difference between Fin1Dx3 and Fin1D turned out to be twice.
- Corrected-Fin can lead to accurate results when compared with an equivalent approach model that models heat conduction between tubes in a more fundamental way like Fin1Dx3 does. Difference between predicted results of both models was between 1% and 2%. Computational cost of Fin1D and Corrected-Fin models are the same. Nevertheless, author would like to emphasize the fact that the present work shows no computational saving or accuracy increase by adding correction terms to an approach that uses the

adiabatic-fin-tip efficiency with regard to a more fundamental approach, regarding the heat conduction between tubes phenomena, like Fin1D.

- By comparison of deviations between Fin1D, Corrected-Fin and Fin1Dx3 models, it was concluded that the main responsible for differences between them were the effects of non-mixed air along fin height.

According to previous conclusions, the final decision of authors about which model to use in the following for modeling MCHXs, it corresponds to the Fin1Dx3 model with continuous fin.

CHAPTER 5

SIMULATION STUDIES

5 SIMULATION STUDIES

In previous chapter, Fin1Dx3 model has been chosen as the best model with regard to computational cost and accuracy reasons. This chapter uses Fin1Dx3 model as simulation tool to study the impact of some design parameters of a MCHX on its performance. The following proposed numerical studies are hardly available in the literature for a MCHX. The goal of the selected case studies is contributing to a better understanding of the influence of some design parameters on MCHX performance.

Along the design process of a MCHX, the first step is choosing the geometric data of tubes and fins such as minor tube dimension, major tube dimension, fin height and fin depth. This choice is based on manufacturing requirements, e.g. costs, tooling and volume production. Given the inlet conditions and mass flow rates for both refrigerant and air, heat transfer area can be generally fixed by imposing a target heat load while face area of the MCHX is obtained from a pressure drop criteria. Fin pitch would have to satisfy a compromise between heat transfer and pressure drop.

Once these areas have been chosen, there are multiple circuitry designs that satisfy the target heat load so that the refrigerant circuitry can be designed in order to optimize the heat exchanger effectiveness by maximizing heat transfer, with some restrictions regarding pressure drop. In the same way, parameters like the aspect ratio (*L/H*) play the same role as the circuitry: several aspect ratios satisfy the performance requirements but just one optimizes the effectiveness. In fact, some simulation software like EVAP-COND (2010) has the capability to optimize the heat load varying the circuitry of a finned tube heat exchanger. Shao et al. (2009) studied the effect of the number of refrigerant passes for a serpentine MCHX working as condenser, with the same face area and heat transfer area. The authors obtained up to 30% differences on heat load only by changing the number of refrigerant passes. Given that the circuitry has an important influence on the heat exchanger performance, the usefulness of simulation software for this purpose is clearly justified, since the optimization via experimentation would take too long, it is difficult and expensive.

Fin cuts are another possible improvement to introduce in a MCHX design. Obviously, the improvement on the heat transfer will be null for a single-pass heat exchanger since all the tubes have the same temperature and the heat conduction between them would be zero. Thus, it is worth assessing the improvement due to fin cuts in a MCHX for different number of refrigerant passes.

On the other hand, depending on the model's assumptions some parameter can be studied or not, e.g. the impact of the aspect ratio (*L/H*) on the heat transfer of a heat

exchanger would be null if it is evaluated with a model which applies the adiabatic-fin-efficiency. This design parameter can only be assessed if model adequately accounts for the heat conduction between tubes.

According to the ideas previously exposed, the authors considered to study some design parameters of a MCHX such as: aspect ratio and number of refrigerant passes. The influence of fin cuts was also studied for different refrigerant circuitry. The impact of all these parameters depends strongly on the heat conduction between tubes, LHC and air-side heat transfer. Hence the need of using a model which takes into account accurately all previous phenomena, otherwise it would not be possible evaluate effects of some of mentioned parameters on MCHX performance. To this end, the simulation studies were carried out with the previously proposed model Fin1Dx3. The Fin1Dx3 model takes into account all these effects and it can simulate any refrigerant circuitry regarding the number of refrigerant passes, tubes number and tube connections. In addition, the model has the option to work in two different modes: continuous fin or cut fin. The reason for these two modes is to be able to evaluate the improvements by cutting the fins on the heat transfer.

The more sensitive the case study is to LHC and to heat conduction between tubes, the larger the impact will be on the performance due to variations of the defined parameters. Impact of LHC and heat conduction between tubes will increase as the temperature gradient on a tube and temperature difference between tubes become larger. That is the reason why a microchannel gas cooler working with CO_2 in transcritical pressures has been chosen as case study. Reasons were explained in the Introduction chapter.

5.1 Simulation methodology and case study description

The MCHX chosen for these studies corresponds to a gas cooler, according to the reasons exposed in the introduction. The gas cooler geometry is based on the gas cooler tested by Yin et al. (2001), which corresponds to a microchannel gas cooler used in automotive applications with CO_2 as working fluid in transcritical conditions. This gas cooler consists of 34 tubes with 3 refrigerant passes. The number of refrigerant passes is a parameter to be studied, from one pass up to the limit that corresponds to a serpentine gas cooler, i.e. refrigerant passes equals the tubes number, without changing the rest of gas cooler dimensions and inlet conditions. Increasing number of refrigerant passes leads to larger velocities of the refrigerant flow. This fact, besides the increase of refrigerant path length produces much larger pressure drop. The limit case (serpentine MCHX) would be, for this reason, of no practical use.

Table 5.1. Geometric characteristics of gas cooler for simulation studies.			
Face area (cm2)	242.5	Refrigerant side area (cm2)	609
Air side area (cm2)	6465	Tubes number of tubes	12
Tube length (mm)	192	Core depth (mm)	16.5
Fin type	Louvered	Fin density (fins/in)	22
Number of ports	11	Port diameter (mm)	0.79
Wall thickness (mm)	0.43	Fin height (mm)	8.89
Fin thickness (mm)	0.1		

The total number of tubes and some geometric dimensions of the gas cooler tested by Yin et al. (2001) (Table 3.3) have been modified so that the change in the number of refrigerant passes will not produce excessive pressure losses for the serpentine case. The total number of tubes was reduced to 12 and the rest of dimensions such as gas cooler width and height were obtained rescaling the original ones proportionally to the tubes number. The resulting geometric data is shown in Table 5.1. The rest of geometric data for fins and tubes were the same as Yin et al. (2001) tested (Table 3.3).

Table 5.2. Operating conditions for simulation studies: based on test n° 2 (Yin et al., 2001).

	Inlet Pressure (kPa)	Pressure drop (kPa)	Inlet temperature (°C)	Outlet temperature (°C)	Mass flow rate (g/s)
CO_2	10792	421.6	138.6	48.2	5.64
Air	100	$61\ 10^{-3}$	43.5	-	87.3

For all scenarios the refrigerant and air side areas, face area and rest of the geometry are the same. Inlet conditions for both fluids in the gas cooler are going to be identical for all simulation studies. Regarding the operating conditions, those corresponding to test nº 2 from Yin et al. (2001) have been chosen. Both the mass flow rate and air flow rate have been modified in order to get the same mass velocities as the original values according to the new geometry. The operating conditions are listed in Table 5.2. Regarding the air, there are two scenarios: with the mass flow rate given in Table 5.2, and with a mass flow rate three times the indicated in Table 5.2.

Regarding the correlations used by the model, they are listed in the Table 3.1.

5.2 Number of refrigerant passes

The number of refrigerant passes is varied from one pass up to the maximum possible number, i.e. 12 passes which corresponds to a serpentine configuration. Fig. 5.1 depicts two samples of the cases studied. The performance differences will be only due to the number of passes since refrigerant area, air side area, face area and rest of the geometry do not change.

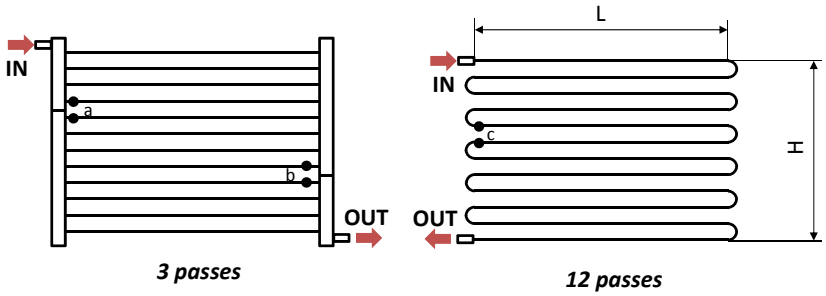

Fig. 5.1 - Schematics of two gas cooler arrangements studied: 3 and 12 refrigerant passes.

Fig. 5.2 shows the results of this study for two different values of the air velocity. As the air velocity is increased, the heat transfer is also increased for all cases due to: the mass flow rate rises since the air velocity is increased with the same face area; the overall heat transfer coefficient increases because the greater the air velocity the larger the air side heat transfer coefficient. When the number of passes is increased the total refrigerant cross-sectional area is reduced so that the refrigerant velocity rises to keep constant the mass flow rate, and it improves the heat transfer coefficient. Thus, for this case study, the figure shows clearly that the heat transfer is always raised, with an asymptotic trend, by increasing the number of passes.

Regarding refrigerant pressure losses, Fig. 5.3 shows the total pressure drop along heat exchanger when the number of refrigerant passes is modified. It has been plotted only the scenario corresponding to the air velocity of 3 m/s because these results do not depend on air velocity. It should be noticed that the case study corresponds to a gas cooler, which does not undergo a phase change.

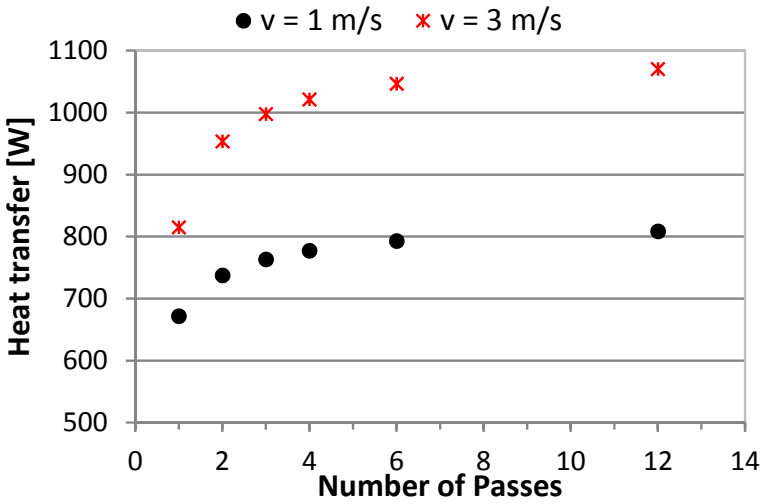

Fig. 5.2 - Heat transfer when number of refrigerant passes is changed in two scenarios: air velocity of 3 m/s and 1 m/s.

In a condenser, the pressure drop leads to a temperature drop during the phase change, therefore the temperature difference between air and refrigerant would go down and the heat transfer would be reduced. In this way, for condensers/evaporators the pressure drop plays an important role in the heat transfer, in fact there is an optimum on the heat transfer when the number of refrigerant passes is studied, because of the opposite influence of the heat transfer coefficients and pressure drop. This conclusion was also exposed by Shao et al. (2009) in their studies for a serpentine microchannel condenser, where they studied the influence on heat transfer of the number of passes.

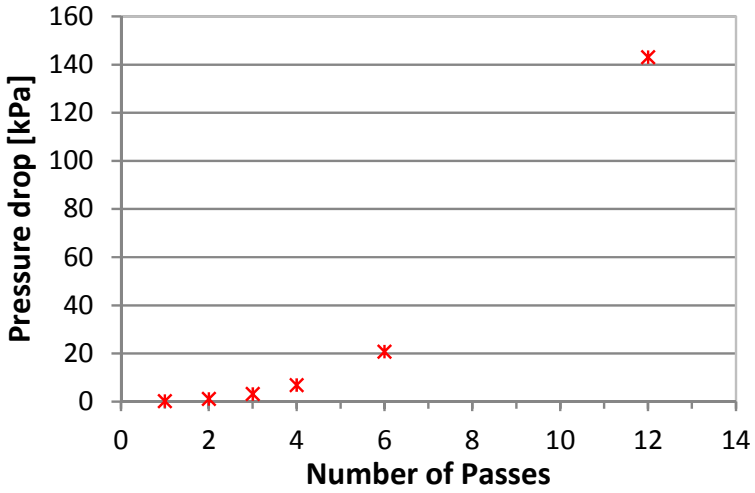

Fig. 5.3 - Refrigerant pressure drop along heat exchanger when number of refrigerant passes is changed.

5.3 Influence of the fin cuts

A technique to improve the effectiveness in air-to-refrigerant heat exchangers is by cutting the fins. The heat conduction between tubes, due to temperature differences from bottom to top fin roots, degrades the heat exchanger effectiveness. By cutting the fins, this heat conduction is avoided.

This technique is indicated for heat exchangers which have large temperature differences between tubes. For example, in a condenser there are tubes with superheated vapor flowing inside which are connected through fins to other tube with saturated vapor inside. Under these conditions large temperature differences can be expected. An extreme case corresponds to a gas cooler arrangement, in which the refrigerant undergoes a temperature variation along the whole gas cooler length, since there is no phase change. Thus the temperature difference between two neighboring tubes can be as large as 50 K.

As it was mentioned in the introduction there only exist few models that take into account heat conduction between tubes. The rest of models always overpredict the heat transfer for the same conditions since they do not account for the effectiveness degradation caused by the heat conduction. The impact expected on the effectiveness by cutting fins is not the same for a finned tube as for a MCHX. In a finned tube heat exchanger the fin cuts can be made perpendicularly to the air flow direction, thus the longitudinal heat conduction between rows of tubes is avoided, which always degrades the effectiveness. In a MCHX the fins are cut along the air flow direction so that the effect introduced by them is not fundamentally the same as for the finned tube case, in fact the improvements on the capacity are lower: Singh et al. (2010) reported capacity improvements of up to 12% for a finned tube heat exchanger whereas Park and Hrnjak (2007) obtained 3.9% for a serpentine microchannel gas cooler. Notice that, fin surfaces commonly used for MCHXs are louvered which have louvers that already prevent the longitudinal heat conduction in fin along the air direction.

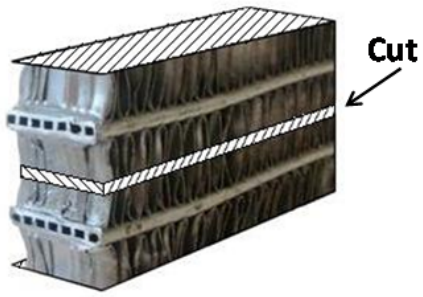

Fig. 5.4 - Schematic of the fin cut arrangement studied.

The fin cuts can be customized according to the working conditions and heat exchanger circuitry. Singh et al. (2010) analyzed different fin cuts arrangements for a finned tube gas cooler. In the present study the fin cuts studied are disposed along the middle section between two neighbor tubes for all the fins of the heat exchanger. Fig. 5.4 shows an example of this fin cut arrangement. The Fin1Dx3 model is developed for a continuous fin, but can be slightly modified to incorporate a cut in a section at half the fin height. This change implies changing two boundary condition of the piecewise function for the fin temperature, which was presented in section 3.1. As consequence of changing the boundary conditions it is also needed to obtain the new matrixes of the model: [*A*], [*B*], [*C*] (section 3.1).

To the authors' knowledge there are no numerical studies for MCHXs about the influence of the refrigerant circuitry on the impact of fin cuts. To this end, the impact of cutting the fins has been evaluated for the same refrigerant passes studied in previous subsection.

The results are shown in Fig. 5.5, where it has been plotted the heat transfer improvement by cutting fins with respect to the solution given by same model and same conditions but without fin cuts, i.e. continuous fins. The heat improvement for one pass is zero because for this arrangement all the tubes have same temperature evolution, resulting null the temperature difference between tubes at the same *X* coordinate. In such a case the adiabatic-fin-tip assumption is fundamentally correct.

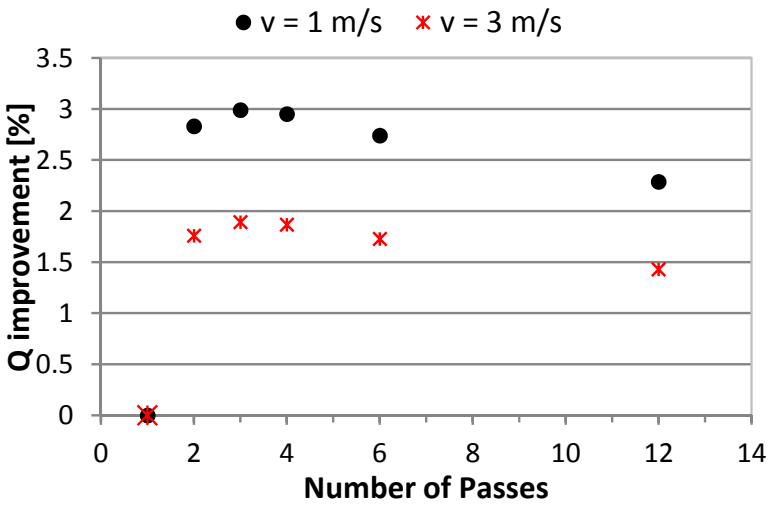

Fig. 5.5 - Improvement of heat transfer by cutting fins with respect to the same conditions but with continuous fin for different number of refrigerant passes and for two scenarios: air velocity of 1 m/s and 3 m/s.

The first interesting fact is that the influence of the air velocity on the parameter studied does not change the trend of the curves, it only moves them vertically. Thus, if

we study the plot for v=1 m/s, when the number of passes is different from one there is always an improvement on the heat transfer by cutting the fins and, for the studied conditions, there is a maximum value for 3 passes, regardless the air velocity. A possible explanation for the presence of a maximum in the heat improvement is described below.

When the number of passes is two, the fin roots which connect two tubes of different passes (central tubes of the heat exchanger) have a large temperature difference that produces a heat conduction flux. As the number of passes is increased the temperature difference between tubes decreases but the number of fins with such a temperature difference rises. Fig. 5.1 illustrates this explanation, where the heat exchanger with 3 passes has two zones with large temperature difference, regions “a” and “b”. The serpentine heat exchanger has a similar and small temperature difference between all the tubes, which can be represented by the temperature difference at zone “c”. Heat exchanger with 3 passes will have only two zones with temperature difference, but the temperature difference between bottom and top of zones “a” or “b” is much higher than corresponding value for region “c” of the serpentine case, though serpentine MCHX has 11 regions with a similar temperature difference to the “c” zone. These opposite effects could be one of the reasons to explain the presence of the maximum depicted in Fig. 5.5.

Regarding the influence of the air velocity on these results, Fig. 5.5 shows that the lower the velocity the larger the improvement. This fact was already pointed out by Singh et al. (2010) in their simulation studies for a finned tube gas cooler.

The maximum improvement that can be obtained depends on the air velocity, but for the scenarios studied this improvement is as much 3%. Similar values were reported by Park and Hrnjak (2007) who measured capacity improvements of up to 3.9% for a serpentine gas cooler.

5.4 Influence of aspect ratio for a serpentine gas cooler

A serpentine MCHX corresponds to a MCHX with a single tube which is bended in order to get a specific number of refrigerant passes. It has the particularity of not having headers therefore it is highly recommended for saving refrigerant charge thanks to its reduced internal volume.

A restriction for these studies is that air side and face area are constants while aspect ratio (*L*/*H*) changes. By observation of the serpentine MCHX design, it is deducible that the air side heat transfer area is proportional to the product: *Np L*. Therefore, to study the isolated effect of the aspect ratio on the performance, *Np L* will have to remain unchanged for all the cases studied. The baseline gas cooler corresponds to the twelve-pass gas cooler studied in subsection 5.2. When aspect ratio changes, gas cooler length becomes larger or shorter so that the number of refrigerant passes will have to change to keep *Np L* constant. Table 5.3 lists the corresponding length *L*, gas cooler height *H*, and aspect ratio, when the number of refrigerant passes *Np* is varied according to previous restrictions.

Table 5.3. Geometric variables in the aspect ratio study for a serpentine gas cooler.

Number of passes	Length (m)	Height (m)	Aspect ratio
2	1.15E+00	2.02E-02	5.70E+01
4	5.76E-01	4.04E-02	1.43E+01
6	3.84E-01	6.06E-02	6.34E+00
8	2.88E-01	8.08E-02	3.56E+00
10	2.30E-01	1.01E-01	2.28E+00
12	1.92E-01	1.21E-01	1.58E+00
14	1.65E-01	1.41E-01	1.16E+00
16	1.44E-01	1.62E-01	8.91E-01

Since the tube length changes, the number of segments used by the model to discretize the gas cooler were also changed in order to keep same accuracy for all cases. Fig. 5.6 shows the results for the predicted heat transfer as function of the aspect ratio. The figure shows the results for the two analyzed cases: the fin is cut and a continuous fin. The figure shows that aspect ratio has no effect on heat transfer when the fin is cut, thus models that apply adiabatic-fin-tip assumption will not be able to study this influence since results are always the same.

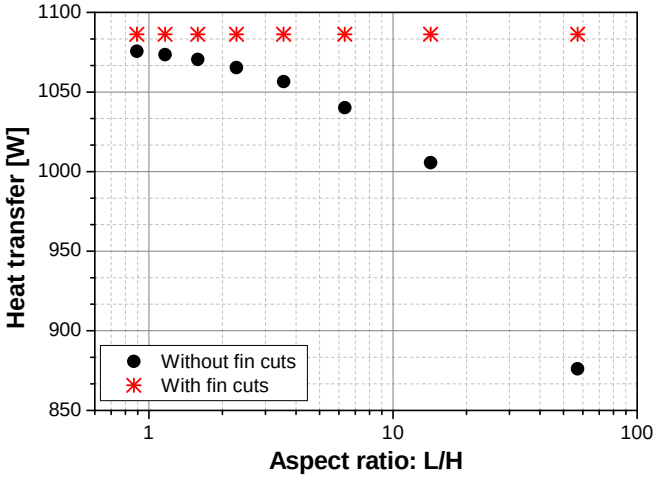

Fig. 5.6 – Heat transfer of the gas cooler when the aspect ratio is varied for two scenarios: continuous fin and fin with cuts.

For the case of continuous fin, Fig. 5.6 shows that heat transfer has a strong dependence on the gas cooler aspect ratio. According to Table 5.3, the highest value of aspect ratio corresponds to *Np*=2 while lowest value correspond to *Np*=16, therefore Fig. 5.6 shows that is preferably using lots of refrigerant passes with a short heat exchanger length instead of few passes with a large length, resulting in an asymptotic trend. An interesting observation is that the asymptote looks to be the capacity for the cut fin case. This fact means that the aspect ratio which maximizes the heat transfer corresponds to the value that minimizes the heat conduction between tubes.

Notice that these conclusions are not affected by pressure losses phenomena because the refrigerant cross-sectional area and total length of refrigerant path are the same for all cases, therefore the pressure losses will be rather the same.

5.5 Conclusions

For application where natural refrigerants are used, MCHX minimizes the impact of their disadvantages, e.g. flammability and high pressures, thanks to its high compactness, reduced volumes and high mechanical strength.

From the designer's point of view, some parameters of MCHXs such as number of refrigerant passes, aspect ratio and effect of fin cuts, are hard and expensive to determine by experimentation. On the other hand, success of simulation tools to this end depends on the model's assumptions, i.e. some parameters produce effects that are due to phenomena that are not taken into account by the model. For instance, the

effect of the aspect ratio cannot be studied by a model that does not account for heat conduction between tubes; otherwise the results would be always the same. The capabilities of Fin1Dx3 model allowed assessing numerically the impact on the heat exchanger performance of: number of refrigerant passes, aspect ratio and effect of fin cuts. Thus, the presented numerical studies are hardly available in literature for MCHXs.

For a gas cooler working with CO_2 under transcritical pressures, the main conclusions of the simulations studies were:

- For a gas cooler where no phase change occurs, heat transfer is always increased by increasing the number of refrigerant passes regardless the increase of pressure drop.
- The fin cuts always increase the heat transfer. In the gas cooler analyzed, the improvement with regard to the continuous fin depends on the air velocity and number of refrigerant passes. The lower the velocity, the greater the capacity improvement. When the number of refrigerant passes is varied, there is an optimum value regardless the air velocity, which is 3 passes for the analyzed case. The improvement in heat transfer was as much as 3%.
- Regarding the aspect ratio of a serpentine heat exchanger, given a heat transfer area and a face area, the best aspect ratio corresponds to a gas cooler with reduced length (*L*) and large height (*H*). The reason is based on the fact that this configuration reduces the heat conduction between tubes.

CHAPTER 6

CONCLUSIONS

6 CONCLUSIONS

Below are summarized the most important conclusions of each chapter. Finally, a summary of the contributions of the thesis to the state of the art in MCHX modeling is presented, and publications resulting of this PhD work are listed.

6.1 Global Conclusions

Along the introduction the usefulness of MCHX and its relatively recent and increasing application in HVAC&R industry was discussed. A simulation model is an interesting tool for the designer and nowadays there only exist few models for this kind of HXs. In the introduction, these models were analyzed and some problems were identified related to the phenomena modeled. The problems and effects identified in the introduction were:

- Different variation of fluid properties for air and refrigerant along a segment.
- Effect of 2D longitudinal heat conduction (2D LHC).
- Heat conduction between tubes along the fin: application of adiabatic-fin-tip assumption.
- Application of the fin theory, which assumes uniform temperature throughout the air in contact with the fin.

The main objective of the thesis is to develop an accurate and suitable model for design purposes of MCHX. To this end the authors decided to study the previous mentioned effects in some applications of MCHX and once the impact of them was assessed, to develop the definitive model.

In order to study and evaluate impact of each phenomenon, Fin2D model was created to obtain very accurate results. It is a very detailed model which allows detecting inaccuracy sources by evaluating the isolate impact of each effect previously mentioned. Fin2D does not use the fin efficiency, accounts for 2D LHC in fins and tubes, accounts for the heat conduction between tubes, and applies a detailed discretization for the air, which is independent of the refrigerant discretization. Fin2D subdivides the heat exchanger into segments and cells (air, refrigerant, fin, tube wall), to which a system of energy conservation equations is applied without traditional heat exchanger modeling assumptions. Few models in literature takes into account these phenomena and all of them apply FEM techniques instead of FVM that is employed by Fin2D, which a priori requires less computational effort.

The scenario analyzed with Fin2D model corresponded to a gas cooler working with CO_2 under transcritical pressure. Main conclusions of the studies carried out with Fin2D model are:

- When classical approaches were analyzed, the error obtained using the ε-NTU method depends on the ε-NTU relationship employed to calculate the effectiveness of each segment. For the studied case, the error is smaller than 3.5% when the relationship for refrigerant mixed and air unmixed (RMAU) is used, whereas the error is smaller than 1% when the relationship for both fluids considered as unmixed (BU) is used. The error becomes larger as the air-side heat transfer coefficient increases. In general, the best option for the studied case is to use the tube-by-tube approach and to consider both fluids as unmixed, though the effect of the mixed refrigerant assumption turned out negligible in the scenarios studied. On the other hand, a tube-by-tube approach can lead to larger errors when long length tubes are simulated because refrigerant properties and heat transfer coefficients can have significant variations, particularly when the refrigerant undergoes a phase change. It was reported that application of a segment-by-segment approach when the RMAU relationship is adopted produces an inconsistency in results.
- For the operating conditions studied, the impact of LHC effects along each direction in fins and tube walls, if considered separately, is not significant. The combined effect is more noticeable and may result in a capacity prediction error of as much as 2.5%, with the LHC_Z in the tube being the dominant effect.
- Using the adiabatic-fin-tip efficiency, which is commonly applied, leads to large errors in heat distribution per tube, and therefore in the prediction of temperature at the tube outlet, when a temperature difference between tubes exists.
- The temperature of air close to the tube wall is very different than the bulk air temperature. This fact could have an important impact on local effects controlling the heat and mass transfer, e.g. dehumidification.

Fin2D model was good to identify the deficiency sources of the classical methodologies in such kind of heat exchangers, but was no good to evaluate the global performance when an actual MCHX is simulated regarding number of tubes and number of refrigerant passes. The main reason which did not allow studying the whole microchannel gas cooler was the large computation time required by Fin2D model. This computational cost is mainly due to the fin surface discretization: the model needs to employ a large number of fin cells because no fin efficiency is used to solve the heat transfer equation along the fin.

6. CONCLUSIONS

Given the main conclusions about the impact of different phenomena and modeling assumptions in a MCHX, a new model was proposed in order to reduce the computational cost but preserving same accuracy. To this end, Fin1Dx3 model was proposed which is based on the Fin2D model but without modeling the negligible effects and changing the model structure and/or discretization. The result is a much faster model with almost the same accuracy as Fin2D model. Due to this computation time reduction, Fin1Dx3 allows analyzing microchannel condensers and gas coolers with any refrigerant circuitry, including serpentine heat exchangers.

Main conclusions about Fin1Dx3 model and its validation are the following:

- The Fin1Dx3 model accounts for all the same effects than Fin2D model except the LHC in the fin along *Z* direction which, in any case, has been found not to be important. Fin1Dx3 is based on a novel discretization methodology for the air and fin wall that only needs three air cells along the *Y* direction. This methodology allows reducing drastically the number of cells to compute, with regard to the Fin2D model, and consequently the simulation time but keeping a high resolution along *Y* direction.
- The large number of fin cells needed by Fin2D model to solve accurately the air-side heat transfer, is compensated in Fin1Dx3 with a novel methodology to describe the air-side heat transfer, using a piecewise function for the fin temperature. This piecewise function, together with the employed air discretization, allows applying in a more fundamental way the analytical solution given by the fin theory.
- The main capabilities of Fin1Dx3 are: 2D-LHC in the tube wall; non-mixed air effects due to temperature difference between bulk air and the air close to the tubes; and it accounts fundamentally for heat conduction between tubes since it does not apply adiabatic-fin-tip assumption.
- The equations have been discretized, with the interesting characteristic of resulting in a system of pseudo-linear equations with respect to the variables of the problem. A numerical scheme has been proposed to solve the problem as a series of explicit steps. The numerical scheme proposed allows computing the three fin cells with the computational effort of just one fin cell.
- Fin1Dx3 model was validated with experimental data, for both condenser and gas cooler. The predicted capacity is within ±5% error, being much more accurate for the gas cooler scenario.
- The study about the influence of the factor φ, which accounts for the effects of un-mixed air flow along Y direction, showed deviations less than 5% for extreme values of φ and for the simulated conditions.

An evaluation of capabilities of Fin1Dx3 model as simulation tool was carried out. To this end, Fin1Dx3 model was compared in terms of computational cost and accuracy against others modeling approaches: Fin2D, a simplified approach based on Fin1Dx3 (Fin1D model), and an approach (Corrected-Fin model) representative of other models from literature (Lee and Domanski, 1997; and Singh et al., 2008). Main conclusions of these comparisons were the following:

- The solving time of Fin1Dx3 has been reduced one order of magnitude with regard to the time employed by Fin2D, whereas the differences on the results are less than 0.3%, which are considered as negligible for practical applications. The solving time difference between Fin1Dx3 and Fin1D turned out to be twice.
- Corrected-Fin can lead to accurate results when compared with an equivalent approach model that models heat conduction between tubes in a less artificial way like Fin1Dx3 does. Difference between predicted results of both models was between 1% and 2%. Computational cost of Fin1D and Corrected-Fin models are the same. Nevertheless, author would like to emphasize the fact that the present work shows no computational saving or accuracy increase by adding correction terms to an approach that uses the adiabatic-fin-tip efficiency with regard to a more fundamental approach, regarding the heat conduction between tubes phenomena, like Fin1D.
- By comparison of deviations between Fin1D, Corrected-Fin and Fin1Dx3 models, it was concluded that the main responsible for differences between them were the effects of non-mixed air along fin height.
- Based on the conclusions, author and directors of the thesis decided to use in the following the Fin1Dx3 model with continuous fin for simulation of MCHXs.

Finally, in order to show the application of the Fin1Dx3 model as simulation tool for design purposes, it was used to carry out numerical studies about the influence of some design parameters of a MCHX on its performance. From the designer's point of view, some parameters of MCHXs are hard and expensive to determine by experimentation. On the other hand, success of simulation tools to this end depends on the model's assumptions, e.g. the effect of the aspect ratio cannot be studied by a model that does not account for heat conduction between tubes; otherwise the results would be always the same. The capabilities of Fin1Dx3 model allowed assessing numerically the impact on the heat exchanger performance of some design parameters for a microchannel gas cooler working with CO_2 under transcritical pressures. These studies consisted of:

- Influence of the number of refrigerant passes on the capacity.

- Influence of the fin cuts on the capacity.
- Influence of the aspect ratio (*L*/*H*) for a serpentine microchannel gas cooler.

The main conclusions of these studies were:

- For a gas cooler where no phase change occurs, heat transfer is always increased by increasing the number of refrigerant passes regardless the increase of pressure drop.
- The fin cuts always increase the heat transfer. In the gas cooler analyzed, the improvement with regard to the continuous fin depends on the air velocity and number of refrigerant passes. The lower the velocity, the greater the capacity improvement. When the number of refrigerant passes is varied, there is an optimum value regardless the air velocity, which is 3 passes for the analyzed case. The improvement in heat transfer was as much as 3%.
- Regarding the aspect ratio of a serpentine heat exchanger, given a heat transfer area and a face area, the best aspect ratio corresponds to a gas cooler with reduced length (*L*) and large height (*H*). The reason is based on the fact that this configuration reduces the heat conduction between tubes.

6.2 Contributions and publications

In conclusion, from the author's point of view, the most important contributions of this thesis to the state of the art in heat exchangers modeling are:

- ✓ The effect of each phenomenon involved in the heat transfer for a MCHX has been evaluated. This analysis allowed identifying the phenomena with the largest effect in the performance of MCHXs.

- ✓ If the classical approach ε-NTU is employed to model heat exchangers, the relationship used to calculate the effectiveness of each segment has to be chosen carefully. An important finding in the thesis is that using the relationship for the arrangement of mixed refrigerant and unmixed air (RMAU) produces an inconsistency in results if a segment-by-segment approach is adopted or vice versa.

- ✓ A unique methodology has been developed to model MCHXs that reduces the computational cost retaining the accuracy. The high accuracy is achieved by using a novel approach to model the air-side heat transfer. This approach also allows getting low computational cost by applying the proposed solving methodology.

- ✓ A high accuracy model for simulation of MCHXs: condensers and gas coolers, has been developed. It has a low computational cost, which is useful for design purposes. This model has been validated against experimental data.

- ✓ The proposed model allows assessing the influence of some important design parameters that are not evaluable by any other model from literature, with a similar computational cost and with such a high accuracy. The model has been applied to perform numerical studies about the influence of these design parameters on the performance of a MCHX. These kind of numerical studies are not present in literature.

- ✓ The thesis has shown that it is possible to take into account the heat conduction between tubes in a less artificial way than other fin efficiency based approaches, which have to add heat conduction terms after assuming adiabatic-fin-tip, what is inconsistent to a certain extent. The alternative methodology, proposed in this work, consists in evaluating the heat transfer by integration of the corresponding fin temperature profile instead of using a fin efficiency which cannot always be defined, e.g. when temperature at fin roots are different. It has been shown that this integration does not represent a serious drawback for the computation, since it can be easily discretized consistently with the rest of governing equations, regardless the number of air-fin cells used. Thus, there is neither accuracy nor computational cost reasons to apply adiabatic-fin-tip assumption when in general it is not satisfied.

The following journal papers were published or are already submitted but pending of acceptation for publication as an outcome of the research conducted in this thesis:

- Martínez-Ballester S., Corberán, José-M., Gonzálvez-Maciá, J., Domanski, P.A., 2011. Impact of Classical Assumptions in Modelling a Microchannel Gas Cooler, International Journal of Refrigeration, 34, 1898-1910.
- Martínez-Ballester S., Corberán, José-M., Gonzálvez-Maciá, J. Numerical Model for Microchannel Condensers and Gas Coolers: Part I – Model Description and Validation, International Journal of Refrigeration, *In press,* DOI: 10.1016/j.ijrefrig.2012.08.023.
- Martínez-Ballester S., Corberán, José-M., Gonzálvez-Maciá, J. Numerical Model for Microchannel Condensers and Gas Coolers: Part II – Simulation Studies and Models Comparison, International Journal of Refrigeration, *In press*, DOI: 10.1016/j.ijrefrig.2012.08.024.

The following conference papers were published as an outcome of the research conducted in this thesis:

- Martínez-Ballester, S., José-M. Corberán, J., Gonzálvez-Maciá, J., 2012. A Novel Approach to Model the Air-Side Heat Transfer in Microchannel Condensers, 6th European Thermal Sciences Conference, Poitiers, France.
- Martínez-Ballester S., Gonzálvez-Maciá, J., Corberán, José-M., 2012. Impact of the Refrigerant Layout and Fin Cuts on the Performance of a Microchannel Condenser and a Gas Cooler, 14th International Refrigeration and Air-Conditioning conference at Purdue, IN, USA.
- Martínez-Ballester S., Corberán, José-M., Gonzálvez-Maciá, J., 2012. Impact of Fin Cuts and Refrigerant Layout on the Performance of a Microchannel Gas Cooler Working with Transcritical CO_2, 10th IIR Gustav Lorentzen Conference on Natural Refrigerants, Delft, The Netherlands.
- Martínez-Ballester S., Corberán, José-M., Gonzálvez-Maciá, J., 2011. Numerical Model for a Microchannel Gas Cooler with any Refrigerant Circuitry, 23rd IIR International Congress of Refrigeration, Prague, Czech Republic.
- Martínez-Ballester S., Gonzálvez-Maciá, J., Corberán, José-M., 2011. Influencia de la Circuitería y Cortes en las Aletas de un Enfriador de Gas de Microcanales, VII Congreso Nacional de Ingeniería Termodinámica, Bilbao, Spain.
- Martínez-Ballester S., Corberán, José-M., Gonzálvez-Maciá, J., Domanski, P.A., 2010. Analysis of Segment-by-Segment ε-NTU Modelling of a Minichannel CO2 Gas Cooler, 13th International Refrigeration and Air-Conditioning conference at Purdue, IN, USA.

6.3 Future work

In order to use this model as a design tool by manufacturers, researchers and academic personnel it has to be slightly developed in following points:

- User's graphical interface (GUI): Currently, definition of heat exchanger geometry, circuitry, operating correlations and correlations was performed by using external files (excel files) or just directly in the source code. A GUI is planned to be developed for definitions of all these parameters.
- Simplification of source code: Thanks to the object oriented programming language used in the thesis, the source code is quite robust and compact. Nevertheless, the model was developed for research on modeling

approaches, so the existing source code can be re-arranged and more closed to changes, i.e. less flexible. This task will allow having a simpler, faster and more compact source code.

- Evaporator Model: Currently, Fin1Dx3 only is valid for condensers since it does not include dehumidification. Fin1Dx3 model will be extended to include dehumidification and then serve also as simulation tool for MCHX evaporators. For an evaporator author and directors foresee that differences in accuracy with regard to other existing models will be larger due to dehumidification. Dehumidification depends strongly on what happens in tube and fin wall, and Fin1Dx3 models much better these phenomena at these locations. Thus the impact of dehumification on performance of a MCHX evaporator is a phenomenon to be studied with Fin1Dx3 model in next future.
- Flow maldistribution: In the governing equations of the Fin1Dx3 model, uniform flow distribution for both fluids was assumed. This assumption is nearly true in a condenser but not for an evaporator. In the air side, the air flow maldistribution is really a problem in defining the air distribution at inlet rather than a problem in governing equations. Despite the fact that Fin1Dx3 model assumed uniform flow distribution for both fluids, the governing equations for modeling the flow distribution was placed at the mixture cells. Thus, their governing equations can be easily modified without affecting the rest of source code.

CHAPTER 7

APPENDICES

7 APPENDICES

7.1 Appendix A: Matrix coefficients for both continuous fin and cut fin.

This appendix contains the matrix coefficients of [*B*] and [*C*]. Following nomenclature has been used:

$$\mathrm{m}_{a(i)} \rightarrow m_{f,a(i)} = \sqrt{\frac{\alpha_{f,a(i)}\, pw_{f,a(i)}}{k_f\ A_{f,a(i)}}}$$

7.1.1 [*B*] for continuous fin

$B_{1,j}$

$$B_{1,1}=-((-1+e^{\varphi H_f m_{a1}})(e^{\varphi H_f (m_{a1}+4 m_{a2}+2 m_{a3})}(m_{a1}-2 m_{a2})(m_{a2}-m_{a3})+e^{2 H_f m_{a2}}(-m_{a1}+2 m_{a2})(m_{a2}-m_{a3})-e^{\varphi H_f m_{a1}+2 H_f m_{a2}}(m_{a1}+2 m_{a2})(m_{a2}-m_{a3})+e^{2\varphi H_f (2 m_{a2}+m_{a3})}(m_{a1}+2 m_{a2})(m_{a2}-m_{a3})-e^{\varphi H_f (m_{a1}+4 m_{a2})}(m_{a1}-2 m_{a2})(m_{a2}+m_{a3})-e^{2 H_f (m_{a2}+\varphi m_{a3})}(-m_{a1}+2 m_{a2})(m_{a2}+m_{a3})-e^{4\varphi H_f m_{a2}}(m_{a1}+2 m_{a2})(m_{a2}+m_{a3})+e^{H_f (2 m_{a2}+\varphi (m_{a1}+2 m_{a3}))}(m_{a1}+2 m_{a2})(m_{a2}+m_{a3})))/(\varphi H_f m_{a1}(e^{2\varphi H_f (m_{a1}+2 m_{a2}+m_{a3})}(m_{a1}-m_{a2})(m_{a2}-m_{a3})+e^{2 H_f m_{a2}}(-m_{a1}+m_{a2})(m_{a2}-m_{a3})-e^{2 H_f (\varphi m_{a1}+m_{a2})}(m_{a1}+m_{a2})(m_{a2}-m_{a3})+e^{2\varphi H_f (2 m_{a2}+m_{a3})}(m_{a1}+m_{a2})(m_{a2}-m_{a3})-e^{2\varphi H_f (m_{a1}+2 m_{a2})}(m_{a1}-m_{a2})(m_{a2}+m_{a3})-e^{2 H_f (m_{a2}+\varphi m_{a3})}(-m_{a1}+m_{a2})(m_{a2}+m_{a3})-e^{4\varphi H_f m_{a2}}(m_{a1}+m_{a2})(m_{a2}+m_{a3})+e^{2 H_f (m_{a2}+\varphi (m_{a1}+m_{a3}))}(m_{a1}+m_{a2})(m_{a2}+m_{a3})))$$

$$B_{1,2}=(((-1+e^{\varphi H_f m_{a1}})^2(e^{H_f m_{a2}}-e^{2\varphi H_f m_{a2}})m_{a2}(e^{2\varphi H_f (m_{a2}+m_{a3})}(m_{a2}-m_{a3})+e^{H_f m_{a2}}(-m_{a2}+m_{a3})-e^{2\varphi H_f m_{a2}}(m_{a2}+m_{a3})+e^{H_f (m_{a2}+2\varphi m_{a3})}(m_{a2}+m_{a3})))/(\varphi H_f m_{a1}(e^{2\varphi H_f (m_{a1}+2 m_{a2}+m_{a3})}(m_{a1}-m_{a2})(m_{a2}-m_{a3})+e^{2 H_f m_{a2}}(-m_{a1}+m_{a2})(m_{a2}-m_{a3})-e^{2 H_f (\varphi m_{a1}+m_{a2})}(m_{a1}+m_{a2})(m_{a2}-m_{a3})+e^{2\varphi H_f (2 m_{a2}+m_{a3})}(m_{a1}+m_{a2})(m_{a2}-m_{a3})-e^{2\varphi H_f (m_{a1}+2 m_{a2})}(m_{a1}-m_{a2})(m_{a2}+m_{a3})-e^{2 H_f (m_{a2}+\varphi m_{a3})}(-m_{a1}+m_{a2})(m_{a2}+m_{a3})-e^{4\varphi H_f m_{a2}}(m_{a1}+m_{a2})(m_{a2}+m_{a3})+e^{2 H_f (m_{a2}+\varphi (m_{a1}+m_{a3}))}(m_{a1}+m_{a2})(m_{a2}+m_{a3})))$$

$$B_{1,3}=((2 e^{(1+2\varphi) H_f m_{a2}}(-1+e^{\varphi H_f m_{a1}})^2(-1+e^{\varphi H_f m_{a3}})^2 m_{a2} m_{a3})/(\varphi H_f m_{a1}(e^{2\varphi H_f (m_{a1}+2 m_{a2}+m_{a3})}(m_{a1}-m_{a2})(m_{a2}-m_{a3})+e^{2 H_f m_{a2}}(-m_{a1}+m_{a2})(m_{a2}-m_{a3})-e^{2 H_f (\varphi m_{a1}+m_{a2})}(m_{a1}+m_{a2})(m_{a2}-m_{a3})+e^{2\varphi H_f (2 m_{a2}+m_{a3})}(m_{a1}+m_{a2})(m_{a2}-m_{a3})-e^{2\varphi H_f (m_{a1}+2 m_{a2})}(m_{a1}-m_{a2})(m_{a2}+m_{a3})-e^{2 H_f (m_{a2}+\varphi m_{a3})}(-m_{a1}+m_{a2})(m_{a2}+m_{a3})-e^{4\varphi H_f m_{a2}}(m_{a1}+m_{a2})(m_{a2}+m_{a3})+e^{2 H_f (m_{a2}+\varphi (m_{a1}+m_{a3}))}(m_{a1}+m_{a2})(m_{a2}+m_{a3})))$$

$$B_{1,4}=(((-1+e^{\varphi H_f m_{a1}})(e^{\varphi H_f (m_{a1}+4 m_{a2}+2 m_{a3})}(m_{a1}-m_{a2})(m_{a2}-m_{a3})+e^{2 H_f m_{a2}}(-m_{a1}+m_{a2})(m_{a2}-m_{a3})-e^{\varphi H_f m_{a1}+2 H_f m_{a2}}(m_{a1}+m_{a2})(m_{a2}-m_{a3})+e^{2\varphi H_f (2 m_{a2}+m_{a3})}(m_{a1}+m_{a2})(m_{a2}-m_{a3})-$$

$$e^{\varphi H_f (m_{a1}+4 m_{a2})} (m_{a1}-m_{a2}) (m_{a2}+m_{a3}) - e^{2 H_f (m_{a2}+\varphi m_{a3})} (-m_{a1}+m_{a2}) (m_{a2}+m_{a3}) - e^{4 \varphi H_f m_{a2}} (m_{a1}+m_{a2}) (m_{a2}+m_{a3}) + e^{H_f (2 m_{a2}+\varphi (m_{a1}+2 m_{a3}))} (m_{a1}+m_{a2}) (m_{a2}+m_{a3}))) / (\varphi H_f m_{a1} ($$

$$e^{2 \varphi H_f (m_{a1}+2 m_{a2}+m_{a3})} (m_{a1}-m_{a2}) (m_{a2}-m_{a3}) + e^{2 H_f m_{a2}} (-m_{a1}+m_{a2}) (m_{a2}-m_{a3}) - e^{2 H_f (\varphi m_{a1}+m_{a2})} (m_{a1}+m_{a2}) (m_{a2}-m_{a3}) + e^{2 \varphi H_f (2 m_{a2}+m_{a3})} (m_{a1}+m_{a2}) (m_{a2}-m_{a3}) - e^{2 \varphi H_f (m_{a1}+2 m_{a2})} (m_{a1}-m_{a2})$$

$$(m_{a2}+m_{a3}) - e^{2 H_f (m_{a2}+\varphi m_{a3})} (-m_{a1}+m_{a2}) (m_{a2}+m_{a3}) - e^{4 \varphi H_f m_{a2}} (m_{a1}+m_{a2}) (m_{a2}+m_{a3}) +$$

$$e^{2 H_f (m_{a2}+\varphi (m_{a1}+m_{a3}))} (m_{a1}+m_{a2}) (m_{a2}+m_{a3}))))$$

$$B_{1,5} = ((4 e^{H_f (m_{a2}+2 \varphi m_{a2}+\varphi m_{a3})} (-1+e^{\varphi H_f m_{a1}})^2 m_{a2} m_{a3}) / (\varphi H_f m_{a1} ($$

$$e^{2 \varphi H_f (m_{a1}+2 m_{a2}+m_{a3})} (m_{a1}-m_{a2}) (m_{a2}-m_{a3}) + e^{2 H_f m_{a2}} (-m_{a1}+m_{a2}) (m_{a2}-m_{a3}) - e^{2 H_f (\varphi m_{a1}+m_{a2})} (m_{a1}+m_{a2}) (m_{a2}-m_{a3}) + e^{2 \varphi H_f (2 m_{a2}+m_{a3})} (m_{a1}+m_{a2}) (m_{a2}-m_{a3}) - e^{2 \varphi H_f (m_{a1}+2 m_{a2})} (m_{a1}-m_{a2})$$

$$(m_{a2}+m_{a3}) - e^{2 H_f (m_{a2}+\varphi m_{a3})} (-m_{a1}+m_{a2}) (m_{a2}+m_{a3}) - e^{4 \varphi H_f m_{a2}} (m_{a1}+m_{a2}) (m_{a2}+m_{a3}) +$$

$$e^{2 H_f (m_{a2}+\varphi (m_{a1}+m_{a3}))} (m_{a1}+m_{a2}) (m_{a2}+m_{a3}))))$$

$B_{2,j}$

$$B_{2,1}=-((-1+e^{\varphi H_f m_{a1}})^2 (e^{H_f m_{a2}}-e^{2\varphi H_f m_{a2}}) m_{a1} (e^{2\varphi H_f (m_{a2}+m_{a3})} (m_{a2}-m_{a3})+e^{H_f m_{a2}} (-m_{a2}+m_{a3})-e^{2\varphi H_f m_{a2}} (m_{a2}+m_{a3})+e^{H_f (m_{a2}+2\varphi m_{a3})} (m_{a2}+m_{a3})))/((-1+2\varphi) H_f m_{a2} (e^{2\varphi H_f (m_{a1}+2m_{a2}+m_{a3})} (m_{a1}-m_{a2}) (m_{a2}-m_{a3})+e^{2H_f m_{a2}} (-m_{a1}+m_{a2}) (m_{a2}-m_{a3})-e^{2H_f (\varphi m_{a1}+m_{a2})} (m_{a1}+m_{a2}) (m_{a2}-m_{a3})+e^{2\varphi H_f (2m_{a2}+m_{a3})} (m_{a1}+m_{a2}) (m_{a2}-m_{a3})-e^{2\varphi H_f (m_{a1}+2m_{a2})} (m_{a1}-m_{a2}) (m_{a2}+m_{a3})-e^{2H_f (m_{a2}+\varphi m_{a3})} (-m_{a1}+m_{a2}) (m_{a2}+m_{a3})-e^{4\varphi H_f m_{a2}} (m_{a1}+m_{a2}) (m_{a2}+m_{a3})+e^{2H_f (m_{a2}+\varphi (m_{a1}+m_{a3}))} (m_{a1}+m_{a2}) (m_{a2}+m_{a3})))$$

$$B_{2,2}=(((e^{H_f m_{a2}}-e^{2\varphi H_f m_{a2}}) (e^{2\varphi H_f (m_{a2}+m_{a3})} (m_{a1} (m_{a2}-2 m_{a3})-m_{a2} m_{a3})-e^{H_f m_{a2}} (m_{a1} (m_{a2}-2 m_{a3})+m_{a2} m_{a3})+e^{2\varphi H_f (m_{a1}+m_{a2}+m_{a3})} (m_{a1} (m_{a2}-2 m_{a3})+m_{a2} m_{a3})+e^{H_f (2\varphi m_{a1}+m_{a2})} (-m_{a1} m_{a2}+2 m_{a1} m_{a3}+m_{a2} m_{a3})+e^{2\varphi H_f (m_{a1}+m_{a2})} (m_{a2} m_{a3}-m_{a1} (m_{a2}+2 m_{a3}))+e^{H_f (m_{a2}+2\varphi (m_{a1}+m_{a3}))} (m_{a2} m_{a3}+m_{a1} (m_{a2}+2 m_{a3}))-e^{2\varphi H_f m_{a2}} (m_{a2} m_{a3}+m_{a1} (m_{a2}+2 m_{a3}))+e^{H_f (m_{a2}+2\varphi m_{a3})} (-m_{a2} m_{a3}+m_{a1} (m_{a2}+2 m_{a3})))/((-1+2\varphi) H_f m_{a2} (e^{2\varphi H_f (m_{a1}+2m_{a2}+m_{a3})} (m_{a1}-m_{a2}) (m_{a2}-m_{a3})+e^{2H_f m_{a2}} (-m_{a1}+m_{a2}) (m_{a2}-m_{a3})-e^{2H_f (\varphi m_{a1}+m_{a2})} (m_{a1}+m_{a2}) (m_{a2}-m_{a3})+e^{2\varphi H_f (2m_{a2}+m_{a3})} (m_{a1}+m_{a2}) (m_{a2}-m_{a3})-e^{2\varphi H_f (m_{a1}+2m_{a2})} (m_{a1}-m_{a2}) (m_{a2}+m_{a3})-e^{2H_f (m_{a2}+\varphi m_{a3})} (-m_{a1}+m_{a2}) (m_{a2}+m_{a3})-e^{4\varphi H_f m_{a2}} (m_{a1}+m_{a2}) (m_{a2}+m_{a3})+e^{2H_f (m_{a2}+\varphi (m_{a1}+m_{a3}))} (m_{a1}+m_{a2}) (m_{a2}+m_{a3})))$$

$$B_{2,3}=(-((e^{H_f m_{a2}}-e^{2\varphi H_f m_{a2}}) (-1+e^{\varphi H_f m_{a3}})^2 (e^{H_f m_{a2}} (m_{a1}-m_{a2})+e^{2\varphi H_f (m_{a1}+m_{a2})} (-m_{a1}+m_{a2})-e^{2\varphi H_f m_{a2}} (m_{a1}+m_{a2})+e^{H_f (2\varphi m_{a1}+m_{a2})} (m_{a1}+m_{a2})) m_{a3})/((-1+2\varphi) H_f m_{a2} (e^{2\varphi H_f (m_{a1}+2m_{a2}+m_{a3})} (m_{a1}-m_{a2}) (m_{a2}-m_{a3})+e^{2H_f m_{a2}} (-m_{a1}+m_{a2}) (m_{a2}-m_{a3})-e^{2H_f (\varphi m_{a1}+m_{a2})} (m_{a1}+m_{a2}) (m_{a2}-m_{a3})+e^{2\varphi H_f (2m_{a2}+m_{a3})} (m_{a1}+m_{a2}) (m_{a2}-m_{a3})-e^{2\varphi H_f (m_{a1}+2m_{a2})} (m_{a1}-m_{a2}) (m_{a2}+m_{a3})-e^{2H_f (m_{a2}+\varphi m_{a3})} (-m_{a1}+m_{a2}) (m_{a2}+m_{a3})-e^{4\varphi H_f m_{a2}} (m_{a1}+m_{a2}) (m_{a2}+m_{a3})+e^{2H_f (m_{a2}+\varphi (m_{a1}+m_{a3}))} (m_{a1}+m_{a2}) (m_{a2}+m_{a3})))$$

$$B_{2,4}=(-(2 e^{\varphi H_f m_{a1}} (e^{H_f m_{a2}}-e^{2\varphi H_f m_{a2}}) m_{a1} (e^{2\varphi H_f (m_{a2}+m_{a3})} (m_{a2}-m_{a3})+e^{H_f m_{a2}} (-m_{a2}+m_{a3})-e^{2\varphi H_f m_{a2}} (m_{a2}+m_{a3})+e^{H_f (m_{a2}+2\varphi m_{a3})} (m_{a2}+m_{a3})))/((-1+2\varphi) H_f m_{a2} (e^{2\varphi H_f (m_{a1}+2m_{a2}+m_{a3})} (m_{a1}-m_{a2}) (m_{a2}-m_{a3})+e^{2H_f m_{a2}} (-m_{a1}+m_{a2}) (m_{a2}-m_{a3})-e^{2H_f (\varphi m_{a1}+m_{a2})}$$

$$(m_{a1}+m_{a2})\ (m_{a2}-m_{a3})+e^{2\varphi H_f (2m_{a2}+m_{a3})}\ (m_{a1}+m_{a2})\ (m_{a2}-m_{a3})-e^{2\varphi H_f (m_{a1}+2m_{a2})}\ (m_{a1}-m_{a2})$$
$$(m_{a2}+m_{a3})-e^{2H_f (m_{a2}+\varphi m_{a3})}\ (-m_{a1}+m_{a2})\ (m_{a2}+m_{a3})-e^{4\varphi H_f m_{a2}}\ (m_{a1}+m_{a2})\ (m_{a2}+m_{a3})+$$
$$e^{2H_f (m_{a2}+\varphi (m_{a1}+m_{a3}))}\ (m_{a1}+m_{a2})\ (m_{a2}+m_{a3}))))$$

$$B_{2,5}=(-(2\ e^{\varphi H_f m_{a3}}\ (e^{H_f m_{a2}}-e^{2\varphi H_f m_{a2}})\ (e^{H_f m_{a2}}\ (m_{a1}-m_{a2})+e^{2\varphi H_f (m_{a1}+m_{a2})}\ (-$$
$$m_{a1}+m_{a2})-e^{2\varphi H_f m_{a2}}\ (m_{a1}+m_{a2})+e^{H_f (2\varphi m_{a1}+m_{a2})}\ (m_{a1}+m_{a2}))\ m_{a3})/((-1+2\ \varphi)\ H_f\ m_{a2}\ ($$
$$e^{2\varphi H_f (m_{a1}+2m_{a2}+m_{a3})}\ (m_{a1}-m_{a2})\ (m_{a2}-m_{a3})+e^{2H_f m_{a2}}\ (-m_{a1}+m_{a2})\ (m_{a2}-m_{a3})-e^{2H_f (\varphi m_{a1}+m_{a2})}$$
$$(m_{a1}+m_{a2})\ (m_{a2}-m_{a3})+e^{2\varphi H_f (2m_{a2}+m_{a3})}\ (m_{a1}+m_{a2})\ (m_{a2}-m_{a3})-e^{2\varphi H_f (m_{a1}+2m_{a2})}\ (m_{a1}-m_{a2})$$
$$(m_{a2}+m_{a3})-e^{2H_f (m_{a2}+\varphi m_{a3})}\ (-m_{a1}+m_{a2})\ (m_{a2}+m_{a3})-e^{4\varphi H_f m_{a2}}\ (m_{a1}+m_{a2})\ (m_{a2}+m_{a3})+$$
$$e^{2H_f (m_{a2}+\varphi (m_{a1}+m_{a3}))}\ (m_{a1}+m_{a2})\ (m_{a2}+m_{a3}))))$$

$B_{3,j}$

$$B_{3,1}=(2\ e^{(1+2\varphi)\,H_f\,m_{a2}}\ (-1+e^{\varphi H_f\,m_{a1}})^2\ (-1+e^{\varphi H_f\,m_{a3}})^2\ m_{a1}\ m_{a2})/(\varphi\ H_f\ m_{a3}\ (e^{2\varphi H_f\,(m_{a1}+2\,m_{a2}+m_{a3})}\ (m_{a1}-m_{a2})\ (m_{a2}-m_{a3})+e^{2\,H_f\,m_{a2}}\ (-m_{a1}+m_{a2})\ (m_{a2}-m_{a3})-e^{2\,H_f\,(\varphi\,m_{a1}+m_{a2})}\ (m_{a1}+m_{a2})\ (m_{a2}-m_{a3})+e^{2\,\varphi H_f\,(2\,m_{a2}+m_{a3})}\ (m_{a1}+m_{a2})\ (m_{a2}-m_{a3})-e^{2\,\varphi H_f\,(m_{a1}+2\,m_{a2})}\ (m_{a1}-m_{a2})\ (m_{a2}+m_{a3})-e^{2\,H_f\,(m_{a2}+\varphi\,m_{a3})}\ (-m_{a1}+m_{a2})\ (m_{a2}+m_{a3})-e^{4\,\varphi H_f\,m_{a2}}\ (m_{a1}+m_{a2})\ (m_{a2}+m_{a3})+e^{2\,H_f\,(m_{a2}+\varphi\,(m_{a1}+m_{a3}))}\ (m_{a1}+m_{a2})\ (m_{a2}+m_{a3})))$$

$$B_{3,2}=(((e^{H_f\,m_{a2}}-e^{2\,\varphi H_f\,m_{a2}})\ (-1+e^{\varphi H_f\,m_{a3}})^2\ m_{a2}\ (e^{H_f\,m_{a2}}\ (m_{a1}-m_{a2})+e^{2\,\varphi H_f\,(m_{a1}+m_{a2})}\ (-m_{a1}+m_{a2})-e^{2\,\varphi H_f\,m_{a2}}\ (m_{a1}+m_{a2})+e^{H_f\,(2\,\varphi\,m_{a1}+m_{a2})}\ (m_{a1}+m_{a2})))/(\varphi\ H_f\ m_{a3}\ (e^{2\varphi H_f\,(m_{a1}+2\,m_{a2}+m_{a3})}\ (m_{a1}-m_{a2})\ (m_{a2}-m_{a3})+e^{2\,H_f\,m_{a2}}\ (-m_{a1}+m_{a2})\ (m_{a2}-m_{a3})-e^{2\,H_f\,(\varphi\,m_{a1}+m_{a2})}\ (m_{a1}+m_{a2})\ (m_{a2}-m_{a3})+e^{2\,\varphi H_f\,(2\,m_{a2}+m_{a3})}\ (m_{a1}+m_{a2})\ (m_{a2}-m_{a3})-e^{2\,\varphi H_f\,(m_{a1}+2\,m_{a2})}\ (m_{a1}-m_{a2})\ (m_{a2}+m_{a3})-e^{2\,H_f\,(m_{a2}+\varphi\,m_{a3})}\ (-m_{a1}+m_{a2})\ (m_{a2}+m_{a3})-e^{4\,\varphi H_f\,m_{a2}}\ (m_{a1}+m_{a2})\ (m_{a2}+m_{a3})+e^{2\,H_f\,(m_{a2}+\varphi\,(m_{a1}+m_{a3}))}\ (m_{a1}+m_{a2})\ (m_{a2}+m_{a3})))$$

$$B_{3,3}=(-((-1+e^{\varphi H_f\,m_{a3}})\ (e^{\varphi H_f\,(2\,m_{a1}+4\,m_{a2}+m_{a3})}\ (m_{a1}-m_{a2})\ (2\,m_{a2}-m_{a3})+e^{2\,H_f\,m_{a2}}\ (-m_{a1}+m_{a2})\ (2\,m_{a2}-m_{a3})-e^{2\,H_f\,(\varphi\,m_{a1}+m_{a2})}\ (m_{a1}+m_{a2})\ (2\,m_{a2}-m_{a3})+e^{\varphi H_f\,(4\,m_{a2}+m_{a3})}\ (m_{a1}+m_{a2})\ (2\,m_{a2}-m_{a3})-e^{2\,\varphi H_f\,(m_{a1}+2\,m_{a2})}\ (m_{a1}-m_{a2})\ (2\,m_{a2}+m_{a3})-e^{2\,H_f\,m_{a2}+\varphi H_f\,m_{a3}}\ (-m_{a1}+m_{a2})\ (2\,m_{a2}+m_{a3})-e^{4\,\varphi H_f\,m_{a2}}\ (m_{a1}+m_{a2})\ (2\,m_{a2}+m_{a3})+e^{H_f\,(2\,m_{a2}+\varphi\,(2\,m_{a1}+m_{a3}))}\ (m_{a1}+m_{a2})\ (2\,m_{a2}+m_{a3})))/(\varphi\ H_f\ m_{a3}\ (e^{2\varphi H_f\,(m_{a1}+2\,m_{a2}+m_{a3})}\ (m_{a1}-m_{a2})\ (m_{a2}-m_{a3})+e^{2\,H_f\,m_{a2}}\ (-m_{a1}+m_{a2})\ (m_{a2}-m_{a3})-e^{2\,H_f\,(\varphi\,m_{a1}+m_{a2})}\ (m_{a1}+m_{a2})\ (m_{a2}-m_{a3})+e^{2\,\varphi H_f\,(2\,m_{a2}+m_{a3})}\ (m_{a1}+m_{a2})\ (m_{a2}-m_{a3})-e^{2\,\varphi H_f\,(m_{a1}+2\,m_{a2})}\ (m_{a1}-m_{a2})\ (m_{a2}+m_{a3})-e^{2\,H_f\,(m_{a2}+\varphi\,m_{a3})}\ (-m_{a1}+m_{a2})\ (m_{a2}+m_{a3})-e^{4\,\varphi H_f\,m_{a2}}\ (m_{a1}+m_{a2})\ (m_{a2}+m_{a3})+e^{2\,H_f\,(m_{a2}+\varphi\,(m_{a1}+m_{a3}))}\ (m_{a1}+m_{a2})\ (m_{a2}+m_{a3})))$$

$$B_{3,4}=(-(4\ e^{H_f\,(m_{a2}+\varphi\,(m_{a1}+2\,m_{a2}))}\ (-1+e^{\varphi H_f\,m_{a3}})^2\ m_{a1}\ m_{a2})/(\varphi\ H_f\ m_{a3}\ (-e^{2\varphi H_f\,(m_{a1}+2\,m_{a2}+m_{a3})}\ (m_{a1}-m_{a2})\ (m_{a2}-m_{a3})-e^{2\,H_f\,m_{a2}}\ (-m_{a1}+m_{a2})\ (m_{a2}-m_{a3})+e^{2\,H_f\,(\varphi\,m_{a1}+m_{a2})}$$

$$(m_{a1}+m_{a2})\ (m_{a2}-m_{a3})-e^{2\varphi H_f (2m_{a2}+m_{a3})}\ (m_{a1}+m_{a2})\ (m_{a2}-m_{a3})+e^{2\varphi H_f (m_{a1}+2m_{a2})}\ (m_{a1}-m_{a2})$$
$$(m_{a2}+m_{a3})+e^{2H_f (m_{a2}+\varphi m_{a3})}\ (-m_{a1}+m_{a2})\ (m_{a2}+m_{a3})+e^{4\varphi H_f m_{a2}}\ (m_{a1}+m_{a2})\ (m_{a2}+m_{a3})-$$
$$e^{2H_f (m_{a2}+\varphi (m_{a1}+m_{a3}))}\ (m_{a1}+m_{a2})\ (m_{a2}+m_{a3}))))$$

$$B_{3,5}=(((-1+e^{\varphi H_f m_{a3}})\ (e^{\varphi H_f (2m_{a1}+4m_{a2}+m_{a3})}\ (m_{a1}-m_{a2})\ (m_{a2}-m_{a3})+e^{2H_f m_{a2}}\ (-m_{a1}+m_{a2})$$
$$(m_{a2}-m_{a3})-e^{2H_f (\varphi m_{a1}+m_{a2})}\ (m_{a1}+m_{a2})\ (m_{a2}-m_{a3})+e^{\varphi H_f (4m_{a2}+m_{a3})}\ (m_{a1}+m_{a2})\ (m_{a2}-m_{a3})-$$
$$e^{2\varphi H_f (m_{a1}+2m_{a2})}\ (m_{a1}-m_{a2})\ (m_{a2}+m_{a3})-e^{2H_f m_{a2}+\varphi H_f m_{a3}}\ (-m_{a1}+m_{a2})\ (m_{a2}+m_{a3})-e^{4\varphi H_f m_{a2}}$$
$$(m_{a1}+m_{a2})\ (m_{a2}+m_{a3})+e^{H_f (2m_{a2}+\varphi (2m_{a1}+m_{a3}))}\ (m_{a1}+m_{a2})\ (m_{a2}+m_{a3})))/(\varphi\ H_f\ m_{a3}\ ($$
$$e^{2\varphi H_f (m_{a1}+2m_{a2}+m_{a3})}\ (m_{a1}-m_{a2})\ (m_{a2}-m_{a3})+e^{2H_f m_{a2}}\ (-m_{a1}+m_{a2})\ (m_{a2}-m_{a3})-e^{2H_f (\varphi m_{a1}+m_{a2})}$$
$$(m_{a1}+m_{a2})\ (m_{a2}-m_{a3})+e^{2\varphi H_f (2m_{a2}+m_{a3})}\ (m_{a1}+m_{a2})\ (m_{a2}-m_{a3})-e^{2\varphi H_f (m_{a1}+2m_{a2})}\ (m_{a1}-m_{a2})$$
$$(m_{a2}+m_{a3})-e^{2H_f (m_{a2}+\varphi m_{a3})}\ (-m_{a1}+m_{a2})\ (m_{a2}+m_{a3})-e^{4\varphi H_f m_{a2}}\ (m_{a1}+m_{a2})\ (m_{a2}+m_{a3})+$$
$$e^{2H_f (m_{a2}+\varphi (m_{a1}+m_{a3}))}\ (m_{a1}+m_{a2})\ (m_{a2}+m_{a3}))))$$

7.1.2 [*B*] for cut fin

When cut fin is modeled a simplified approach is used in Fin1Dx3_Cut. The required evaluation of boundary conditions turns out very simple if the fin cut has a total height given by (1-2φ)H_f, i.e. the fin cut is not just a line but it has finite dimensions, what it is totally true. A very thin cut will correspond to the case when (1-2φ)H_f tends to be zero, what implies that φ tend to be 0.5.

For this model the fin cut is a discontinuity so that calculation of $T_{f2}(Y)$ is not done and T_{a2} does not change along Y and its impact on HX performance is null since air flow rate of this cell tends to be zero. Important consequences of this discontinuity is that equations for fin *f1* and fin *f3* are decoupled and the number of the unknown constants of Eq. (3.14) (C_1, C_2, C_3, C_4, C_5, C_6) is reduced to four constants: (C_1, C_2, C_5, C_6), which are calculated with following boundary conditions:

$$\begin{cases} T_{f1}(Y=0) = T_{fB} \\ T_{f3}(Y=H_f) = T_{fT} \\ \left.\dfrac{dT_{f1}}{dY}\right|_{Y=\varphi H_f} = 0 \\ \left.\dfrac{dT_{f3}}{dY}\right|_{Y=(1-\varphi)H_f} = 0 \end{cases}$$

$B_{1,j}$

$$B_{1,1}=(1-e^{2\varphi H_f m_{a1}})/(\varphi H_f m_{a1}(e^{2\varphi H_f m_{a1}}+1))$$

$$B_{1,2}=0$$

$$B_{1,3}=0$$

$$B_{1,4}=-B_{1,1}$$

$$B_{1,5}=0$$

$B_{2,j}$

T_{f2} will not be evaluated because $f2$ corresponds to the fin cut and it is a discontinuity. In order to maintain same equations structure and solving methodology the way to solve this discontinuity is to make null all the elements related to T_{f2}:

$$B_{2,1}=0$$

$$B_{2,2}=0$$

$$B_{2,3}=0$$

$$B_{2,4}=0$$

$$B_{2,5}=0$$

$B_{3,j}$

$$B_{3,1}=0$$

$$B_{3,2}=0$$

$$B_{3,3}=(1-e^{2\varphi H_f m_{a3}})/(\varphi H_f m_{a3}(e^{2\varphi H_f m_{a3}}+1))$$

$$B_{3,4}=0$$

$$B_{3,5}=-B_{3,3}$$

7.1.3 [*C*] for continuous fin

$C_{1,j}$

$$C_{1,1}=((-1+e^{\varphi Hf\, m_{a1}})\, m_{a1}\, (e^{\varphi Hf\,(m_{a1}+4\,m_{a2}+2\,m_{a3})}\,(m_{a1}-m_{a2})\,(m_{a2}-m_{a3})+e^{2\,Hf\,m_{a2}}\,(-m_{a1}+m_{a2})\,(m_{a2}-m_{a3})-e^{\varphi Hf\,m_{a1}+2\,Hf\,m_{a2}}\,(m_{a1}+m_{a2})\,(m_{a2}-m_{a3})+e^{2\,\varphi Hf\,(2\,m_{a2}+m_{a3})}\,(m_{a1}+m_{a2})\,(m_{a2}-m_{a3})-e^{\varphi Hf\,(m_{a1}+4\,m_{a2})}\,(m_{a1}-m_{a2})\,(m_{a2}+m_{a3})-e^{2\,Hf\,(m_{a2}+\varphi\,m_{a3})}\,(-m_{a1}+m_{a2})\,(m_{a2}+m_{a3})-e^{4\,\varphi Hf\,m_{a2}}\,(m_{a1}+m_{a2})\,(m_{a2}+m_{a3})+e^{Hf\,(2\,m_{a2}+\varphi\,(m_{a1}+2\,m_{a3}))}\,(m_{a1}+m_{a2})\,(m_{a2}+m_{a3}))/(e^{2\,\varphi Hf\,(m_{a1}+2\,m_{a2}+m_{a3})}\,(m_{a1}-m_{a2})\,(m_{a2}-m_{a3})+e^{2\,Hf\,m_{a2}}\,(-m_{a1}+m_{a2})\,(m_{a2}-m_{a3})-e^{2\,Hf\,(\varphi\,m_{a1}+m_{a2})}\,(m_{a1}+m_{a2})\,(m_{a2}-m_{a3})+e^{2\,\varphi Hf\,(2\,m_{a2}+m_{a3})}\,(m_{a1}+m_{a2})\,(m_{a2}-m_{a3})-e^{2\,\varphi Hf\,(m_{a1}+2\,m_{a2})}\,(m_{a1}-m_{a2})\,(m_{a2}+m_{a3})-e^{2\,Hf\,(m_{a2}+\varphi\,m_{a3})}\,(-m_{a1}+m_{a2})\,(m_{a2}+m_{a3})-e^{4\,\varphi Hf\,m_{a2}}\,(m_{a1}+m_{a2})\,(m_{a2}+m_{a3})+e^{2\,Hf\,(m_{a2}+\varphi\,(m_{a1}+m_{a3}))}\,(m_{a1}+m_{a2})\,(m_{a2}+m_{a3}))$$

$$C_{1,2}=((2\,e^{\varphi Hf\,m_{a1}}\,(e^{Hf\,m_{a2}}-e^{2\,\varphi Hf\,m_{a2}})\, m_{a1}\, m_{a2}\, (e^{2\,\varphi Hf\,(m_{a2}+m_{a3})}\,(m_{a2}-m_{a3})+e^{Hf\,m_{a2}}\,(-m_{a2}+m_{a3})-e^{2\,\varphi Hf\,m_{a2}}\,(m_{a2}+m_{a3})+e^{Hf\,(m_{a2}+2\,\varphi\,m_{a3})}\,(m_{a2}+m_{a3}))/(e^{2\,\varphi Hf\,(m_{a1}+2\,m_{a2}+m_{a3})}\,(m_{a1}-m_{a2})\,(m_{a2}-m_{a3})+e^{2\,Hf\,m_{a2}}\,(-m_{a1}+m_{a2})\,(m_{a2}-m_{a3})-e^{2\,Hf\,(\varphi\,m_{a1}+m_{a2})}\,(m_{a1}+m_{a2})\,(m_{a2}-m_{a3})+e^{2\,\varphi Hf\,(2\,m_{a2}+m_{a3})}\,(m_{a1}+m_{a2})\,(m_{a2}-m_{a3})-e^{2\,\varphi Hf\,(m_{a1}+2\,m_{a2})}\,(m_{a1}-m_{a2})\,(m_{a2}+m_{a3})-e^{2\,Hf\,(m_{a2}+\varphi\,m_{a3})}\,(-m_{a1}+m_{a2})\,(m_{a2}+m_{a3})-e^{4\,\varphi Hf\,m_{a2}}\,(m_{a1}+m_{a2})\,(m_{a2}+m_{a3})+e^{2\,Hf\,(m_{a2}+\varphi\,(m_{a1}+m_{a3}))}\,(m_{a1}+m_{a2})\,(m_{a2}+m_{a3})))$$

$$C_{1,3}=((4\,e^{Hf\,(m_{a2}+\varphi\,(m_{a1}+2\,m_{a2}))}\,(-1+e^{\varphi Hf\,m_{a3}})^2\, m_{a1}\, m_{a2}\, m_{a3})/(e^{2\,\varphi Hf\,(m_{a1}+2\,m_{a2}+m_{a3})}\,(m_{a1}-m_{a2})\,(m_{a2}-m_{a3})+e^{2\,Hf\,m_{a2}}\,(-m_{a1}+m_{a2})\,(m_{a2}-m_{a3})-e^{2\,Hf\,(\varphi\,m_{a1}+m_{a2})}\,(m_{a1}+m_{a2})\,(m_{a2}-m_{a3})+e^{2\,\varphi Hf\,(2\,m_{a2}+m_{a3})}\,(m_{a1}+m_{a2})\,(m_{a2}-m_{a3})-e^{2\,\varphi Hf\,(m_{a1}+2\,m_{a2})}\,(m_{a1}-m_{a2})\,(m_{a2}+m_{a3})-e^{2\,Hf\,(m_{a2}+\varphi\,m_{a3})}\,(-m_{a1}+m_{a2})\,(m_{a2}+m_{a3})-e^{4\,\varphi Hf\,m_{a2}}\,(m_{a1}+m_{a2})\,(m_{a2}+m_{a3})+e^{2\,Hf\,(m_{a2}+\varphi\,(m_{a1}+m_{a3}))}\,(m_{a1}+m_{a2})\,(m_{a2}+m_{a3})))$$

$$C_{1,4}=(-(m_{a1}\,(e^{2\,\varphi Hf\,(m_{a1}+2\,m_{a2}+m_{a3})}\,(m_{a1}-m_{a2})\,(m_{a2}-m_{a3})-e^{2\,Hf\,m_{a2}}\,(-m_{a1}+m_{a2})\,(m_{a2}-m_{a3})-e^{2\,Hf\,(\varphi\,m_{a1}+m_{a2})}\,(m_{a1}+m_{a2})\,(m_{a2}-m_{a3})-e^{2\,\varphi Hf\,(2\,m_{a2}+m_{a3})}\,(m_{a1}+m_{a2})\,(m_{a2}-m_{a3})-$$

$$e^{2\varphi Hf\,(m_{a1}+2\,m_{a2})}\,(m_{a1}-m_{a2})\;(m_{a2}+m_{a3})+e^{2\,Hf\,(m_{a2}+\varphi\,m_{a3})}\,(-m_{a1}+m_{a2})\;(m_{a2}+m_{a3})+e^{4\,\varphi Hf\,m_{a2}}\,(m_{a1}+m_{a2})\;(m_{a2}+m_{a3})+e^{2\,Hf\,(m_{a2}+\varphi\,(m_{a1}+m_{a3}))}\,(m_{a1}+m_{a2})\;(m_{a2}+m_{a3}))/(e^{2\,\varphi Hf\,(m_{a1}+2\,m_{a2}+m_{a3})}\,(m_{a1}-m_{a2})\;(m_{a2}-m_{a3})+e^{2\,Hf\,m_{a2}}\,(-m_{a1}+m_{a2})\;(m_{a2}-m_{a3})-e^{2\,Hf\,(\varphi\,m_{a1}+m_{a2})}\,(m_{a1}+m_{a2})\;(m_{a2}-m_{a3})+e^{2\,\varphi Hf\,(2\,m_{a2}+m_{a3})}\,(m_{a1}+m_{a2})\;(m_{a2}-m_{a3})-e^{2\,\varphi Hf\,(m_{a1}+2\,m_{a2})}\,(m_{a1}-m_{a2})\;(m_{a2}+m_{a3})-e^{2\,Hf\,(m_{a2}+\varphi\,m_{a3})}\,(-m_{a1}+m_{a2})\;(m_{a2}+m_{a3})-e^{4\,\varphi Hf\,m_{a2}}\,(m_{a1}+m_{a2})\;(m_{a2}+m_{a3})+e^{2\,Hf\,(m_{a2}+\varphi\,(m_{a1}+m_{a3}))}\,(m_{a1}+m_{a2})\;(m_{a2}+m_{a3}))$$

$$C_{1,5}=((8\;e^{Hf\,(m_{a2}+\varphi\,(m_{a1}+2\,m_{a2}+m_{a3}))}\,m_{a1}\;m_{a2}\;m_{a3})/(e^{4\,\varphi Hf\,m_{a2}}\,(m_{a1}+m_{a2})\;(-m_{a2}+e^{2\,\varphi Hf\,m_{a3}}\,(m_{a2}-m_{a3})-m_{a3})+e^{2\,Hf\,m_{a2}}\,(m_{a1}-m_{a2})\;(-m_{a2}+m_{a3}+e^{2\,\varphi Hf\,m_{a3}}\,(m_{a2}+m_{a3}))+e^{2\,\varphi Hf\,m_{a1}}\,(e^{4\,\varphi Hf\,m_{a2}}\,(m_{a1}-m_{a2})\;(-m_{a2}+e^{2\,\varphi Hf\,m_{a3}}\,(m_{a2}-m_{a3})-m_{a3})+e^{2\,Hf\,m_{a2}}\,(m_{a1}+m_{a2})\;(-m_{a2}+m_{a3}+e^{2\,\varphi Hf\,m_{a3}}\,(m_{a2}+m_{a3})))))$$

$C_{2,j}$

$$C_{2,1}=-(4\ e^{Hf\ (m_{a2}+2\varphi\ m_{a2}+\varphi\ m_{a3})}\ (-1+e^{\varphi Hf\ m_{a1}})^2\ m_{a1}\ m_{a2}\ m_{a3})/(e^{2\varphi Hf\ (m_{a1}+2\ m_{a2}+m_{a3})}\ (m_{a1}-m_{a2})\ (m_{a2}-m_{a3})+e^{2\ Hf\ m_{a2}}\ (-m_{a1}+m_{a2})\ (m_{a2}-m_{a3})-e^{2\ Hf\ (\varphi\ m_{a1}+m_{a2})}\ (m_{a1}+m_{a2})\ (m_{a2}-m_{a3})+e^{2\varphi Hf\ (2\ m_{a2}+m_{a3})}\ (m_{a1}+m_{a2})\ (m_{a2}-m_{a3})-e^{2\varphi Hf\ (m_{a1}+2\ m_{a2})}\ (m_{a1}-m_{a2})\ (m_{a2}+m_{a3})-e^{2\ Hf\ (m_{a2}+\varphi\ m_{a3})}\ (-m_{a1}+m_{a2})\ (m_{a2}+m_{a3})-e^{4\varphi Hf\ m_{a2}}\ (m_{a1}+m_{a2})\ (m_{a2}+m_{a3})+e^{2\ Hf\ (m_{a2}+\varphi\ (m_{a1}+m_{a3}))}\ (m_{a1}+m_{a2})\ (m_{a2}+m_{a3}))$$

$$C_{2,2}=(-(2\ e^{\varphi Hf\ m_{a3}}\ (e^{Hf\ m_{a2}}-e^{2\varphi Hf\ m_{a2}})\ m_{a2}\ (e^{Hf\ m_{a2}}\ (m_{a1}-m_{a2})+e^{2\varphi Hf\ (m_{a1}+m_{a2})}\ (-m_{a1}+m_{a2})-e^{2\varphi Hf\ m_{a2}}\ (m_{a1}+m_{a2})+e^{Hf\ (2\varphi\ m_{a1}+m_{a2})}\ (m_{a1}+m_{a2}))\ m_{a3})/(e^{2\varphi Hf\ (m_{a1}+2\ m_{a2}+m_{a3})}\ (m_{a1}-m_{a2})\ (m_{a2}-m_{a3})+e^{2\ Hf\ m_{a2}}\ (-m_{a1}+m_{a2})\ (m_{a2}-m_{a3})-e^{2\ Hf\ (\varphi\ m_{a1}+m_{a2})}\ (m_{a1}+m_{a2})\ (m_{a2}-m_{a3})+e^{2\varphi Hf\ (2\ m_{a2}+m_{a3})}\ (m_{a1}+m_{a2})\ (m_{a2}-m_{a3})-e^{2\varphi Hf\ (m_{a1}+2\ m_{a2})}\ (m_{a1}-m_{a2})\ (m_{a2}+m_{a3})-e^{2\ Hf\ (m_{a2}+\varphi\ m_{a3})}\ (-m_{a1}+m_{a2})\ (m_{a2}+m_{a3})-e^{4\varphi Hf\ m_{a2}}\ (m_{a1}+m_{a2})\ (m_{a2}+m_{a3})+e^{2\ Hf\ (m_{a2}+\varphi\ (m_{a1}+m_{a3}))}\ (m_{a1}+m_{a2})\ (m_{a2}+m_{a3})))$$

$$C_{2,3}=(-((-1+e^{\varphi Hf\ m_{a3}})\ m_{a3}\ (e^{\varphi Hf\ (2\ m_{a1}+4\ m_{a2}+m_{a3})}\ (m_{a1}-m_{a2})\ (m_{a2}-m_{a3})+e^{2\ Hf\ m_{a2}}\ (-m_{a1}+m_{a2})\ (m_{a2}-m_{a3})-e^{2\ Hf\ (\varphi\ m_{a1}+m_{a2})}\ (m_{a1}+m_{a2})\ (m_{a2}-m_{a3})+e^{\varphi Hf\ (4\ m_{a2}+m_{a3})}\ (m_{a1}+m_{a2})\ (m_{a2}-m_{a3})-e^{2\varphi Hf\ (m_{a1}+2\ m_{a2})}\ (m_{a1}-m_{a2})\ (m_{a2}+m_{a3})-e^{2\ Hf\ m_{a2}+\varphi Hf\ m_{a3}}\ (-m_{a1}+m_{a2})\ (m_{a2}+m_{a3})-e^{4\varphi Hf\ m_{a2}}\ (m_{a1}+m_{a2})\ (m_{a2}+m_{a3})+e^{Hf\ (2\ m_{a2}+\varphi\ (2\ m_{a1}+m_{a3}))}\ (m_{a1}+m_{a2})\ (m_{a2}+m_{a3})))/(e^{2\varphi Hf\ (m_{a1}+2\ m_{a2}+m_{a3})}\ (m_{a1}-m_{a2})\ (m_{a2}-m_{a3})+e^{2\ Hf\ m_{a2}}\ (-m_{a1}+m_{a2})\ (m_{a2}-m_{a3})-e^{2\ Hf\ (\varphi\ m_{a1}+m_{a2})}\ (m_{a1}+m_{a2})\ (m_{a2}-m_{a3})+e^{2\varphi Hf\ (2\ m_{a2}+m_{a3})}\ (m_{a1}+m_{a2})\ (m_{a2}-m_{a3})-e^{2\varphi Hf\ (m_{a1}+2\ m_{a2})}\ (m_{a1}-m_{a2})\ (m_{a2}+m_{a3})-e^{2\ Hf\ (m_{a2}+\varphi\ m_{a3})}\ (-m_{a1}+m_{a2})\ (m_{a2}+m_{a3})-e^{4\varphi Hf\ m_{a2}}\ (m_{a1}+m_{a2})\ (m_{a2}+m_{a3})+e^{2\ Hf\ (m_{a2}+\varphi\ (m_{a1}+m_{a3}))}\ (m_{a1}+m_{a2})\ (m_{a2}+m_{a3})))$$

$$C_{2,4}=(-(8\ e^{Hf\ (m_{a2}+\varphi\ (m_{a1}+2\ m_{a2}+m_{a3}))}\ m_{a1}\ m_{a2}\ m_{a3})/(e^{2\varphi Hf\ (m_{a1}+2\ m_{a2}+m_{a3})}\ (m_{a1}-m_{a2})\ (m_{a2}-m_{a3})+e^{2\ Hf\ m_{a2}}\ (-m_{a1}+m_{a2})\ (m_{a2}-m_{a3})-e^{2\ Hf\ (\varphi\ m_{a1}+m_{a2})}\ (m_{a1}+m_{a2})\ (m_{a2}-m_{a3})+e^{2\varphi Hf\ (2\ m_{a2}+m_{a3})}$$

$$(m_{a1}+m_{a2})\ (m_{a2}-m_{a3}) - e^{2\varphi Hf\ (m_{a1}+2\,m_{a2})}\ (m_{a1}-m_{a2})\ (m_{a2}+m_{a3}) - e^{2\,Hf\ (m_{a2}+\varphi\,m_{a3})}\ (-m_{a1}+m_{a2})$$

$$(m_{a2}+m_{a3}) - e^{4\,\varphi Hf\ m_{a2}}\ (m_{a1}+m_{a2})\ (m_{a2}+m_{a3}) + e^{2\,Hf\ (m_{a2}+\varphi\,(m_{a1}+m_{a3}))}\ (m_{a1}+m_{a2})\ (m_{a2}+m_{a3}))))$$

$$C_{2,5} = ((m_{a3}\ (e^{2\,\varphi Hf\ (m_{a1}+2\,m_{a2}+m_{a3})}\ (m_{a1}-m_{a2})\ (m_{a2}-m_{a3}) - e^{2\,Hf\ m_{a2}}\ (-m_{a1}+m_{a2})\ (m_{a2}-m_{a3}) +$$

$$e^{2\,Hf\ (\varphi\,m_{a1}+m_{a2})}\ (m_{a1}+m_{a2})\ (m_{a2}-m_{a3}) + e^{2\,\varphi Hf\ (2\,m_{a2}+m_{a3})}\ (m_{a1}+m_{a2})\ (m_{a2}-m_{a3}) +$$

$$e^{2\,\varphi Hf\ (m_{a1}+2\,m_{a2})}\ (m_{a1}-m_{a2})\ (m_{a2}+m_{a3}) - e^{2\,Hf\ (m_{a2}+\varphi\,m_{a3})}\ (-m_{a1}+m_{a2})\ (m_{a2}+m_{a3}) + e^{4\,\varphi Hf\ m_{a2}}$$

$$(m_{a1}+m_{a2})\ (m_{a2}+m_{a3}) + e^{2\,Hf\ (m_{a2}+\varphi\,(m_{a1}+m_{a3}))}\ (m_{a1}+m_{a2})\ (m_{a2}+m_{a3}))) / (e^{2\,\varphi Hf\ (m_{a1}+2\,m_{a2}+m_{a3})}$$

$$(m_{a1}-m_{a2})\ (m_{a2}-m_{a3}) + e^{2\,Hf\ m_{a2}}\ (-m_{a1}+m_{a2})\ (m_{a2}-m_{a3}) - e^{2\,Hf\ (\varphi\,m_{a1}+m_{a2})}\ (m_{a1}+m_{a2})\ (m_{a2}-m_{a3}) +$$

$$e^{2\,\varphi Hf\ (2\,m_{a2}+m_{a3})}\ (m_{a1}+m_{a2})\ (m_{a2}-m_{a3}) - e^{2\,\varphi Hf\ (m_{a1}+2\,m_{a2})}\ (m_{a1}-m_{a2})\ (m_{a2}+m_{a3}) -$$

$$e^{2\,Hf\ (m_{a2}+\varphi\,m_{a3})}\ (-m_{a1}+m_{a2})\ (m_{a2}+m_{a3}) - e^{4\,\varphi Hf\ m_{a2}}\ (m_{a1}+m_{a2})\ (m_{a2}+m_{a3}) +$$

$$e^{2\,Hf\ (m_{a2}+\varphi\,(m_{a1}+m_{a3}))}\ (m_{a1}+m_{a2})\ (m_{a2}+m_{a3})))$$

7.1.4 [*C*] for cut fin

The same approach applied for getting coefficients of matrix [*B*] in case of cut fin has been applied to get the coefficients of matrix [*C*].

$C_{1,j}$

$$C_{1,1} = m_{a1}\,(e^{2\varphi H_f m_{a1}} - 1)/(e^{2\varphi H_f m_{a1}} + 1)$$

$$C_{1,2} = 0$$

$$C_{1,3} = 0$$

$$C_{1,4} = -C_{1,1}$$

$$C_{1,5} = 0$$

$C_{2,j}$

$$C_{2,1} = 0$$

$$C_{2,2} = 0$$

$$C_{2,3} = m_{a3}\,(1 - e^{2\varphi H_f m_{a3}})/(e^{2\varphi H_f m_{a3}} + 1)$$

$$C_{2,4} = 0$$

$$C_{2,5} = -C_{2,3}$$

7.2 Appendix B: Experimental data used for validation of model

7.2.1 Gas cooler

All data related to the gas cooler used in this thesis for model's validation and other numerical studies is extracted from Yin et al. (2001), which is summarized below.

Gas cooler geometry

Gas Cooler Characteristics	
Mass (kg)	2.3
Face Area (cm^2)	1950
Core Depth (cm)	1.65
Core Volume (cm^3)	3320
Airside Area (m^2)	5.2
Refrigerant Side Area (m^2)	0.49
Fin Density (fins/in)	22
Louver Angle (deg)	23
Tube Length (mm)	545
Number of Ports	11
Port Diameter (mm)	0.79
Web Thickness (mm)	0.70
Wall Thickness (mm)	0.43
Fin Height (mm)	8.89
Fin Thickness (mm)	0.10
Louver Height (mm)	7.16
Louver Pitch (mm)	0.99
Number of Louvers	2x6
Louver redirection Length (mm)	1.7
Louver entry Length (mm)	1.7
Header tube diameter (mm)	2@7
Inlet/exit elbow tube diameter (mm)	7

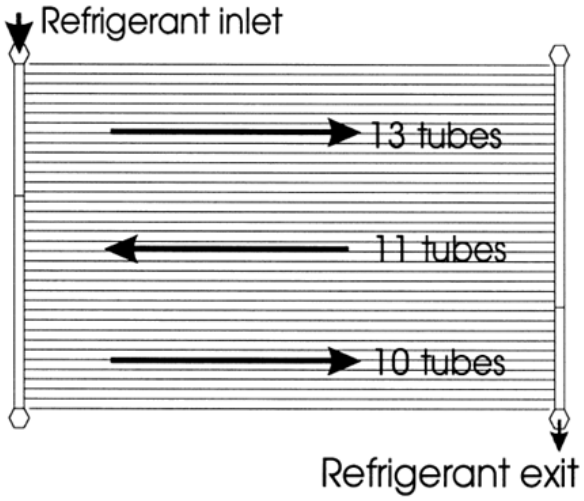

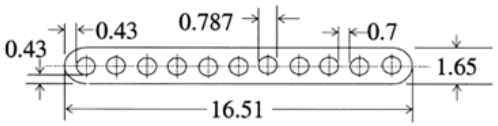

Yin et al. (2001)

Operating conditions

Test [#]	m_r [g/s]	$P_{r,in}$ [kPa]	ΔP_r [kPa]	$T_{r,in}$ [°C]	$T_{r,out}$ [°C]	m_a [g/s]	$T_{a,in}$ [°C]	ΔP_a [Pa]
1	34.74	11007	137.7	108.9	48.2	542	43	43
2	56.36	10792	421.6	138.6	50.2	701	43.5	61
3	39.98	12014	155.4	125.4	49	699	44.3	62
4	26.39	12464	62.7	115.8	58	457	55.1	45
5	37.84	10937	116.3	124.7	49	537	42.7	46
6	22.37	9556	60.9	97.9	45.8	453	43.1	39
7	27.12	10982	97.5	101.2	56	459	53.9	46
8	27.48	9333	99	91	45.5	452	43	39
9	31.49	8858	103.6	66.5	38.4	452	31.8	34
10	24.07	14390	25.4	113.3	45.4	452	43	40
11	22.08	10555	28.2	103	35.9	453	32.4	34
12	22.06	11392	37.2	114.8	46.8	437	43.4	38
13	25.17	8386	91.1	87.4	36.8	451	31.5	32
14	38.49	10278	197.9	118.9	48.4	537	43.3	47
15	19.6	12460	27.6	126.6	46	454	43.5	40
16	44.31	9061	337.3	104	46.4	541	43.4	47
17	21.67	9514	24	102	36.9	451	32.4	34
18	23.56	9841	52.7	107.1	46	452	42.8	39
19	45.58	8587	344.3	101.7	45	536	42.7	46
20	24.68	8460	67.3	89	37.2	451	31.8	33
21	47.53	8677	389.9	97.8	45.1	535	42.7	46
22	25.92	9387	92.2	97	45.7	455	43.1	40
23	26.6	8435	78	81.3	37.2	453	32.2	34
24	25.98	10014	84.4	96.6	46.5	461	42.9	40
25	42.73	9713	239.4	108	47.5	539	43.2	48
26	25.25	8328	66.2	84.4	36.8	453	32.4	34

Test [#]	m_r [g/s]	$P_{r,in}$ [kPa]	ΔP_r [kPa]	$T_{r,in}$ [°C]	$T_{r,out}$ [°C]	m_a [g/s]	$T_{a,in}$ [°C]	ΔP_a [Pa]
27	25.11	9593	78.5	96.9	45.7	453	43	41
28	43.12	9200	286.9	105.4	46.3	539	42.9	47
29	26	8331	59.1	81.2	36.9	453	32.1	35
30	37.69	10259	166	120.9	48.6	540	43.7	49
31	22.83	9537	18.9	93.8	37.4	450	32.1	34
32	26.04	7659	73.8	78.2	32.5	454	26.8	32
33	25.45	8359	66.1	87.3	36.7	456	31.7	35
34	32.63	9242	145	83.3	45.5	455	43.3	38
35	26.06	9349	93.2	94.1	45.2	536	43.8	47
36	25.55	9385	85.3	95.4	44.9	710	43.6	66
37	24.72	7826	57.1	79.9	33.4	448	26.8	31
38	26.23	8204	81.9	82.3	36.4	449	32.4	34
39	20.78	9833	46.2	106.8	46	451	43.6	40
40	34.86	10735	168.9	129.8	48.7	540	43.7	48
41	32.91	9879	150.5	110.5	47.3	502	43.7	44
42	31.47	10315	127.9	116	48.3	501	44.1	45
43	29.95	10772	109.4	121.1	48.2	502	43.7	45
44	28.82	11251	92.8	125.8	48.1	501	43.6	45
45	27.94	11745	84	130.3	48	501	43.7	45
46	23.02	8303	29.6	83.3	33.1	455	26.7	29
47	22.9	8413	31	85.5	33.7	447	27	31

7.2.2 Condenser

All data related to the gas cooler used in this thesis for model's validation and other numerical studies is extracted from García-Cascales et al. (2001), which is summarized below.

Condenser geometry

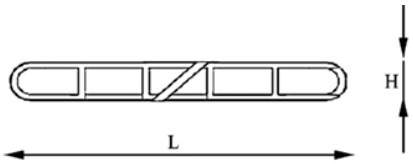

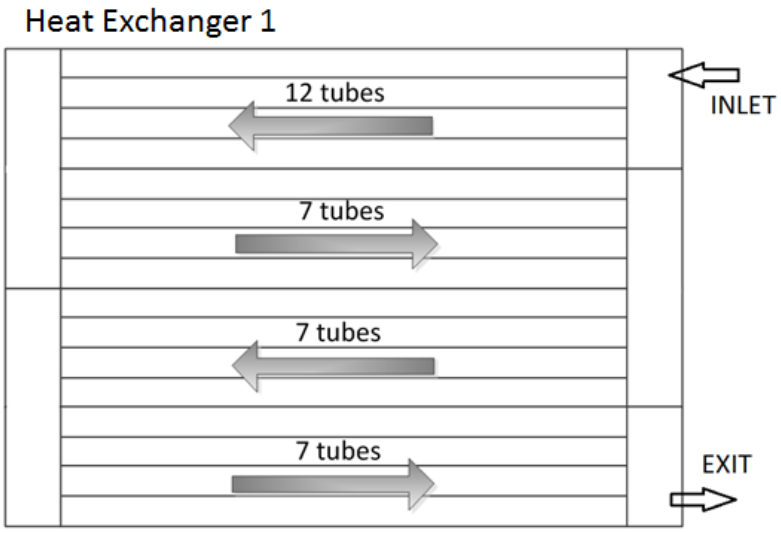

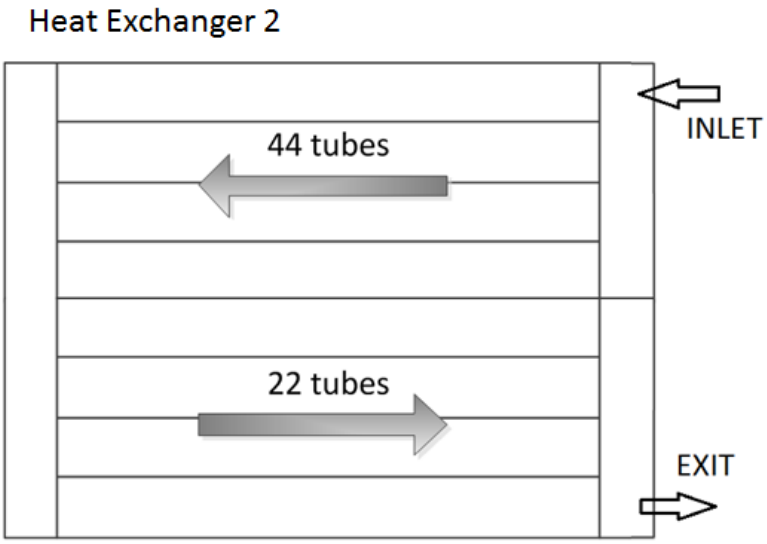

	Heat Exchanger 1	Heat Exchanger 2
Tubes	33	66
Fin type	Louvered fins	Louvered fins
Fins per inch	12	10
Core width (mm)	534.56	889
Finned length (mm)	482.6	641

Operating conditions

Test	t1.1	t1.2	t1.3	t1.4	t2.1	t2.2	t2.3	t2.4
Secondary fluid - Air								
Inlet air dry-bulb T (°C)	35	34.98	34.92	34.99	35.02	35.01	35.01	35
Inlet air wet-bulb T (°C)	22.74	22.69	22.7	22.79	21.62	21.15	21.61	21.71
Outlet air dry-bulb T (°C)	42.18	42.66	43.21	43.9	42.24	42.79	43.41	44.19
Atmospheric pressure (kPa)	98.6	98.6	98.64	98.62	99.22	99.22	99.21	99.21
Volumetric flow rate (m^3/h)	1877.19	1625.38	1375.56	1126.41	7334	6342	5369	4388
Refrigerant - R410A								
Inlet temperature (°C)	79.57	79.47	79.5	79.85	79.24	79.44	79.73	79.65
Inlet pressure (kPa)	2977.29	2977.88	2975.76	2977.6	2978.78	2980.38	2974.51	2975.85
Outlet temperature (°C)	42.77	42.7	42.93	42.68	42.71	42.39	42.5	42.58
Outlet pressure (kPa)	2955.81	2959.47	2960.29	2965.82	2943.88	2950.35	2949.01	2954.95
Outlet saturation (°C)	48.35	48.4	48.41	48.49	48.17	48.27	48.25	48.33
Outlet subcooling (°C)	5.577	5.705E+00	5.487E+00	5.812E+00	5.460E+00	5.880E+00	5.740E+00	5.750E+00
Mass flow rate (kg/s)	0.023765	0.019645	0.019645	0.016881	0.09236	0.08508	0.07681	0.0681
Pressure Drop (kPa)	2.066E+01	1.763E+01	1.464E+01	1.103E+01	3.419E+01	2.944E+01	2.490E+01	2.040E+01
Heat Transferred (kW)	4.754	4.362	3.923	3.386	18.446	17.064	15.424	13.657

REFERENCES

Agarwal, A., Bandhauer, T.M., Garimella, S. , 2010. Measurement and modeling of condensation heat transfer in non-circular microchannels, Int. J. Refrigeration, 33(6), 1169–1179.

Asinari, P., 2004. Finite-volume and Finite-element Hybrid Technique for the Calculation of Complex Heat Exchangers by Semiexplicit Method for Wall Temperature Linked Equations (SEWTLE). Numerical Heat Transfer Part B-Fundamentals, 45, 221-247.

Asinari, P., Cecchinato, L., Fornasieri, E., 2004. Effects of Thermal Conduction in Microchannel Gas Coolers for Carbon Dioxide. Int. J. Refrigeration 27(6), 577-586.

Ayad, F., Benelmir, R., Souayed, A., 2012. CO2 evaporators design for vehicle HVAC operation, Applied Thermal Engineering, 36, 330–344.

Bertsch, S.S., A. Groll, E.A., Garimella, S.V., 2008. Refrigerant flow boiling heat transfer in parallel microchannels as a function of local vapor quality, International Journal of Heat and Mass Transfer, 51 (19–20), 4775–4787.

Brix W., Kærn, M.R., Elmegaard, B., 2009. Modelling refrigerant distribution in microchannel evaporators, Int. J. Refrigeration , 32(7), 1736–1743.

Brix W., Kærn, M.R., Elmegaard, B., 2010. Modelling distribution of evaporating CO2 in parallel minichannels, Int. J. Refrigeration , 33 (6), 1086–1094.

Cavallini A., Censi G., Del Col D., Doretti L., Longo G.A., Rossetto L., 2002. In-tube condensation of halogenated refrigerants. ASHRAE Trans., 108 (1), pp. 146–161.

Cavallini, A., Del Col, D., Doretti, L., Matkovic, M., Rossetto, L., Zilio, C., 2005. Condensation Heat Transfer and Pressure Gradient Inside Multiport Minichannels, Heat Transfer Engineering, 26(3), 45–55.

Cavallini, A., Del Col, D., Matkovic, M., Rossetto, L., 2009. Frictional pressure drop during vapour–liquid flow in minichannels: Modelling and experimental evaluation, International Journal of Heat and Fluid Flow, 30(1), 131–139.

Chen, T., Garimella, S.V., 2011. Local heat transfer distribution and effect of instabilities during flow boiling in a silicon microchannel heat sink, International Journal of Heat and Mass Transfer, 54(15–16), 3179–3190.

Churchill S.W., 1977. Friction-factor Equation Spans All Fluid Flow Regimes. Chemical Engineering, 7: 91-92.

CoilDesigner, 2010.Tool to Aid in the Design, Simulation and Optimization of Air-Cooled Heat Exchangers, http://ceee.umd.edu/isoc/software/index_coildesigner.htm , University of Maryland, Center for Environmental Energy Engineering, MD, USA.

Corberán J.M., Gonzálvez J., Montes P., Blasco R., 2002. 'ART' a Computer Code to Assist the Design of Refrigeration and A/C Equipment. International Refrigeration and Air Conditioning Conference at Purdue, IN, USA.

Corberán, J.M., De Cordoba, P.F., Gonzalvez, J., Alias, F., 2001. Semiexplicit Method for Wall Temperature Linked Equations (SEWTLE): A General Finite-Volume Technique for the Calculation of Complex Heat Exchangers. Numer. Heat Transfer, Part B 40, 37-59.

Domanski, P.A., Choi, J.M., Payne, W.V., 2007. Longitudinal Heat Conduction in Finned-Tube Evaporator. 22nd IIR International Congress of Refrigeration, Beijing, China.

EVAP-COND, 2010. Simulation Models for Finned Tube Heat Exchangers with Circuitry Optimization, http://www.nist.gov/el/building_environment/evapcond_software.cfm, National Institute of Standards and Technology, Building and Fire Research Laboratory, Gaithersburg, MD, USA.

Fernando, P., Palm, B., Ameel, T., Lundqvist, P., Granryd, E., 2008. A minichannel aluminium tube heat exchanger – Part II: Evaporator performance with propane. Int. J. Refrigeration , 31(4), 681–695.

Fernando, P., Palm, B., Lundqvist, P., Granryd, E., 2004. Propane heat pump with low refrigerant charge: design and laboratory tests, Int. J. Refrigeration , 27(7), 761–773.

Friedel L., 1980. Pressure drop during gas/vapor-liquid flow in pipes. Int. Chem. Eng., July, 20, pp. 352–367.

Fronk, B.M., Garimella S., 2011. Water-Coupled Carbon Dioxide Microchannel Gas Cooler for Heat Pump Water Heaters: Part II – Model Development and Validation, Int. J. Refrigeration, 34, 17-28.

García-Cascales, J.R., Vera-García, F., Gonzálvez-Maciá, J., Corberán-Salvador, J.M., Johnson, M.W., Kohler, G.T., 2010. Compact Heat Exchangers Modeling: Condensation. Int. J. Refrigeration 33, 135-147.

REFERENCES

Garimella, S., Agarwal, A., Killion, J.D., 2005. Condensation Pressure Drop in Circular Microchannels, Heat Transfer Engineering, 26(3), 28–35.

Gnielinski V., 1976. New Equations for Heat and Mass Transfer in Turbulent Pipe and Channel Flow. Int. Chem. Eng. 16 (2), 359-368.

Hrnjak, P., 2010. Developments in Charge Reduction and Microchannel Technology, Sustainable Refrigeration and Heat Pump Technology Conference, Stockholm, Sweden, 2010.

Hrnjak, P., Litch, A.D., 2008. Microchannel heat exchangers for charge minimization in air-cooled ammonia condensers and chillers, Int. J. Refrigeration , 31(4), 658–668.

IDAE, 2005. Aire acondicionado a nuestras necesidades reales. http://www.idae.es/, Instituto para la Diversificación y Ahorro de la Energía (IDAE).

IEC 60335-1, 2010. International Standard: Household and similar electrical appliances - Safety - Part 1: General requirements. International Electrotechnical Commission.

IMST-ART, 2010.Simulation tool to assist the selection, design and optimization of refrigeration equipment and components, http://www.imst-art.com , UniversitatPolitècnica de Valéncia, Insituto de IngenieríaEnergética, Spain.

Incropera, F. P., DeWitt, D.P., 1996. Fundamentals of Heat and Mass Transfer, fourth ed. John Wiley and Sons, New York.

Jiang, H.B., 2003. Ph. D. Thesis, Development of a Simulation and Optimization Tool for Heat Exchanger Design. University of Maryland, USA.

Jiang, H.B., Aute, V., Radermacher, R., 2006.Coildesigner: a General-Purpose Simulation and Design Tool for Air-To-Refrigerant Heat Exchangers. Int. J. Refrigeration 29 (4), 601-610.

Joardar, A., Jacobi, A.M., 2005. Impact of leading edge delta-wing vortex generators on the thermal performance of a flat tube, louvered-fin compact heat exchanger, International Journal of Heat and Mass Transfer, 48 (8), 1480–1493.

Kandlikar, S.G., 2002. Fundamental issues related to flow boiling in minichannels and microchannels, Experimental Thermal and Fluid Science, 26(2–4), 389–407.

Kandlikar, S. G., and Grande, W. J., 2002. Evolution of Microchannel Flow Passages--Thermohydraulic Performance and Fabrication Technology. Heat Transfer Eng., 25(1), pp. 3-17.

Kays W.M., London A.L., 1984, Compact Heat Exchangers, 3rd ed. McGraw-Hill, New York.

Kew, P.A., Reay, D.A., 2011. Compact/micro-heat exchangers – Their role in heat pumping equipment, Applied Thermal Engineering, 31(5), 594–601.

Kim, M.H., Bullard, C.W.,2001. Development of a microchannel evaporator model for a CO2 air-conditioning system, Energy, 26(10), 931–948.

Kim M.-H., Bullard C., 2002, Air-Side Thermal Hydraulic Performance of Multi-Louvered Fin Aluminum Heat Exchangers, Int. J. Refrigeration, 25: 390-400.

Kim, M.H., Pettersen, J., Bullard, C.W., 2004. Fundamental process and system design issues in CO2 vapor compression systems, Progress in Energy and Combustion Science, 30(2), 119–174.

Kim, M.H., Sumin, S., Bullard, C.W., 2002. Effect of inlet humidity condition on the air-side performance of an inclined brazed aluminum evaporator, Int. J. Refrigeration , 25(5), 611–620.

Klein, S.A, 2004. Engineering Equation Solver, F-Chart Software, Madison, WI (USA).

Kulkarni, T., Bullard, C.W., Cho, K., 2004. Header design tradeoffs in microchannel evaporators, Applied Thermal Engineering, 24(5–6), 759–776.

Lee, J., Domanski, P.A., July 1997. Impact of Air and Refrigerant Maldistributions on the Performance of Finned-Tube Evaporators with R-22 and R-407C. Report No.: DOE/CE/23810-81.

Lemmon, E.W., McLinden, M.O., M.L. Huber. 2002. REFPROP, Version 7.0. U.S. Department of Commerce, Maryland.

Li, Q., Flamant, G., Yuan, X., Neveub, P., Luo, L. 2011. Compact heat exchangers: A review and future applications for a new generation of high temperature solar receivers, Renewable and Sustainable Energy Reviews, 15(9), 4855–4875.

Lia, B., Peuker, S., Hrnjak, P.S., Alleyne, A. G., 2011. Refrigerant mass migration modeling and simulation for air conditioning systems, Applied Thermal Engineering, 31(10), 1770–1779.

Moallem, E., Cremaschi, L., Fisher, D.E., Padhmanabhan, S., 2012. Experimental measurements of the surface coating and water retention effects on frosting

performance of microchannel heat exchangers for heat pump systems, Experimental Thermal and Fluid Science, 39,, 176–188.

Moallem, E., Padhmanabhan, S.Cremaschi, L., Fisher, D.E., 2012. Experimental investigation of the surface temperature and water retention effects on the frosting performance of a compact microchannel heat exchanger for heat pump systems, Int. J. Refrigeration , 35(1), Pages 171–186.

MPower, 2010. Modine's Custom Vapor Compression System Design, http://www.modine.com/v2portal/page/portal/hvac/hvacCoolingCoilsDefault/hvac_com/cooling_coils/level_3_content2_040.htm, Modine Manufacturing Company, Racine, WI, USA, and Universitat Politècnica de València, Spain.

Nielsen, K.K., Engelbrecht, K., Christensen, D.V., Jensen, J.B., Smith A., Bahl, C.R.H., 2012. Degradation of the performance of microchannel heat exchangers due to flow maldistribution, Applied Thermal Engineering, 40, 236–247.

Oliet, C., Oliva, A., Castro, J., Pérez-Segarra, C.D., 2007a. Parametric studies on automotive radiators, Applied Thermal Engineering, 27(11–12), 2033–2043

Oliet, C., Pérez-Segarra, C.D., Castro, J., Oliva, A., 2010. Modelling of fin-and-tube evaporators considering non-uniform in-tube heat transfer, International Journal of Thermal Sciences, 49(4), 692–701.

Oliet, C., Pérez-Segarra, C.D., Danov, S., Oliva, A., 2007b. Numerical simulation of dehumidifying fin-and-tube heat exchangers: Semi-analytical modelling and experimental comparison, International Journal of Refrigeration, 30(7), 1266–1277.

Palm, B., 2007. Refrigeration systems with minimum charge of refrigerant, Applied Thermal Engineering, 27(10), 1693–1701.

Park, C.Y., Hrnjak, P., 2007. Effect of Heat Conduction through the Fins of a Microchannel Serpentine Gas Cooler of Transcritical CO2 System. Int. J. Refrigeration 30 (3), 389-397.

Patankar, S.V., 1980. Numerical Heat Transfer and Fluid Flow.Hemisphere, New York.

Pettersen, J., Hafner, A., Skaugen, G., 1998. Development of compact heat exchangers for CO2 air-conditioning system, Int. J. Refrigeration , 21 (3), 180–193.

Qi, Z., Chen, J., Radermacher, R., 2009. Investigating performance of new mini-channel evaporators, Applied Thermal Engineering, 29(17–18), 3561–3567.

Qu, X. , Shi, J., Qi, Z., Chen, J., 2011. Experimental study on frosting control of mobile air conditioning system with microchannel evaporator. Applied Thermal Engineering, 31 (14–15), 2778–2786.

Ramos-Alvarado, B., Li, P., Liu, H., Hernandez-Guerrero, A., 2011. CFD study of liquid-cooled heat sinks with microchannel flow field configurations for electronics, fuel cells, and concentrated solar cells, Applied Thermal Engineering, 31(14–15), 2494–2507.

Revellin, R., Mishima, K., Thome, J.R., 2009. Status of prediction methods for critical heat fluxes in mini and microchannels, International Journal of Heat and Fluid Flow, 30(5), 983–992.

Revellin, R., Thome, J.R., 2007. Adiabatic two-phase frictional pressure drops in microchannels, Experimental Thermal and Fluid Science, 31(7), 673–685.

Shao, L.L., Yang, L., Zhang, C.L., Gu, B., 2009. Numerical Modeling of Serpentine Microchannel Condensers. Int. J. Refrigeration 32 (6), 1162-1172.

Shao, L.-L., Yang, L., Zhang, C.-L., 2010. Comparison of heat pump performance using fin-and-tube and microchannel heat exchangers under frost conditions, Applied Energy, 87(4), 1187–1197.

Singh, V., 2009. Development of an Advanced Heat Exchanger Model for Steady State and Frosting Conditions, Doctoral Thesis, University of Maryland, College Park, USA.

Singh, V., Aute V., Radermacher, R., 2008.Numerical Approach for Modeling Air-To-Refrigerant Fin-And-Tube Heat Exchanger with Tube-To-Tube Heat Transfer. Int. J. Refrigeration 31 (8), 1414-1425.

Singh, V., Aute V., Radermacher, 2010. Investigation of Effect of Cut Fins on Carbon Dioxide Gas Cooler Performance, HVAC&R Reasearch, 16(4), 513-527.

Thome, J.R., 2004. Boiling in microchannels: a review of experiment and theory, International Journal of Heat and Fluid Flow, 25, 128–139.

Veje, C., Süss, J., 2004. The Transcritical CO2 Cycle in Light Commercial Refrigeration Applications. 6th G. Lorentzen Conf. on Natural Working Fluids, Glasgow, Scotland.

Webb, R.L., 1994. Principles of Enhanced Heat Transfer. John Wiley and Sons, New York.

Xia, Y., Zhong, Y., Hrnjak, P.S., Jacobi, A.M., 2006. Frost, defrost, and refrost and its impact on the air-side thermal-hydraulic performance of louvered-fin, flat-tube heat exchangers, Int. J. Refrigeration , 29 (7), 1066–1079.

Ye, L., Tonga, M.W., Zeng, X., 2009. Design and analysis of multiple parallel-pass condensers, Int. J. Refrigeration , 32, 1153–1161.

Yin J.M., Bullard C.W., Hrnjak P.S., 2001. R-744 Gas Cooler Model Development and Validation. Int. J. Refrigeration 24 (7), 692-701.

Zhang, P., Hrnjak, P.S., 2010. Air-side performance of a parallel-flow parallel-fin (PF2) heat exchanger in sequential frosting, Int. J. Refrigeration , 33(6), 1118–1128.

Zhao, C.Y., Lu T.J., 2002. Analysis of microchannel heat sinks for electronics cooling, International Journal of Heat and Mass Transfer, 45(24), 4857–4869.

Zhao, Y., Ohadi, M.M., Radermacher, R., 2001. Microchannel Heat Exchangers with Carbon Dioxide Report No.: ARTI-21CR/10020-01.

Zhong, Y., Joardar, A., Gu, Z., Park, Y.-G., Jacobi, A.M., 2005. Dynamic dip testing as a method to assess the condensate drainage behavior from the air-side surface of compact heat exchangers, Experimental Thermal and Fluid Science, 29 (8), 957–970.

Zilio, C., Brown, J.S., Schiocheta, G., Cavallini, A., 2011. The refrigerant R1234yf in air conditioning systems, Energy, 36 (10), 6110–6120.

Zilio, C., Cecchinato, L., Corradi, M., Schiochet, G., 2007. An Assessment of Heat Transfer Through Fins in a Fin-and-Tube Gas Cooler for Transcritical Carbon Dioxide Cycles. HVAC&R Res. J. 13 (3), 457-469.